Developing Biosensor Technology to Monitor Biofilm Formation on Voice Prosthesis in Throat Cancer Patients Following Total Laryngectomy

A dissertation submitted to the University of Kent for the degree of Doctor of Philosophy in the Faculty of Electronic Engineering

2019

Viktorija Makarovaite

School of Engineering and Digital Arts

Developing Biosensor Technology to Monitor Biofilm Formation on Voice Prosthesis in Throat Cancer Patients Following Total Laryngectomy

Abstract

Voice prostheses (used to replace an excised larynx in laryngectomy patients) are often colonised by the yeast *Candida albicans*, yet no monitoring technology for *C. albicans* biofilm growth until these devices fail. With the current interest in smart technology, understanding the electrical properties of *C. albicans* biofilm formation is necessary. There has been great interest in Passive Radio Frequency Identification (RFID) for use with implantable devices as they provide a cost-effective approach for sensing. The main drawback of RFID sensors is the need to overcome capacitive loading of human tissue and, thus, low efficiency to produce a high read range sensor design. This is further complicated by the size restriction on any RFID design to be implemented within a voice prosthesis as this medical device is limited to less than 3 cm in overall size. In order to develop such a voice prosthesis sensor, we looked at three separate aspects of *C. albicans* colonisation on medical devices within human tissue. To understand if it is possible to detect changes within a moist environment (such as the mouth), we developed a sensor capable of detecting minute dielectric changes (accuracy of ± 0.83 relative permittivity and ± 0.05 S·m-1 conductivity) within a closed system. Once we understood that detection of dielectric changes within a liquid solution were possible, to overcome human tissue capacitive loading of RFID sensors. Adjusting backing thickness or adding a capacitive shunt into the design could limit this tissue effect and even negate the variability seen between human tissues. Without developing these methods, implementation of any RFID device would be difficult as human tissue variability would not be compensated for properly. Finally, biofilm growth in terms electrical properties. As *C. albicans* biofilm matures, there is a loss in capacitance (the biofilm becomes increasingly hydrophobic) prior to 24 hours after which the biofilm thickness shifts the resonance leading to a slow gain in capacitance. Understanding all of these aspects allowed us to develop two final voice prosthesis sensors producing read ranges above 60 cm and 10 cm within a tissue phantom. Ultimately, this showed the possibility of developing cost-effective passive RFID sensor technology for monitoring microbial biofilm formation within human tissue, leading to more effective real-time clinical care.

Viktorija Makarovaite

47,252/ 124 pages

2019

School of Engineering and Digital Arts

Acknowledgments

I would like to express my gratitude to my supervisors, Prof. John Batchelor and Dr. Campbell Gourlay, for their support throughout the years. I especially appreciate all the time they've taken to help edit all my work and guide my publications. Many thanks for the assistance provided by Simon Jakes before his retirement without whom many of my early designs would not have been prototyped. Also, a big thanks to both the KFG and Antenna's groups for all their support. Thank you to Simon Holder and Aaron Hillier for their help with the polymer adjustments needed to make my devices function properly. I would like to thank my friends and family for the support they've given, especially during this final year. Finally, the biggest thanks to my dog Beanie for being cute and helping with my stress levels.

My heartfelt thanks.

Ethics Approval # 0551920

Table of Contents

1 Chapter 1: Introduction

This project aimed at developing biosensor technology capable of monitoring *Candida albicans* biofilm growth on voice prosthesis in throat cancer patients following a total laryngectomy. There was not any patient testing for the voice prosthesis sensor but rather use of a gelatine body phantom to imitate the throat tissue of a cancer patient. Any non-invasive testing was completed utilizing volunteers (with University of Kent ethical approval) and consisted of external readings intended for the improvement of human body phantoms to represent human tissues more accurately in terms of dielectric properties. Additionally, some sensor designs were attached externally to volunteer forearms as wearable sensors with negligible harm. The thesis structure was separated into five main chapters: Introduction; Background Information; Project Aims (which include the four main papers); Concluding thoughts; and References.

The background chapters will describe *C. albicans* disease, virulence and biofilm growth on medical devices followed by the detection methods currently utilised. The largest section of this chapter will involve the description of the chosen sensor type for development as well as other common biosensors used for microbial detection. This will show that a radio frequency identification-based sensor was chosen as the main method for detection as it was able to produce a fully passive, wireless system capable of detection outside the body. The final portion of this section will include the summary of the main background topics to show the importance of this project. Chapter 3 will incorporate the project aims describing what research needed completion to develop technology capable of monitoring biofilm growth upon a voice prosthesis while within the body. Also, it will include the correlating journal publications developed based on the project aims. Chapter 4 will include the concluding thought of the finished project and suggestions for what else needs to be included as well as any issues

remaining with the completion of the topic. Finally, Chapter 5 is comprised of all references employed throughout the thesis except for Chapter 3 as Chapter 3 includes separate references as each included journal article is formatted based on the IEEE Sensors Journal requirements. Altogether, this should present why the project was developed which concluded in a functional RFID sensor for monitoring biofilm formation on voice prosthesis in throat cancer patients following total laryngectomy.

2 Chapter 2: Background Information

Understanding *Candida albicans* as a disease is necessary to develop a sensor capable of monitoring biofilm growth on a voice prosthesis while within the body. This disease is linked to *C. albicans* gene expression as well as the general growth environment. Slight variations in gene expression can cause a commensal *C. albicans* to become pathogen even changes to iron acquisition or CO_2 availability play an important role in virulence of this pathogen. When it comes to *C. albicans* biofilm growth on medical devices, there is much research in the role of saliva as a medical device surface coating and effect on virulence. Biofilm growth on medical devices vary based on location, type of medical device or even surface roughness and hydrophobicity. All these must be known for a full understanding of *C. albicans* biofilm development on medical devices. The main methods involved in *Candida species* detection, or any microbial detection, often require *in vitro* growth, require expensive equipment for detection or just unable to perform real-time monitoring. In the case of current biosensors, most published devices are incapable of wirelessly detecting microbial growth, specifically within the body. Therefore, utilising some of the current methods capable of wireless sensing, as seen within the field of radio frequency identification, would be ideal to overcome these shortcomings.

2.1 Disease and Virulence

Within the last few decades there has been an increase in a wide spectrum of fungal infections ranging from acute and self-limiting to severe or even life-threatening diseases. [1] A majority of these increases are attributed to advances in medicine particularly in fields of chemotherapy and transplant surgery (bone marrow and solid organ, particularly) as well as the global AIDS emergence. [2] This upsurge in immunocompromised patients has allowed for the emergence of numerous human disease associated fungal species with a segment even

capable of inducing disease within immunocompetent hosts. [1] Many factors play a role in disease and virulence of any specific microbial species but often these have genetic links and environmental factors.

2.1.1 Fungal Burden and Disease

Nearly 90% of all reported fungi related deaths (about 1.5 million per year) and the primary fungal pathogens in clinical isolates can be categorized within four genera: *Candida, Cryptococcus, Pneumocystis* and *Aspergillus.* [1, 2] Invasive diseases caused by *Aspergillus spp.* are reported to be linked with over 200,000 annual deaths within the global immunocompromised population. *Cryptococcus spp*. induced meningitis alone caused over 500,000 reported deaths in sub-Saharan Africa while *Pneumocystis spp.* associated pneumonia (in immunocompromised populations) has nearly an 80% mortality rate with 400,000 global death per annum. *Candida spp*. bloodstream infections have a 40 % mortality rate in cases of sepsis with an overall global incidence of 400, 000 annum cases. However, these reported fungal burdens do not account for the millions (and billions) of individuals suffering from non-lethal fungal diseases such as dermatophytosis (estimated at over 1.7 billion cases per annum). [1] Most of these have over the counter remedies as seen with athletes' foot (commonly due to *Trichophyton rubrum*) affliction. The main issues arise because diagnosis is difficult, less drugs are available in comparison to other microorganisms and the occurrence of drug resistance with prolonged exposure. [3, 4] Fungal infections occur as superficial, allergic, invasive or systemic infections with systemic being the most serious and life threatening. [3] One of the most studied fungal pathogens is *Candida albicans*.

C. albicans is generally considered to be an opportunistic pathogen and is a unicellular fungus. In healthy individuals, *C. albicans* and other *Candida spp*. tend to be part of the normal flora found on the skin, mucosal surfaces, gastrointestinal and urogenital tracts, and vaginal canal. [5] *C. albicans* can cause a variety of diseases with the most common being oropharyngeal

candidiasis and vulvovaginal candidiasis. [6] Oropharyngeal candidiasis usually occurs secondary to diabetes or HIV-induced immunodeficiency and can predict the progression of HIV symptoms. Most of the HIV and AIDS associated *Candida spp.* infections occur from commensal associated strains.[7] In systemic or invasive *C. albicans* infection, *C. albicans* gains entry into the bloodstream by penetrating the epithelial barrier before disseminating throughout the body and reaching other organs. [8] *C. albicans* has the highest prevalence of any fungal pathogen (other than dermatophytes) with being the 4th main cause of bloodstream infections within the United States. [9]

C. albicans tends to be not a very virulent species until given the opportunity to become a pathogen often due to mechanical injury or gastrointestinal perforation, or some type of immunodeficiency. *C. albicans* adaptation to its environment by expressing specific infection associated genes contributes its pathogenicity along with morphological transition, adhesion and hydrolytic enzyme secretion, phenotypic switching and iron acquisition. [7]

2.1.1.1 *C. albicans Hyphal Transition*

C. albicans can transition between a blastopore (single celled budding yeast) to hyphae (elongated rod form). Blastopores are thought to enable dissemination whereas hyphal cells facilitate tissue invasion. [7] This morphological transition is controlled by gene regulation and a complex network of signalling pathways. [10, 11] Environmental signals such as serum, neutral pH, prolonged exposure to 37°C, 5% CO_2 atmosphere, nutrient starvation and N-acetyl-D-glucosamine presence all contribute to the activation of the signalling network. [12-16] For example, one such pathway is the cyclic AMP-protein Kinase A (cAMP-PKA) pathway. It activates cAMP production by sensing an environmental signal using adenylyl cyclase Cyr1. When serum is present, then *C. albicans* will utilise GTPase Ras1 to activate Cyr1 by directly interacting with the Ras-associated domain of Cyr1 with Ras1. [7] Also, G protein-coupled receptor 1 (Gpr1) senses amino acid presence in the environment activates Cyr1 using Gpα2.

[17] Intracellular cAMP levels are increased by Cyr1 activation which can then bind Bcy1 subunit of PKA releasing Tpk1 and Tpk2 subunit of PKA. [18] Active PKA can then regulate transcription factor Efg1 enhancing the expression of hyphal genes such as ALS3 (adhesion), HGC1 (hyphal formation) and HWP1 (adhesion). [7]

MAPK (mitogen-activated protein kinase) cascade, also, plays a role *C. albicans* morphogenesis using Cst20 (MAPK kinase kinase), Ste11 (MAPK kinase kinase), Hst7 (MAPK kinase), and Cek1 (MAPK). Cek1 has been shown to phosphorylate a transcription factor (Cph1) helps hyphal growth on solid media but has no effect when in liquid media or in the presence of serum. Availability of nitrogen also affect *C. albicans* morphology.[7, 19] During nitrogen limitation, MEP2 gene (controlled by the transcription factors Gat1 and Gln3) is upregulated possibly leading to activation of the cAMP-PKA pathway a Cph1-dependent pathway. [7, 20]I t has been shown that GTPase Rhb1 is involved in MEP2 expression nitrogen limitation signalling. [21]

Environmental pH can trigger *C. albicans* morphogenesis using Rim101 (a zinc-finger-containing transcription factor) regulation which is in active in acidic condition. [22, 23] When the environment becomes neutral or alkaline then Rim13 can cleave Rim101 C-terminal portion altering gene expression of morphogenesis by activating a protein. [24] *C. albicans* itself can change the environmental pH by extruding of ammonia during glucose deprivation. [25] *C. albicans* can also experience hypoxia induced hyphal transition in a matrix dependent manner with Efg1 and Cfz1 transcription factors. [26] These all form a complex signalling pathway leading to hyphal formation or yeast form. This allows *C. albicans* to adapt to variable niches just by changing gene expression or extracellular proteome secretion of which mostly include secreted enzymes such as hydrolases and adhesins through the classical pathway. However, there are many enzymes which are found in both disease and commensal *C. albicans* colonisation. [27]

2.1.1.2 *Activity of Adhesins*

The initial step leading to *C. albicans* infection is the adherence to host cells. *C. albicans* commonly causes mucosal infections by first adhering and colonising epithelial cells. *C. albicans* cell wall contains carbohydrates and proteins which can interact with the external environment and allow for adherence to host cells or biomaterials such as medical devices usually forming biofilms. Biofilms are less susceptible to antifungal agents and host defences than planktonic cells providing a continual reservoir for infection. Adhesins (mostly glycosylphosphatidylinositol modified wall proteins) help *C. albicans* adherence along with other factors (such as salivary proteins). Three gene families (Als, Hwp, and Iff/Hyr) are the main adhesins found in *C. albicans*. [28] The Als protein family (agglutin-like sequences) is a common family of adhesins with eight Als genes encoding glycoproteins on the cell wall. Depletion of these genes have shown that they play a key role in adherence to host cells. The Hwp family sharing a conserved 42-aa repeat unit; it should be noted that there is a link between gene repeats and adherences where longer repeats produced greater adherence. [28] Hwp family proteins (Hwp1, Eap1) along with Int1 (integrin-like protein) also play a role in *C. albicans* adherence where Hwp1 is present in the hyphal cell wall allowing for adherence to epithelial cells and is required for biofilm formation. Eap1 is not only required for biofilm formation, but also for binding to polystyrene surfaces. Int1 has been shown to play a role in adherence and colonisation of murine intestinal epithelium. Also, Adhesins play a key role in *C. albicans* adherence when secreted as extracellular proteomes.[7, 27-29]

2.1.1.3 *Hydrolytic Enzyme Activity*

C. albicans secretes many hydrolytic enzymes which help with nutrient acquisition, dissemination throughout a host and help modulate the host immune responses. [7] Secreted aspartyl proteases (Saps) are expressed differently during *C. albicans* various stages and are secreted more readily during biofilm formation rather than throughout planktonic cell

formation. [7, 27] Saps likewise play a role in modulating the host immune response at different pH levels and sites, and are associated with the cell wall formation. [7, 27] Phospholipase A to D (PLA to PLD) help hydrolyse glycerophospholipids on the host cell membrane playing a key role in tissue invasion which destroys and degrades the host tissue. [7, 30] Also, PLB is the main active phospholipase in *C. albicans.* [31] Moreover, *C. albicans* secretes a serine peptidase and more than nine lipases which degrade extracellular matrix components and human serum proteins, and hydrolyse triacylglycerols. [30, 32, 33] Many of these enzymes are present within extracellular proteome secretion along with adhesins and other enzymes. [27]

2.1.1.4 *C. albicans phenotypic switching*

C. albicans survival is enhanced by phenotypic switching by causing the pathogen to become more virulent. [7] The most common switching occurs between white hemispherical colonies (W) and grey/opaque flat colonies (O). This switching also affects the cells size, hyphal formation, properties of the cell surface, composition of the membrane, biofilm formation, drug susceptibility, metabolism, and also facilitate mating.[34] It has been shown that when the PEP1 gene is present on a W cell when usually seen only in an O cell, then this W cell has increased virulence. Murine models show that W cells tend to colonise kidneys and O cells taken from the kidneys switch to a W state. This regulation has been found to be majorly controlled by WOR1 gene with additional help of WOR2, Efg1 and Czf1 in feedback loops. Deletion of the WOR1 gene will lock a cell in the W phase. [7] Also, some phenotype transcription factors (Tec1 particularly) have been linked to biofilm formation on silicone elastomers which are regulated by the Ras1/cAMP pathways. It has also been shown that phenotype switching plays a role in host colonisation: W colonies are more virulent for systemic mouse models; O colonies are more virulent in cutaneous models as they more readily infiltrate skin surface. [34]

2.1.1.5 *Iron acquisition of C. albicans*

C. albicans acquires iron during infection, as iron within a host is usually sequestered within specialized proteins, requiring utilization of siderophore or haemoglobin-iron uptake. [35] Free forms of iron inhibit cell growth while causing cells to be more susceptible to neutrophil damage. [36] Als3 facilitates iron acquisition from the host ferritin while Rbt51 helps utilise hemin and haemoglobin-iron. [7] Iron availability can also affect the drug resistance of biofilms [13] as *C. albicans* cell wall antigen composition and adhesion properties are affected by iron deprivation. [7] Iron therapy can also be used to treat infection especially in patients who have high iron availability. Using chelators can help with multi-drug resistant species as these lower the iron levels within a patient. With medication such as Ciclopirox olamine, their activity is increased due to iron limitation as they act to reduce the available iron within the tissue particularly as a topical treatment. [37] *C. albicans* caused endothelial cell damage is iron-dependent and Arn1 (a siderophore transporter) is needed for epithelial penetration. [38] Iron acquisition of *C. albicans* is facilitated by a "regulatory circuit" of transcription factors (including Sfu1, Hap43, and Sef1) and a complex system. [7] Sef1 was shown to promote virulence in bloodstream infections by inducing iron uptake whereas Sfu1 negates Sef1 and promotes commensalism. [39, 40] Whereas Hap43 acts as a repressor of transcription within this regulatory circuit due to iron deprivation [41] along with other transcription factors.

It should be noted that 70% of available iron within the host can be found within haemin and haemoglobin and with the haemolytic activity of *C. albicans* can uptake this iron via extracellular membrane proteins such as those part of the CFEM domain. Specifically, iron uptake from haem for *C. albicans* is due to the proteins Rbt5, Pga10, Pga7 and Csa2 which help move the iron into the plasma membrane through the cell wall. Also, iron acquisition can change based on *C. albicans* stage of infection: initial infection has a link with strong iron

uptake even with low iron availability while late stage infection as tissue damage increases the iron uptake is not as strong. For systemic infections, Sef1 (with low iron availability) has a nuclear localisation while stress response liked with biofilm adhesion such as Hog1 increase with tissue damage and high iron. Iron- acquisition can play a role in host-pathogen interaction by utilising the host iron availability for necessary niche adaptations and change in transcription factors.[35]

2.1.2 *C. albicans* Biofilm Formation

Candida albicans forms biofilms in four distinct stages: (1) surface attachment and colonisation of yeast cells, (2) growth and proliferation of these cells ultimately forming a basal layer of attaching microcolonies, (3) growth of ellipsoid cells attached end to end (pseudohyphae) and then extensive cylindrical cell chains (hyphae) which is connected with the production of extracellular matrix (ECM) material, and (4) yeast cell dispersion from the biofilm to form new biofilms at other sites. [42-48] Also, there are six transcription regulators controlling the formation of *C. albicans* biofilms, made of three cell types (yeast, pseudohyphae and hyphae) within an extracellular matrix, to form an interwoven transcriptional network (exhibited in Fig.1). [49]

These regulators are sequence-specific DNA-binding proteins that regulate transcription which include: Brg1, Tec1, Efg1, Rob1, Bcr1 and Ndt80. [8] Within this network, each transcription regulator can control the other five regulators and most genes are controlled by more than a single regulator at a time. Positive regulation is thought to be the basis for most of this control with 15% of the genes in the C. *albicans* genome comprising this network. Other *Candida spp.* are likely regulated by other transcription regulators and/ or target genes but still like the six regulators of *C. albicans*. [49]

In a different study, biofilm formation was also shown to be controlled by the transcription regulators Efg1, Tec1, and Bcr1 as well as *C. albicans* adenylyl cyclase (Cyr1 (Cdc35)) and

Tpk2 (protein kinase A subunit). [50] Biofilms can be formed in either a Cyr1- dependent or independent pathway and/ or an adenosine monophosphate (cAMP) dependent or independent matter. [51] Cyr1 is involved in C. *albicans* phenotype switching, invasive filamentous growth and biofilm formation. Specifically, the activating G-protein Ras1 of Cyr1 is required for yeast to hypha conversion. [50] During hyphal development, cAMP signalling increases along with activation of PKA (protein kinase A) and an increase in hyphal growth transcription genes. [52] The cAMP dependent pathway utilising *C. albicans* biofilms were more impervious to human polymorphonuclear leukocytes and other small molecules as well as contained more β-glucan in their extracellular matrix acting as antifungal components. [50, 51]

It has been shown that early and mature biofilms exhibit differing gene profiles. It is believed that these differences could be due to the changes in morphology and structure of a biofilm over time or due to changes in the metabolic or quorum sensing process. [53] As attachment of *C. albicans* onto a surface initiates biofilm formation, it is understandable that early growth during biofilm formation (up to 12 hours) genes involved with attachment are upregulated such as the family of adhesins known as ALS (agglutin-like sequences) genes. [37, 53-55] ALS1 was up-regulated 12-fold and ALS2 was upregulated 4-fold compared to planktonic *C. albicans* as well as was only present during this early time point in the biofilm formation. [53] Transcription of genes involved in protein synthesis, stress, transport, metabolism (cell wall, amino acid, and energy production) and carbohydrate processing are up regulated during intermediate biofilm formation while genes dealing with DNA processing and cell cycle are downregulated. Also, some down-regulation is evident in genes involved with protein synthesis, transport, cytoskeleton, and carbohydrate processing during intermediate biofilm formation.

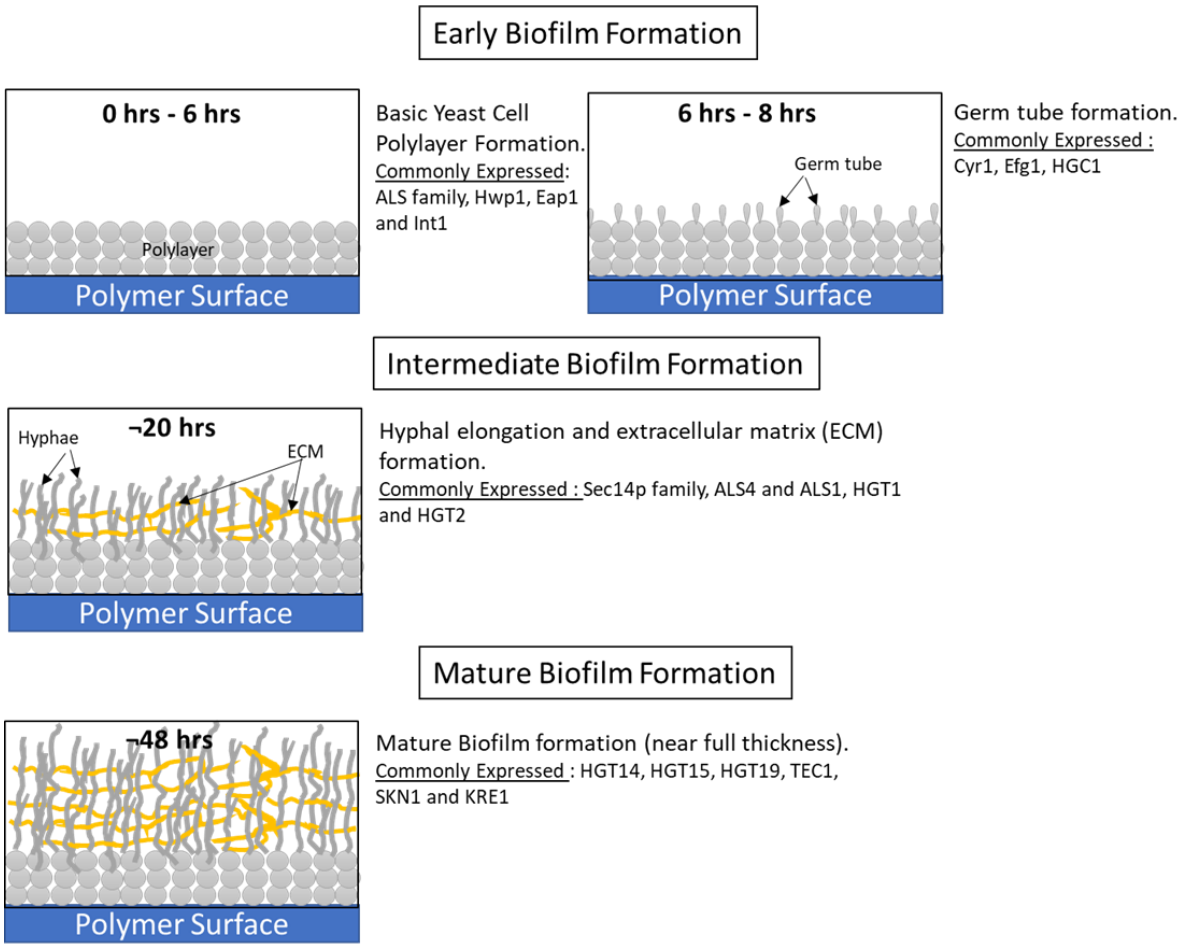

Figure 1 *Candida albicans* biofilm formation. Separated into three main stages of biofilm formation: early, intermediate and mature. Also, some common regulators involved in each stage are expressed.

Mature biofilms which contain a basal layer of *C. albicans* cells, an extensive matrix production and filamentous morphotype layering exhibit up-regulation of genes which encode protein processing, transport, DNA/cell cycle, carbohydrate processing, energy and metabolism were found to be upregulated while genes involved with DNA processing, cell cycle, transcription, protein synthesis and transport were downregulated. Specifically, adherence (ALS4 and ALS1), general metabolism (CGT, ICL1, MLS1, PCK1 and PDK1) and cell wall metabolism (ECE1 and SAP5) as well as hyphal formation (HWP2) genes are all upregulated during *C. albicans* biofilm formation. [53] Also, amino acid permeases such as DAO2, DIP5, GAP6 and GNP1. [53]

Genes involved with hyphal morphology changes are upregulated in mature biofilms compared to early ones. For example, a transcription factor with hyphal morphogenesis involvement

(TEC1) is up-regulated 2.4-fold in a mature biofilm. [56] An extracellular polymeric matrix is required for the formation of a mature biofilm which is composed of glucose, protein, carbohydrate and small amounts of hexosamine and phosphorus. [53, 57] Therefore, it is understandable that genes involved with β-1-6 glucan synthesis and ERG25 transcription (SKN1 and KRE1) are upregulated in a mature biofilm. ERG25 plays a role in C4-demethylation of ergosterol biosynthesis intermediates as a C-4 methyl sterol oxidase. [53] This suggests that this upregulation increases the conversion of lanosterol to nonergosterol intermediates (eburicol and 14-methyl fecosterol). Transcripts ENG1 and SWC1, involved in β-1-3 glucan degradation with a β-1-3 glucosidase activity were downregulated in mature biofilms (at 24 hours). [53, 58]

The genes encoding the malate synthase and isocitrate lyase enzymes (MSL1 and ICL1) part of the glyoxylate cycle, which allow two carbon molecules as the energy source, are over 2-fold upregulated in a mature biofilm. This can become necessary when overtime the glucose levels decrease at the silicone surface needing for *C. albicans* to utilise additional carbon sources as would be allowed by the use of the glyoxylate cycle. [53] Up-regulation of efflux pumps, slow growth, plasma membrane ergosterol content alteration, and antimicrobial decreased perfusion through the matrix have all been suggested as ways that *C. albicans* gains resistance to various antifungals. [53, 58, 59] Early biofilm resistance has been attributed to the increased transcription of MDR1 and CDR1 (efflux pumps genes). [58, 59] During intermedia and mature biofilm formation the resistance has been noted to occur by the upregulation of a phosphatidylinositol transfer protein of the Sec14p family (PDR16). [53, 60] It is also possible to differentiate between intermediate and mature biofilms by regulation of amino acid synthesis and sulphur metabolism genes. Intermediate biofilms exhibited eighteen gene changes while mature biofilms had twenty-one genes in comparison to a planktonic yeast cell. Many of the genes involved in *C. albicans* biofilm formation of an intermediate to mature

biofilm (post 12 hours of attachment) are listed in Table 2.1; However, it should be noted that over 40% of genes present were not able to be categorised and the function still needs to be deciphered. Increased expression of glucose transporters, HGT1 and HGT2 (a 52-fold increase), was seen in intermediate biofilms whereas mature biofilms expressed both the HGT1 and HGT2 at a lower level but also increased the expression of other glucose transporters such as HGT14, HGT15 and HGT19. It is possible that nutrient starved mature biofilms require more access to glucose and thus need more glucose transporters or excess glucose is needed to produce the carbohydrate matrix as normally seen in a mature biofilm. [53]

Table 2.1: Genes differentially regulated during intermediate and mature biofilm formation

	Upregulated Transcripts		**Downregulated Transcripts**	
Category	**Genes**	**No. genes (%)**	**Genes**	**No. genes (%)**
Amino acid	*AGP2, ARG1, CAN1, CDG1, CPA1, CPA2, SMM1*	6 (5)	*GLT1*	1 (4)
Carbohydrate	*CAT8, CIT1, DLD3, FBP1, GAL1, GAL10, HGT1, HGT2, HGT14, KGD1, MLS1, PAM16, PCK1*	13 (10)	*UGP1, PFK2*	2 (7)
Cell wall	*BGL2, CYC3, ECE1, FMP45, orf19.6489*	5 (4)	*CWH43, SCW11*	2 (7)
Cytoskeleton	*SDA1*	1 (1)	*DYN1, IQG1*	2 (7)
DNA/Cell Cycle	*AAH1,* orf19.1005, orf19.5845	3 (2)	*HHF1, HHF22, HTA2, PCL2, POL30, RNR3, TMP1, orf19.7634*	8 (30)

Energy/Metabolism	*ALD6, AOX2, ARG8, COX11, COX 17, CTN1, GUT2, ICL1, INO1, NCE103, NDE1, OYE22, OYE23, YAT2, orf19.361*	15 (12)		
Fatty Acid	*FAA2, orf19.732*	2 (2)		
Heat Shock Protein	*HSP30*	U1 (1)		
Hyphal	*RLP1*	1 (1)		
Iron	*CFL2, FRE10, ISU1, SIT1*	4 (3)		
Plasma Membrane	*ERG25, PDR16*	2 (2)	*ERG7, PLB1*	2 (7)
Resistance/Stress	*AQY1, EBP1, MDR1, SOD6, YHB3*	5 (4)		
Transcription/Protein	*CIC1, DBP1, DBP7, MRPL33, MRT4, MSS116, MTO1, PEX4, REX2, RLP7, RPC19 RRN11, SAP5, SOF1, UGA32, orf19.124*	16 (13)		
Transport	*GNP1, JEN2, LEU5, OAC1, SFC1, TIM9, TNA1*	7 (6)		
Unknown		43 (35)		10 (37)
Remade from [53].				

2.1.3 Commensal or Disease-linked Biofilm Gene Expression:

As *Candida albicans* is considered an opportunistic pathogen and found as part of the normal human flora (particularly of the gastrointestinal (GI) tract and oral cavity), therefore

distinguishing a true *Candida* infection can be difficult. The fungal cell surface can guide the differentiation of a true infection from commensal growth. When infection does occur this often links with either candidemia and/ or candidiasis, particularly in immunocompromised individuals. [61] One of the most common forms of bloodstream infection is due to *C. albicans*; a recent study found that *C. albicans* caused at least 33% of blood stream infection within 2008 till 2011 in the US (Atlanta and Baltimore) and a 14.5% increase in hospital patient mortality [61, 62]; this rate has not decreased within the last 20 years. [62] When looking at invasive candidiasis, a high GI tract burden of *C. albicans* (as well as other *Candida* species) has been viewed as a likely risk factor. [61]

2.1.3.1 *Commensal Gene expression:*

This variability between normal colonisation of the GI tract (and other locations) compared to *C. albicans* in a biofilm have been related to variability seen in gene expression. Studies which compared gene expression of biofilms grown on a variety of polymer materials in comparison to liquid-grown planktonic cells, had an upregulation of 1,805 gene out of a total of 6,000 *C. albicans* genes possible. Similarly, gene expression during colonisation of commensal *C. albicans* (isolated from murine models) found that 741 genes were upregulated in this non-disease model compared to liquid-grown planktonic cells. [61]

The disease-linked and commensal *C. albicans* biofilms shared an upregulation of only 361 genes, suggesting that the diseased-associated biofilms upregulate over 1,400 more genes during the disease process to account for biofilm adaptations. This shared overexpression was associated with metabolic processes, cell adhesion and redox processes suggesting that these genes promote growth within a host. [61, 63] Many of the disease-linked biofilm genes were associated with protein translation. [63] Other studies have showed the same protein translation gene upregulation during biofilm states compared to commensal colonisation which down-regulated the same genes. [63, 64] Similarly, the *C. albicans* gene orf19.6090 (homolog to the

widely studied *Saccharomyces cerevisiae* gene NSR1), which help with pre-rRNA processing, is upregulated in disease-linked biofilm but not GI tract commensal growth. Also, a mutant lacking this gene produced lower biofilm mass suggesting a biofilm growth defect. [65]

Also, disease-associated *C. albicans* biofilms overexpress beta-1, 3 glucan (β-glucan) (part of the extracellular matrix and, also, present in fungal cell walls) linked genes. [61, 63] This can be seen with glucan synthase enzymes; three genes (GSC1, GSL1 and GSL2) in *C. albicans* are thought to play a role in activity of glucan synthase. [49, 61, 66] GSL1 and GSL2 are not yet fully understood; however, it was shown that CZF1 (transcription factor encoding gene) deletion influences GSL1 and the removal of the gene induced a clear overexpression of GSL1. This suggests that CZF1 regulates *C. albicans* cell wall integrity by repressing β-glucan synthesis. This correlates with another publication suggesting there is a down-regulation of GSL1 during filamentation which CZF1 positively regulates. [66] GSC1 gene product synthesizes β-glucan and is upregulated during biofilm formation in rat models. [61, 67] All three genes are upregulated in only the biofilm models and not commensal models which is understandable as *C. albicans* biofilms have an extensive extracellular matrix production compared to commensal colonisations. [61]

Determining the difference between a commensal colonisation or a disease-linked biofilm growth of *C. albicans* has, also, a correlation with the expression of cell surface proteins which usually function in adhesion. So far 45 upregulated genes were found within biofilm rather than commensal colonisation that regulate cell surface proteins (ten regulate adhesion and eight expressed during hyphae formation). The 10 genes linked to adhesion include ALS2, ALS4, CSH1, HWP2, and XOG1 for hyphal adhesion and ALS6, BGL", IFF4, PRAT1 and SAP10 for non-hyphal adhesion. However, these genes are not extensively studied so known function could change with time. This commensal or disease linked gene expression can be altered depending on growth surface and environment. Having *C. albicans* grow within host tissue

compared to non-host tissue biomaterial surface allows for the upregulation of ulterior genes to induce better material adhesion and colonisation. [61]

2.2 *Candida albicans* Growth on Medical Biomaterials:

Microbial biofilm formation results in the production of polymeric substance within the extracellular matrix such as the thin strand (or amorphous sheet) polysaccharides that surround the cells and connect them to the material surface or each other. [68] When quantifying volume within a biofilm, the extracellular components rather than cells compose most of the volume allowing for the cells to be highly antimicrobial resistance (1000-fold higher) compared to planktonic cells. [68-72] This developed anti-microbial resistance can lead to devastating medical device-related consequences such as systemic infections, device removal requirement and often tissue necrosis following colonisation. [68-73]

Ability to form a biofilm is linked with *Candida* species pathogenesis. Planktonic cells are not able to as easily induce an infection compared to cells from biofilms. [61] For example, mortality rates for wax moth larvae varied greatly between *C. albicans* strains with the ability to form a biofilm or with a non-biofilm forming mutation. The strains unable to form a biofilm had much lower mortality rates. [74] A mouse model showed a similar result, when the candidemia model used planktonic (grown in a non-biofilm form) cells for infection compared to cells that detached from a biofilm directly, the mortality rate was much lower. This was particularly interesting as both cell types chosen for this candidemia model were in the yeast form. [47] When looking at human infection, *Candida* biofilm forming strains are linked with much higher rates of mortality and morbidity compared to non-biofilm forming strains. [75]

Ultimately, management of biofilm formation on medical devices can be both costly and difficult. *Candida* species, particularly *Candida albicans,* is frequently associated with medical device failure and colonisation especially when looking at bloodstream or urinary tract infections. [69, 73] As the majority of *Candida* species are opportunistic pathogens, other

factors must be involved in order to allow the formation of these biofilms on medical devices: material contact surface, hyphae formation and device environment. [73]

2.2.1 *Candida albicans* and Surface Attachment:

Biofilm infections can be detected on an implantable device only after an infection has already occurred; most commonly due to device failure, inflammation of surrounding tissue or (more rarely) bloodstream systemic infection. [76] This always necessitates revision or replacement as it is difficult to treat due to a development of drug resistance by mature *C. albicans* biofilms. [76, 77] Also, lack of symptoms can occur with colonisation that is usually followed by a low grade fewer or is completely aseptic. [78, 79]

Candida albicans biofilm formation occurs by first attachment to device surface followed with phenotype dimorphic switching from planktonic cells (once enough cell attachment occurs) leading to extracellular matrix formation of polymeric material. [76] The mature extracellular matrix forms a dense network of polysaccharides, protein, carbohydrates, extracellular DNA strands and a combination of all *C. albicans* forms (yeast, hyphae and pseudohyphae). [73, 76, 77] The growth of the biofilm allows the yeast cells to develop hyphae/pseudohyphae and extend away from the attached basal cell layer creating a filamentous layer which then (once mature) can slough off planktonic cells for possible migration to other areas of the body or device. This release of planktonic cells has led to blood stream infections lethal for immunocompromised patients especially after any surgical trauma or can interfere with patient healing. [76] Yeast attachment is dependent on the material's contact surface. [73] The contact surface can also be altered to a more hospitable environment by the presence of a conditioning film or by changes in the surface roughness and hydrophobicity.

This becomes a more serious problem as *C. albicans* is able to colonise most medical device surfaces in use even on smooth surfaces made of Teflon$^{TM.}$ [76] Biofilm formation has been noted on all medical polymers, metals, ceramics and even tissue derived materials (such

collagen fillers). Biofilm formation has been published for joint prosthetics, cardiac devices, voice prosthesis and catheters (vascular, parenteral and peritoneal and urinary). [77] Basically, any medical device made from polyvinyl chloride (PVC) or polyurethane can be colonised by *C. albicans* easily if given the opportunity (usually due to a host- weakened state). [76] There is enough evidence that *C. albicans* can form on the surface of medical devices made from silicone elastomers, polystyrene and others. [78] Surface of the device can affect biofilm morphology and formation.

2.2.1.1 *Roughness and Hydrophobicity:*

Material surface roughness and hydrophobicity has been shown to increase microbial attachment with increased roughness. For example, when varying levels of roughness and hydrophobicity on materials such as PVC, polystyrene, stainless steel, polycarbonate, hydroxy apatite and polyte trafluoroethylene, there was a correlation between *C. albicans* adhesions and increased surface roughness. The same was seen with poly (methyl methacrylate) (PMMA)-based polymers, where an increase in the contact angle lowered C. albicans adhesion while surface roughness increased it. This was seen independent of the conditioning surface with serum suggesting surface roughness plays a larger role in *C. albicans* adhesion than serum conditioning of the material surface. [78, 80]

Similarly, increased hydrophobicity can cause increased *C. albicans* attachment to material surface. It has been shown that *C. albicans* will adhere more readily to hydrophobic non-polar surfaces rather than hydrophilic ones; higher-energy surfaces have a correlation with higher microbial attachment. For example, *C. albicans* will more readily colonise a titanium surface over a silicone surface due to the slight increase of surface roughness of titanium compared to silicone. One suggestion for surface roughness causing more of an effect of C. albicans attachment is that increased roughness, increases the surface area available for cell attachment as well as has lower shear forces. Material porosity can also play a role in *C. albicans*

attachment by increasing the surface area as well. Roughness, pores or cracks have been shown to house the biofilms during formation when visualised three-dimensionally. [78]

When it comes to the environment surrounding medical devices known to promote *C. albicans* biofilm formation then factors such as high-glucose, cell surface hydrophobicity and even gentle shaking are culprits. Most of these are the initial interactions that can help modulate biofilm formation.

2.2.1.2 *Surface Conditioning Film:*

Many of these initial interactions are due to nonspecific factors such as yeast cell adhesins recognising ligands on device surface (serum proteins, salivary factors, and other natural coatings) or cell surface hydrophobicity and electrostatic forces. [77, 78] Many non-specific factors that enhance *Candida* species biofilm formation are part of the conditioning film of medical devices. This film occurs as body fluids interact with the device surface allowing for host protein and cell deposition. Conditioning films can provide binding receptor sites for planktonic *C. albicans* acting as part of the early adhesion step of biofilm formation on both biological and inanimate surfaces. This can lead to a 2-fold increase in biofilm formation when a conditioning film is present, particularly in the early adherence stage. [81] This can modulate biofilm morphology.

Exposing a biomaterial surface to any medium rich in proteins, carbohydrates, cells, and other natural coatings have been shown to increase *Candida species* attachment by changing the conformation of the material surface. [78, 81] This usually leads to a dynamic modification or conditioning of the material surface which tends to be a coating process with a chemical composition change. This dynamic process can cause change within the material surface as well as within the surrounding tissue closest to the material surface in a surface-medium interaction. For example, serum and saliva have been reported to enhance attachment on pre-conditioned materials. It should be noted that the surface conditioning will vary based on the

location of the implant and can affect *C. albicans* attachment. Also, residual mono/disaccharides or ion concentrations can affect adhesion to material surface. Metal ions have been shown to enhance adhesion of *Candida* to polymeric surfaces as ion concentration helps determine biofilm structure. Divalent ions (Ca2+ and Mg2+) promote adhesion to material surface. Other ion concentrations (Co2+, Ag+, Zn2+ and other similar ions) can inhibit *C. albicans* pathogenicity by blocking yeast to hyphae transition. [78] There has been much study of the role of saliva for *C. albicans* attachment to medical devices.

2.2.1.2.1 Role of Saliva:

The oral cavity is coated by salivary components which can play a role in colonisation and adherence of microorganisms. [82] Food digestion and wetting (mucins and amylases), tooth surface remineralisation and protection (mucins and proline proteins) or oral cavity host defences (lysozymes and defensins) are all key functions of salivary proteins. [82, 83] For *Candida albicans*, basic proline-rich (bPRP) proteins, mucin and statherin are salivary receptors. [82] *C. albicans* adherence to epithelial cells [84], voice prostheses silicone rubber [85], oral bacteria [86] and hydroxyapatite beads (tooth enamel model) [87] is increased in the presence of saliva [82]. Salivary proteins allow for the increased adherence of *C. albicans* yeast cells to silicone rubber of voice prostheses. [85] Homes *et al.* stated that the increased *in vivo* adherence occurs due to released salivary proteins from the silicone rubber which was incubated with whole saliva at a concertation dependent manner. [82, 85]

Also, if the concentration of whole saliva is increased for silicone pre-treatment before the addition of microorganisms then *C. albicans* adherence also increases; increase of 50% of saliva in the assay led to an almost double increase of *C. albicans* binding to the silicone (from around 7% with 30% saliva in assay to around 13% when increased to 50% saliva in assay). [85] A previous *in vitro* study, which utilised lateral flow, did not document any increased *C. albicans* adherence to silicone rubber or PVC because of saliva biomaterial pre-treatment as

seen in the Holmes *et al.* studies. [85, 88] However, Jones *et al* did note that when the microorganisms were treated with whole saliva (not the biomaterials) then there was an increase in adherence. They suspect that saliva altered surface properties of the biomaterials (silicone and PVC) by reducing the advancing and receding contact angles and the micro-rugosity. It is likely that salivary proteins must bind *Candida spp.* yeast cells prior to the yeast cell binding of silicone for adherence to be affected. Jones *et al.* also noted that *C. tropicalis* and *C. albicans* adherence was decreased by incubation in 5% v/v carbon dioxide to PVC and silicone while *C. krusei* adherence was increased. They suspect this phenomenon to be due to carbon dioxide increasing the cell surface hydrophobicity and zeta potential. [88] Both these experiments utilised yeast cells rather than hyphal cells because hyphal cells have a tendency to clump extensively causing adherence quantification difficult. [89]

Holmes *et al.* showed that only certain saliva proteins bind to silicone and after using a probe with antibodies to SPLUNC2 (short palate, lung, and nasal epithelium clone 2), SPLUNC2 was one such protein. [82, 85] SPLUNC2 is depleted from a saliva sample on binding with silicone and can be recovered when eluted from the silicone. Therefore, Holmes *et al.* utilised SPLUNC2, a ~36-kDa hydrophobic protein, as the possible saliva protein which altered *C. albicans* adherence. [82, 85] SPLUNC2 is a member of the PLUNC (palate, lung and nasal epithelium clone) gene family currently known as the BPIF (bactericidal permeability increasing fold- containing) family. [90, 91] It is secreted by salivary glands and gingival epithelial cells. [83, 85]

BPIF family is structurally similar to lipopolysaccharide binding proteins (LPS), however, SPLUNC2 is only present in the oral cavity secreted by salivary gland serous cells. [82] Khovidhunkit *et al*. also reported that a hamster orthologue of SPLUNC2 has *C. albicans* activity, colony forming units (CFU) were decreased in liquid culture. [92] Holmes *et al*. suggested that the reduction of CFUs, seen by Khovidhunkit *et al.,* does not reflect yeast cell

death but rather yeast agglutination. [82] Holmes *et al.* exhibited that radiolabelled *C. albicans* binds whole saliva at a ~36-kDa band size protein as well as to a 28-kDa polypeptide and ~60-kDa dimer of SPLUNC2 preparation while the control protein PavAr had no binding. SPLUNC2 can be glycosylated with several isoforms which can explain the smaller 28-kDA polypeptide present on which *C. albicans* can bind to. Holmes *et al.* showed that *C. albicans* binding to silicone follows a dose-dependent manner with the amount of SPLUNC2 solution used as pre-treatment. Higher percentage of SPLUNC2 induced increased *C. albicans* binding ($P \leq 0.05$; Student's t-test). [82]

Binding was due to SPLUNC2 activity rather than as a result of buffers or assay procedures because PAVAr recombinant protein control did not show binding with *C. albicans* as seen with the SPLUNC2 samples. [82] SPLUNC2 contains 249 amino acids and is commonly seen in two bands (N-glycosylated (Asn (124) and Asn (132)) and non-glycosylated). [83] This SPLUNC2 sample used in the experiment was not glycosylated exhibiting that glycosylation is not required for *C. albicans* binding but rather SPLUNC2 binding to voice prostheses occurs selectively along with other known salivary proteins such as bPRPs, mucin and statherin. [82] When looking at mixed microorganism biofilms, *C. albicans* adherence was much higher when the silicone rubber contained bound *S. aureus* and *R. dentocariosa* than just buffer. In buffer, adhering bacteria could inhibit *C. albicans* binding to silicone more readily than when the same bacteria were present in saliva. However, *C. albicans* had higher initial adherence to silicone with no bacterial presence in buffer rather than saliva but much higher adherence in the presence of other adhering bacteria after the initial 2-hour incubation period ($p<0.05$, Student *t*-test). Only a few specific bacteria enhanced *C. albicans* adherence significantly (*R. dentocariosa* and *S. aureus*). [93] A similar result was seen by Mei *et al*., when *C. albicans* biofilm formation was observed; *C. albicans* more readily adhered to silicone without the

presence of other adhering bacteria but formed more hyphae when other bacteria were present. [94]

When comparing saliva samples from patients and healthy volunteers, the patient samples were more likely to induce *C. albicans* adherence. [85] However, the groups were not fully matched as the patient group had undergone radiotherapy and were older which are known factors to affect saliva composition. [85, 95, 96] It was determined that selective protein adsorption to the silicone surface had concentrated specific salivary peptides on the silicone. These polypeptides detected were at ~40 and 52 kDa and the 40 kDa polypeptide was not present in saliva samples collected after incubation with silicone suggesting silicone adsorbed it. [85]

2.2.2 Growth on Medical Devices:

Candida species biofilm growth has been reported on many medical devices including implantable ports and shunts, catheters, intrauterine devices, endotracheal tubes, prosthetic devices, and dentures. Indwelling devices have been linked with increased nosocomial infections. [97] Table 2.2 exhibits the current scale of biofilm growth on the most widely used medical devices; *C. albicans* is the most common fungal coloniser of these devices. [97, 98] It is important to understand that unless the medical device is removed once a biofilm forms, the device will act as a reservoir for the infection that ultimately is protected from both host defence and antifungal therapy. [98] However, removal is not always feasible or can even lead to secondary complications such as bleeding and inflammation. [97] This suggests that unless symptoms occur or the device fails, it is unlikely that microbial colonisation will be detected. Long term studies of microbial growth (140 days) on medical materials found that biofilm formation initially showed 80% coverage of the medical material until near day 42 when there was a large biofilm detachment; however, this also occurred to a smaller extent at days 7, 21, 63, 91, 105 and 133 suggesting a near bi-weekly biofilm detachment with proliferation settling

between 60% to 10% coverage of the material. [99] This often occurs because *C. albicans* can evade the host's immune system to continue colonising most medical devices without interruption. Therefore, it is important to understand both the colonisation and immune evasion of *C. albicans* to minimize the effect of the biofilm growth on the devices' function.

Table 2.2: *Candida* species and infection rates of the most common devices in use yearly

Devices		**Yearly Utilisation**	**Risk of Infection (%)**	**Main *Candida* species involved**
Catheters	Central and Peripheral	~5 million	3 to 8	*albicans, glabrata* and *parapsilosis*
	Haemodialysis and peritoneal	~240k	1 to 20	*albicans* and *parapsilosis*
	Urinary	>10 million	10 to 30	*albicans*
Tubes and	Endotracheal	>1 million	10 to 25	*albicans* and *glabrata*
	neurosurgical	~40k	6 to 15	*albicans*
Prosthesis	Intracardiac	~400k	1 to 3	*albicans, glabrata, parapsilosis* and *tropicalis*
	Joints	~600k	1 to 3	*albicans, glabrata* and *parapsilosis*
Oral devices	Voice prosthesis	>1k	50 to 100	*albicans* and *tropicalis*
	Dentures	>1 million	5 to 10	*albicans* and *glabrata*

Table remade from [98].

2.2.2.1 *Host-Pathogen Interaction on Medical devices:*

C. albicans biofilms can easily evade the host immune system particularly when medical devices are involved. For example, when *C. albicans* is cocultured with peripheral mononuclear cells (such as monocytes or macrophages), it can more readily colonise silicone. This is accomplished by localising the monocytes within the basal layer of the biofilm allowing

C. albicans to continue normal extracellular matrix thickening without phagocytosis; It even showed a two-fold increase in the biofilm thickness. [100] In general, monocyte activity for biofilms was half of what was seen with *C. albicans* planktonic cells. [101, 102] However, the cocultured samples did have increased proinflammatory cytokine levels of IL-1b but down-regulated other proinflammatory cytokines (TNF-a) and anti-inflammatory cytokines (IL-10 and 6, MIP1β) suggesting a complicated interaction between the host and the biofilm. [100] The physical structure of the *C. albicans* biofilm matrix is the key component in resistance to phagocytosis as even glycosylated *C. albicans* mutants (which were more readily phagocytosed than the wildtype strain as planktonic cells) had the same inhibition to phagocyte migration similar to the wildtype when in biofilm. [102] *C. albicans* can evade antimicrobial peptides present in body fluids (such as saliva) by secreting aspartyl proteases which inhibit the peptides killing activity by cleaving histatin 5. Secretion of Msb2 glycodomin also inactivated (with binding) antimicrobial peptides such as LL-37. These has been linked to the *C. albicans* high-osmolarity glycerol (HOG) pathway. [103] Also, for infections stages in murine host models, there was an overexpression of 14 host proteins related to leukocyte and erythrocyte associate inflammation (C-reactive protein, alarmin S100-A9 and myeloperoxidase) and a predominant presence of polymorphonuclear (PMN) cells during biofilm formation. [104] PMN cells had a similar response to *C. albicans* biofilms in comparison to planktonic cells. [101]

Mature biofilms do not trigger the production of reactive oxygen species by neutrophils; disruption of the biofilm matrix increased neutrophil activity against *C. albicans*. However, when comparing neutrophil activity with a mucosal surface or a device surface, neutrophil activity was low and there was no migration throughout the biofilm. Also, the extracellular matrix formed by *C. albicans* on had a much thicker layer which contained 98% of host proteins such as haemoglobin, alpha globulins and albumin. [101] It should be remembered that mature biofilms contain an extracellular matrix consisting of protein, carbohydrates, lipids and DNA

which are ultimately different than *C. albicans* cell wall components such as a linear α-1,2-branched α-1,6 mannan (5 to 10-fold larger than the cell wall branched mannans). Also, many of the cell wall proteins are absent from the extracellular matrix instead it is mainly composed of host origin matrix-associated proteins. [105] In theory this could be the reason of the host immune systems inability to recognise biofilm infections in comparison to planktonic cell colonisation as biofilms are able to utilise host proteins to circumvent host immune responses. Similar to what is seen in 'asteroid bodies' produced by fungal cells, calcium salt mediated crystallisation and precipitation around a yeast cell in a crown-like structure. These structures contain imbedded host components, mostly antibody and antigen complexes, which protect the internal yeast from the host environment as the internal yeast cell continues to remain viable and capable of division. [103] These main evasion properties (summarised in Table 2.3) rely on some type of shielding of the fungal cells with the biofilm from the host immune response. This ability to evade the host allows for *C. albicans* colonisation of the medical devices, which tends to be preluded by adherence to the medial device surface.

Table 2.3: *Candida* albicans main components in the host immune evasion summary

Component	**Function**	**Host Response Effect**
Mannan molecule	Cell wall component; polysaccharide	Dectin-1 receptor unable to recognize β-1,3-glucans
Transferrin Receptors	Utilizing host transferring proteins; binding iron	Balancing iron needs within host
Asteroid Bodies	"Crown-like" structure used to protect yeast from hostile environment	Immobilizes immune components (IgGs and IgMs); interrupts humoral immune response
Biofilm Formation	Adherence to surfaces; protect yeast from hostile environment	Avoid neutrophil phagocytosis; No ROS activation; innate immune evasion; Reduced susceptibility to antimicrobials

Table remade from [103]

Adhesion to biomaterials depends on material-intrinsic properties such as surface area and topography but, *in vivo*, peptide adsorption to the biomaterial from the adjoining body fluids is important for adherence and quantification. Adsorbed proteins attach to the surface without masking the inherent biomaterial properties allowing for the original physicochemical properties of the biomaterial to dictate the composition, conformation and amount of these adsorbed proteins. [106] Attachment is known to be related to the biomaterial surface wettability, roughness, prior protein adsorption and even microbial species or strain. [106, 107] Hydrophilic material tends to be more resistant to both fungal and bacterial growth adhesion while hydrophobic material increase adherence. [108, 109] Cell division, coadhesion, coaggregation and extracellular matrix production help biofilm formation after microorganism colonisation of (and adherence to) a surface. [107] Once adherence occurs, the cells multiply in the z-axis to form a basal polylayer of tightly packed cells to help anchor the biofilm to the attachment surface. Biofilm formation has also been shown to depend on the density of the inoculum: low-density inoculum leads to sparse and patchy cell mounds but high-density inoculum leads to uniform films across the attachment surface. [110] However, it should be noted that different types of medical devices within different host body locations can have varying *C. albicans* colonisation. For example, variability in colonisation can be seen for medical device categories such as catheters, implantable devices and oral cavity devices just based on surrounding environment.

2.2.2.2 *Catheters:*

Catheters cover a large group of medical devices in use, the majority of which fall into three main categories: intravenous, dialysis and urinary. Intravenous catheters have an increased role in nosocomial bloodstream infections which have led to increased cost and patient morbidity. [79, 97] It has been shown (same as previously described), early phase

biofilm formation to a catheter surface mostly consists of yeast cell attachment without the formation of an extracellular matrix while mature biofilm contained yeast cells and hyphae within a thick extracellular matrix. [97] Also, due to surface hydrophobicity, roughness and surface conditioning, different catheter materials can induce *Candida* biofilm formation to varying capacities. For example, one of the first publicans on the effect of catheter material *C. albicans* biofilm formation showed that *C. albicans* can readily colonise (foremost) latex catheters followed by SE, polyvinyl chloride, polyurethane and colonise silicone the least readily. [45] It was also shown that modifying the catheter surface with the addition of 6% polyethylene oxide can alter biofilm formation. The polyethylene oxide modification reduced *C. albicans* biofilm formation by 78%. This study also presented that increased contact angles for polyether urethane catheters had an inverse relationship to biofilm formation. [111] The majority of central venous catheters are all colonised by microbial biofilms, however only a third of these infections are due to *Candida* but with an overall highest crude mortality. [79] Even though colonisation can occur at any point during the hospitalisation, it most frequently occurs due to skin induced extraluminal catheter colonisation and within the first week for central venous catheter and within the first 30 days for vascular catheters. For urinary catheters, the risk increases approximately 10% per day the catheter is not removed. [112]

Infection can also occur due to hematogenous seeding (infection moving from one location to another) or intraluminal colonisation of the device itself. More rarely it is possible due to an infected infusate that flows within the catheter. [79] Also, anywhere from 20 to 70 percent of reported candidemia is due to the presence of a catheter. [113] The best treatment for most catheter related *Candida* infections require catheter removal and antifungal treatment till two weeks of negative blood and no symptoms are seen; without removal of the catheter, the patient prognosis is poor with higher rates of mortality and duration of infection. [79] However, it should be noted that catheter associated *C. albicans* biofilms had more than 128-fold increase

resistance to fluconazole (a common *C. albicans* antifungal medication) compared the same strain with planktonic grown cells only. Therefore, antifungal resistance might need to be determined.

Dialysis (haemodialysis and peritoneal) catheter biofilm contamination is a known complication for patients undergoing dialysis treatment. This can be seen with the high mortality and morbidity rates for *Candida* peritonitis in patients with end-stage renal disease. *C. albicans* is one of the main species isolated in both haemodialysis and peritoneal dialysis catheters. Diagnosis can be easily missed as symptoms are non-specific, but *Candida* contamination and positive culture of the dialysis effluent will confirm an infection had occurred. The main treatment for these infections is also the removal of the catheter with antifungal therapy, but what makes these infections especially harmful is the need to discontinue dialysis treatment and loss of ultrafiltration till infection clearance. [79]

In indwelling urinary catheters, *C. albicans* is one of the main causes of urinary tract infections. Infection occurs most commonly during the actual catheterisation process by either having the catheter surface already colonised or by allowing infection to occur when microorganism move from the external periurethral catheter surface towards the bladder. However, there is a difference between urinary tract colonisation and infection as *C. albicans* can be found as a non-commensal on skin. Asymptomatic candiduria is also a common occurrence for a large portion of ICU patients, the treatment would require the removal of the catheter but rarely antifungal treatment as morbidity and candidemia chances are low. However, injury to the area can cause an infection due to a colonised IUT device. It is also known that a rare foetal *Candida* infection is always linked with a retained IUT device. IUT device removal is recommended to limit this rare occurrence or a continuous check for infection at a minimum followed by antifungal therapy if an infection is found. [79]

2.2.2.3 *Implantable Devices:*

Implantable access ports and shunts are usually used for long term therapy. Venous ports, most often seen in long-term anti-cancer therapy and drug administration, have *Candida* species infection as the most common complication associated with these devices with a difficult differential diagnosis. For any suspicion of infection, the device will be removed automatically. Neurosurgical shunts also suffer from infection as a common complication; however, bacterial infection is more prevalent than fungal infections. Over the last few decades, infections due to *Candida* have steadily been increasing. In these shunts, biofilms tend to colonise the silicone elastomer tubing and infection occurrence is thought to occur at point of placement but transient candidemia may also be a cause. These cases tend to have non-specific symptoms such as nausea and vomiting, lethargy, and mental fogginess with fever as well as negative blood cultures. A positive *Candida* result of the shunt liquid tends to be indicative of an infection. For both ports and shunts, removal of the device is inevitably followed by antifungal therapy. [79]

Biofilm formation on prosthetic devices usually occurs because of some type of *Candida* species, particularly *C. albicans*. Valve endocarditis is known to occur after *C. albicans* colonisation of intracardiac prosthetic devices often at the time or before (present on device itself) surgery. Echocardiography with positive blood cultures are usually diagnostic for this type of infection which will require device removal and debridement surgery followed by antifungal therapy. Even if this infection is caught early, mortality remains high as these patients tend to be especially immunocompromised. Other cardiac devices (such as defibrillators and pacemakers) are, also, susceptible to this type of infection. Looking at prosthetic joints, *C. albicans* infections are rare but contamination is thought to occur during implantation by exposure to skin commensals or by transient candidemia. This type of infection

would also often require device removal, debridement of adjacent tissue and systemic antifungal therapy. [79]

2.2.2.4 *Oral Cavity Devices:*

When it comes to medical devices placed within or near the oral cavity (such as endotracheal tubes, voice prosthesis and dentures), there is a rich reservoir for infection available just due to normal flora (20–75 % of the general population) as these sites are not sterile. *Candida albicans* can be a risk factor infection within the respiratory tract especially for ventilator-associated pneumonia and infection is prevalent as early as 48 to 72 hours after intubation. [79, 112] It is believed that gastropulmonary reflux or oropharynx contamination can cause the initial organism adherence on endotracheal tubes. When this occurs, the mature biofilms can disseminate aggregates from the main biofilm body towards the lower respiratory tract. [79] Voice prostheses can also be readily colonised by *C. albicans* (75% of the reported infections) and form a biofilm upon the material surface. This often leads to device failure and subsequent removal as build-up of the biofilm upon the valve of the prosthesis causes air leakage and increased air flow resistance making the device non-functional. Failure can even lead to aspiration pneumonia as the voice prosthesis design shelters any biofilm growth on the material surface from antimicrobial activity. This often occurs because the voice prosthesis (due to oesophageal presence) experiences continuous chemical, mechanical and even microbial stimuli. It has been reviewed that changing dietary components can lower biofilm formation particularly with use of probiotics and dairy products as well as use of prophylactic antifungals and synthetic saliva. Surface coating techniques have a tendency to function *in vitro* but not always *in vivo* as seen with serum coating of voice prosthesis. [114] Surface coating of dentures behave similarly to voice prosthesis coatings.

Biofilm accumulation on denture material is one of the main causes of stomatitis with *Candida*-associated version accounting for anywhere between 11% to 67% of all infections. [79, 97]

This results in mucosal tissue inflammation underneath the denture particularly for maxillary rather than mandibular dentures. [115] Surface roughness within the acrylic material of most dentures promotes *C. albicans* biofilm growth by increasing the surface area available for attachment. [79] *C. albicans* biofilm formation in denture-associated infection produce a thin and heterogeneous biofilm formation (unlike catheter growth) with no biphasic appearance and thick hyphae formation within the extracellular matrix. [97, 116] Injury to denture adjacent mucosa after biofilm formation is thought to be the first step towards stomatitis showing an intricate extracellular network of both dimorphic forms. [79] There have been recent studies which found nineteen salivary proteins (majority of which were immunoglobulin associated) associated with denture stomatitis based on proteomic analysis. Four of the secreted proteins (STAT, CYTN, CAH6 and PPIA) showed much higher levels in stomatitis patients. Particularly, STAT and CYTN had increased expression with *Candida* biofilm formation rather than with planktonic cells. [115]

2.3 Current Methods for Detection of *Candida:*

Standard *Candida* species detection methods are laborious (often exceeding 2 to 4 days for identification), which can lead to delayed treatment as species identification can determine medical treatment due to variable antifungal resistance. [117] Also, it can lead to prolonged hospitalisation (compared to non-*Candida* bloodstream infections [118]) and increased cost [119] compared to other types of microbial infections. The need for rapid diagnosis allowed for new detection methods to be developed able to perform identification and/ or antimicrobial susceptibility testing. [117] Also, many of these methods are challenged when needing to quantify many small analogous samples. Most techniques for *Candida* detection are separated into three broad groups: microscopy, traditional and novel. [118]

2.3.1 Microscopy:

Microscopic examination utilises either non-specific or specific staining techniques for organism identification. Calcofluor white is the main non-specific stain able to react with a fungal cell wall containing β 1–3 and β 1–4 glucan, which can be visualised with fluorescent microscopy at 347 nm (range 300 to 412 nm). [117, 120] If bound, it shines with a bright green-blue colour and can be enhanced with the addition of potassium hydroxide (KOH). [117] Oligonucleotide probes are utilised in FISH (fluorescence in situ hybridization) staining techniques which bind to specific *Candida* genes, commonly on the 18S region of rRNA while enhanced FISH staining with peptide nucleic acid (PNA) targets the 26S region. [117] The main draw of this type of specific staining is that it reduces the chances for false positives as often seen with calcofluor white staining, however is not recommended for use directly on liquid samples but requires growth in culture. [117]

2.3.2 Traditional Methods:

Traditional methods utilise different types of carbohydrate media for *Candida* species detection with growth. Some of the most common growth-based detection utilises carbohydrate assimilation and fermentation reactions as species identification tools. [117] Within this section both biochemical and media characterisation of *Candida species* will be discussed.

2.3.2.1 *Biochemical Characterisation:*

Biochemical characterisation can be automated with use of the API 20C AUX kits (bioMerieux-Vitek) [121], the Auxacolor system (Sanofic Diagnostics Pasteur) [122], RapID™ YEAST PLUS System (Thermo Scientific) [123] and a few others. [117] Once a yeast culture is available (7 to 14 days), the diagnostic systems described can take anywhere from 4 to 72 hours to deliver an identification. A positive result depends on either the change in colour (Auxacolor and RapID™) or turbidity (API 20C AUX) where a majority of clinically relevant *Candida* species can produce a distinct biochemical profile. [117, 122, 123] However, most of

these systems have misidentification possibilities (anywhere from around 7% to 15%) and can require further testing for validation. Therefore, the recommendation remains that any carbohydrate identification method must be accompanied with morphological identification to determine a *Candida* species accurately. [117] Morphological identification can be accomplished with microscopy and/ or based on media growth of the organism.

2.3.2.2 *Media Growth:*

Sabouraud glucose agar (SGA) is the traditional media for fungal growth which can be further cultured onto media such as Corn Meal-Tween 80 agar for morphological differentiation. Chromogenic media can improve *Candida* species identification by causing a change in colour or texture of fungal colonies during growth. These media types contain enzyme reactive chromogenic substrates which correspond to different *Candida* species with an accuracy above 94% for *C. albicans*, *C. glabrata*, *C. Tropicalis* and *C. krusei*. This is particularly useful in mixed cultures where SGA is unable to differentiate between morphology of yeast colonies for 47% of mixed isolates. However, just as with carbohydrate identification methods, there are chances for misidentification when using chromogenic media (varied based on manufacturer). To overcome these issues, both morphology and colour of the colonies and yeast cells should be considered when identifying the species. [117]

Blood culture identification is a simple automated process only requiring 10 ml of patient blood injected within a minimum of two blood bottles containing specific broth media for organism growth and identification. Any positive samples will have microscopy performed and subcultured onto appropriate growth media. Morphology and characteristics of *Candida* species taken directly from blood culture do not vary from specimens when grown with other common media such as SAB; however, direct isolation from positive blood bottles allowed for more rapid identification when using chromogenic media as there was no need for any additional isolation steps. [117] BD Bactec™ and VersaTREK™ systems are some of the most

common blood culture systems in use today, which respond to CO_2 and pH changes within the blood as detection for microbial growth. [124] However, even with these automated systems, *Candida* identification is still a laborious process and not able to do rapid identification nor available for point of care use. Even with automation blood culture bottles, a minimum need of at least 14 hours before a blood culture bottles are recognised as infected by the automated system is necessary. [124]

2.3.2.3 *Molecular Methods:*

Non-molecular diagnostics (such as microscopy and culture) with their low-sensitivity (and the dependence on proper personnel training for identification) are still the primary method used for invasive fungal infection diagnosis with the addition of molecular based methods for detection of rare species. [124] *Candida* species identification requires patient serum samples as the human humoral response to any yeast infection produces antibodies to a multitude of *Candida* epitopes with high sensitivity and specificity allowing for rapid identification.

2.3.2.3.1 Antibody Identification:

Serological diagnosis most commonly includes agglutination, immunoprecipitation, immunoblotting and enzyme-linked immunosorbent assays (ELISA). As *Candida* is a common skin commensal, it is suggested that antigenic rather than antibody diagnosis is preferable as regardless of infection, *Candida* antibodies will be present. A common method for this type of serology is latex-agglutination tests, with a preference for monoclonal antibodies to *Candida* antigens as these are less likely to detect commensal *Candida* colonisation compared to polyclonal antibodies. Beta-glucan assays are able to detect the presence of fungal species within a sample and can be useful for the detection of candidemia, particularly catheter-associated candidemia as beta-glucan abundance in biofilms can be more than 4 times in comparison to planktonic cell colonisation. [113] However, beta-glucan cannot distinguish

normal flora colonisation (as it is a major component of most fungal cell walls), but using specific cut-off values can increase the positive predictive value (PPV) to above 80% for concentrations 60 pg/ml. [125] It should be noted that a higher rate of false-positive is likely in patients with hematologic malignancies but it is possible to improve this with a minimum of 2 consecutive tests rather than a single beta-glucan assay as this increases the specificity to almost 99% but still a low sensitivity near 50%. [126] Beta-glucan assays should be treated as an adjunct test rather than a primary test.

2.3.2.3.2 Nucleic Acid Identification:

Molecular diagnostics ultimately rely on sample preparation as DNA extraction and purification will determine if an accurate *Candida* identification occurs and have been extensively reviewed in [117]. This can be enhanced by concentrating target DNA, removing any contamination or debris present in sample and removal of any hybridization inhibitors. DNA microarrays utilise solid substrate attached DNA probes (target sequence complement) which is labelled for easy detection with hybridization. [127] However, microarray sensitivity is lower than PCR techniques due to DNA amplification capabilities. Amplification techniques can be either isothermal or nonisothermal, but both are able to greatly increase nucleic acid quantities. Overall, nucleic acid identification techniques have high sensitivity and specificity for *Candida* screening; However, these hinge on the time-consuming sample purification and nucleic acid extraction steps before identification can occur. [117]

A novel approach to utilising nucleic acids can be seen in the development of specific aptamers to yeast as a cost-effective alternative to traditional molecular identification. For example, [128, 129] developed an aptamer able to bind curdlan (linear unbranched (1→3)-β-D-glucan) with high sensitivity and specificity. Also, an approach to aptamer development that targets environmental changes rather than specific species could also allow for broad infection detection; A streptavidin- binding aptamer was developed in [130] which has a 100-fold

decrease in affinity when the pH drops from 7.4 to 5.2. The advantage of this type of non-specific target aptamer is that it does not require a specific target structure to function rather a change in the environment. [130] As it is known that *C. albicans* biofilm growth produces a pH change, this could be applied to direct blood detection of *Candida* growth in future applications.

2.3.3 Novel technology:

The advantages and disadvantages of all the main standard methods of microbial detection are summarized in Table 2.4. However, it should be noted that traditional methods have more difficulty identifying rare species of *Candida* unlike the presented novel technology. [131] This will ultimately produce a higher reliance on novel technology as new species emerge.

2.3.3.1 *Microfluidics:*

The next step in nucleic acid identification of fungi includes microfluidic systems (such as made for the SlipChip® [132]) including many microarrays, which can be used to detect multiple *Candida* species using blood samples. [117] This specific device is able to identify the most common species of *Candida* with a total identification capability of 20 pathogens by using dielectrophoresis and multiplex PCR amplification. [117, 132] Digital microfluidic systems (such as droplet-based) allow for a quicker turnaround time of less than an hour after DNA extraction with a smaller sample requirement. These utilise electrowetting control to move the droplet sample to various chip regions (commonly 'thermal zones' with varying temperatures) as necessary allowing for easier on-chip PCR processing. [117] Comparing conventional PCR to these on-chip microfluidic PCR process produce similar sensitivities for fungal species identification (69% to 56%, respectively). [117] Within these chips, it is also possible to reduce the identification step to less than 20 minutes by utilising optical sensing to

detect internal reflectance fluorescence. [133] Pathogen identification within these microfluidic chips is, however, unable to determine the viability of the pathogen within the sample as it only detects based on nucleic acid identification. [117] However, the capability to detect multiple pathogens provide an advantage to microfluidics.

2.3.3.2 *Spectroscopy and Resonance:*

Comparably to microfluidic chips, spectroscopy cannot determine viability of detected pathogen as identification results from distinct molecular structure of the sample (such as fungal cell and DNA) as seen within the spectrum scattering. A novel spectroscopy (surface-enhanced Raman spectroscopy) can identify *Candida* species (similarly to an immunoassay) by utilising nanoparticles to attach to or near the fungal pathogen within a sample of interest aiding the visualisation of the Raman scattering. [117] Magnetic field-based techniques such as nucleic magnetic resonance (NMR) could also be used for *Candida* species identification; NMR identifies organisms based on nuclei absorbance and electromagnetic radiation remittance when a magnetic field is applied. It has one key advantage over other techniques due to the ability to identify organisms without the need for purification for highly turbid samples (blood, urine, serum etc.). [117] In miniaturized-on NMR approach, magnetic nanoparticles bind targets to form magnetic clusters which affect the spin-spin relaxation time of the sample leading to a decrease reading. For example, T2 Biosystem Inc. system utilises a PCR tube to detect *Candida* (using a magnetic-nanoparticles attached to a PCR amplicon) with a sensitivity of 10 CFU/ml.[133] Recently, the T2Candida® Panel for the T2DX system was released able to detect clinically relevant *Candida* species within 3-5 hours directly from collected patient whole blood samples. [134]

2.3.3.3 *Proteomic Based Detection:*

Mass spectrometry (MS) measures the ratio of mass to charge (m/z) of ionized compounds. [135] A common proteomic approach for pathogen detection within the last few

years utilise the matrix assisted laser desorption ionization (MALDI) MS (reviewed in [135]) analysis where samples are coated with a matrix (energy-absorbent) solution and allowed to crystallize with drying process. The sample can then be laser beam ionized to form protonated ions and separated based on the formed ions' m/z ratio. This can all be analysed for sample identification with different MALDI MS approaches such as time of flight (TOF); TOF determines the required time for an ion to travel a known length of tubing within the MS system. [135] From previous publications, the MALDI-TOF was able to identify 100% of clinical *Candida* isolates. [136, 137] In vulvovaginitis patients, MALDI-TOF was able to recognise 94% of isolates with the remaining 6% unidentified due to lack in the database rather than an incorrect identification; with an improvement to the database, it is likely that this would increase the identification percent to 100% as seen within the other publications. [138] However, it should be noted that correct identification with commercial MALDI-TOF systems heavily rely on a substantial and thorough organism database as it is only possible to determine an unknown organism if the database already contains the peptide mass fingerprint (PMF) of the collected sample. This requires a standardisation for PMF analysis and database entry as parameters such as growth media and temperature can affect the organism and cause identification problems.

Table 2.4: Summary of Available Methods for Fungal Identification and Detection

Method		**Advantage**	**Disadvantage**
Traditional	Culture and biochemical	Sensitive and Inexpensive	Time consuming

	Serology	Faster than Traditional methods; Can Identify organism and any produced toxins	More time consuming and less sensitive/ specific than nucleic-acid detection; Currently only available for a small number of organisms; Requires large quantities of antigen
	Molecular (Real-time and Multiplex PCR)	Sample culture not required; Rapid with high sensitivity and specificity; Reduced contamination due to closed tube system; Simultaneous detection of multiple pathogens using multiplex-PCR	Thermal cycler precision dependant; Requires trained laboratory personnel
Microscopy and Staining	Calcofluor white and FISH	Rapid identification directly from smears; FISH staining has specificity of molecular methods	FISH limited by antigen availability; Requires trained laboratory personnel
Novel	DNA sequencing	Gold standard using 16S rDNA and 18S rDNA; Identification of both fastidious and uncultivable species	Expensive; Requires trained laboratory personnel and identification software; Currently not for routine use
	Microfluidics and Microarray	Large scale screening and detection of clinical isolated	Expensive; Requires trained laboratory personnel
	Spectroscopy	High specificity and sensitivity	Cannot determine pathogen viability; Requires nanoparticles for identification
	NMR	Rapid; High sensitivity and specificity; Sample isolation and purification not needed for turbid samples such as whole blood	Requires PCR amplicon and magnetic nanoparticles

	MALDI-TOF MS	Rapid; High sensitivity and specificity; Routine use less expensive than both molecular and serology methods; Does not require trained laboratory personnel	High initial cost of system; reliant on database
Table remade from [117, 133, 135].			

2.4 Biosensors:

Current microbial growth detection relies on direct and indirect methods which have numerous utilisation issues, particularly the time requirements for growth or even the reliance on symptom identification by clinicians before identification request. Therefore, there is a need to develop more reliable techniques, particularly ones which can detect adhesion and biofilm formation in real-time. For that reason, many techniques have been developed looking at impedance and other electrochemical properties to identify microorganism growth in a real-time environment mostly using biosensors.

2.4.1 Common Biosensors for Microbial Detection:

Biosensor approaches for microbial growth detection rely on both direct and/or indirect methods. Common methods include electrochemical spectroscopy (EIS), constant phase elements, impedimetric measurements and fibre optic sensors. Other than the fibre optic approach, most of the common biosensors published rely on *in vitro* detection of microbial growth which can provide detection at a lower cost and with equivalent sensitivity and specificity to the current methods utilised within hospital and laboratory settings (such as microscopy or microfluidics). Fibre optic approaches have been published which are capable of real-time monitoring of microbial growth on medical devices yet lack true wireless capabilities.

2.4.1.1 *Electrochemical Impedance Spectroscopy (EIS):*

Most current impedance research in identifying microbial growth relies on using electrochemical impedance spectroscopy (EIS). In EIS a small sinusoidal voltage at a chosen frequency is applied to a surface to be read where a probe then reads the resulting current this can be repeated using many differing frequencies or with only a single frequency. This type of impedance is calculated by the current-voltage ratio. This does not require special reagents or labels to be utilised. A similar biosensor utilises field-effect modulation in a semiconductor by charged particles such as ion-sensitive field-effect transistors (ISFETs) and can be used in semi conducting nanowires, carbon nanotubes, potentiometric structures, and thin film transistors. These measure the interaction of semiconductor charge carrier and external charges with low ionic strength enhanced sensitivity. This electrolyte-insulator-semiconductor interface exhibits channel conductance or capacitance due to the response of the field-effect sensors. [139] Recently, EIS was able to detect *C. albicans* growth by utilising antibodies functionalised membrane on electrodes. [140] The authors were able to detect *C. albicans* within an hour of growth and as little as 10 CFU/mL were needed for detection. [140] However, as most published yeast detection methods, growth outside of the body is required. These devices are unable to detect growth on medical devices within the body in real-time.

2.4.1.2 *Constant Phase Element Sensor (CPE):*

Ionic changes in culture media can be affected by metabolic activity of microorganism such as altering low conductive nutrients or substrates (such as proteins and carbohydrates) into components of high conductance. For optimal yeast growth, monitoring pH levels of environmental/ media substrates is needed because when uncontrolled growth occurs, the media pH reduces due to carbon dioxide and H+ ion release leading to further yeast growth affect. Biswas *et al*. developed a sensor which can monitor H+ ion concentration in the medium while not affecting the microorganism due to a polymer film covering of the sensor probe. This

sensor detects changes in the phase angle inside the culture medium with microbial growth and pH drop. A phase angle difference between the two inputs of the probe give the ionic concentration measure within the polarising medium. A schematic view of this type of probe and activity over a range of different frequencies as well as a schematic of the detection circuit help exemplify that only a change in ion concentration and not frequency affects the phase angle. [141] Often CPE sensors are combined with EIS systems such [142, 143] to help overcome shortcomings of EIS systems alone when dealing with antibody or peptide detections (often dealt with yeast biofilms. [14] These are often used, as stated, to determine change in culture conductivity [142-144] during microbial growth; however as with EIS, EIS-CPE based sensors are non-invasive and require the microbial or peptide detection to occur outside of the body. Therefore, making the systems unusable for real-time monitoring of microbial growth within the human body.

2.4.1.3 *Indirect Impedance Microbial Growth Detection:*

Microbial growth can be effectively detected using indirect impedance techniques which have been implemented for food spoilage recognition. Johnson *et al* developed an indirect impedimetric sensor which would be able to detect complex microbial combinations and growth based on carbon dioxide production. In the fermentation process, CO_2 is a by-product and a respiration primary product determined by the energy generating pathway of each microorganism present. For the Johnson *et al* sensor, the CO_2 production was measured by its reaction to potassium hydroxide (KOH) causing a detectable conductance change in the media. This measured the impedance caused by CO_2 when run through a KOH agar solution. [145]

This study showed that as microbial accumulation and growth occurs, conductance decreases over time. Also, it was determined that the larger the starting bacteria concentration the lower the detection time necessary to identify bacterial presence. The same was seen in another study

which looked at the yeast *Saccharomyces cerevisiae*. It showed that as the concentration of the yeast increased, the conductance decreased along with the necessary time for detection. [146] This shows that conductance can be used to detect microbial growth over time even with an indirect method especially when working with difficult specimens and analytes such as KOH detection of CO_2.

2.4.1.4 *Optical Fibre Sensors:*

Zhong *et al*. were able to monitor biofilm growth of *Rhodopseudomonas palustris* on polydimethylsiloxane in a photobioreactor. [147] The biofilm cells were separated from the media and measured with two U-shaped gold coated fibre-optic probes. The reference probe analysed the liquid concentration in the separated culture media while the sensor was able to detect the exponential phase growth of the biofilm with 0–536 μm thickness. [147] A similar sensor also was able to detect biofilm growth and hydrogen production with a similar use of a reference probe and sensor. Authors suggested to improve sensitivity by increasing the surface roughness during measurement of the liquid-phase within the biofilm. This particular system obtained a linear relationship at a 0 to 120 μm biofilm thickness with the highest hydrogen production at 115 μm. [148] *C. albicans* growth could also be detected by utilising Concanavalin A protein hydrogels to bind the cell surface mannan proteins. [149] Once this cross-link occurs it causes a visually detectable diffraction shift. The presented sensor in [149] can detect around 32 CFU/mL and is also able to distinguish between mannan present and non-present microbial species (commonly seen within fungal versus bacterial pathogens).

Fibre sensors have been used for biofilm formation monitor of medical device surfaces in real-time. Kurmoo *et al.* used polyvinyl chloride (PVC) endotracheal tubing to demonstrate real time monitoring of *P. aeruginosa* as this species is often the cause of this device's failure. [150] The LPG sensors were placed within the endotracheal tube lumen and utilised as refractive index sensors. The lumen was chosen as it showed the highest microbial colonisation and was

determined the likely cause of microbial dispersion within the lungs. Bacterial attachment and biofilm formation were indicated by a sensor surface change in medium refractive index. This allowed for a link between the inverse of the biofilm growth and the optical attenuation wavelength shift with an empirical formula. Therefore, the system was able to quantify biofilm growth above 81 μg/ cm^2 in vitro but possibly adapted for in vivo use. [150] Another non-invasive optical detection of biofilm growth utilized low-coherence interferometry (LCI) and optical coherence tomography (OCT). [151] As it only had a penetration depth of up to 2 to 3 mm (based on tissue type), the optical fibre sample arm had to be directly inserted within the sample region (middle ear). As the beam is transversely scanned, the optical system provides cross-sectional images of the sample region which allows the computer software to determine the biofilm layer based on an algorithm leading to a sensitivity of 68% and specificity of 98%. [151] However, even with [150] being placed within the presumptive body, the systems were not wireless as a spectrometer or a sensor attached to a computer [151] were necessary for the detection to occur. Therefore, there is a need for a true wireless, low cost system to be developed for biofilm detection within the body in real-time.

2.4.2 RFID Microbial Detection:

Radio frequency identification (RFID) sensors have various applications in fields such as pharmaceutical, warehousing, agricultural, industrial, food safety, and security. They are easier to install than tethered sensors because they have small form factors and can be installed at high densities with lower costs because of the lack of excess wiring on components. Also, in comparison to optical sensors, RFID sensors can perform measurements without needing the packaging to be transparent. Thickness shear mode [152], magnetic acoustic resonance [153] and resonant inductor-capacitor-resistor (LCR) transducers (Fig. 2) represent the most common categories of battery free wireless RFID sensors. Magnetic acoustic resonance relies on mechanical wave propagation able to detect small cyclic displacements in a medium (same

theory as seen in magnetic resonance imaging (MRI)). [153] Thickness shear mode sensors usually utilise variable length delay lines rather than a lumped IC chip for RFID detection. [152] Most of these sensors are capable of passive sensing of physical, chemical and biological changes of their desired target. These approaches could offer a fully wireless microbial detection system at low cost.

2.4.2.1 *Basic Principle:*

The LCR circuit RFID tag is the approach with the most potential and cost effectiveness for medical use and microbial growth identification as it can be easily utilised in ultra-high frequency (UHF) applications for long distance detection (furthest compared to other common sensor methods) and easy manipulation of dielectric solutions to affect impedance. [154] In addition, based on previous publications for LCR based systems, a detectable change in impedance only occurs when 10^3 to $3x10^7$ cells/ml are present making this a viable and previously tested option for microbial detection. [155] LCR also has the advantage of utilising standard IC chips increasing robustness (and repeatability) of sensor function when developing more than a single copy of the device.

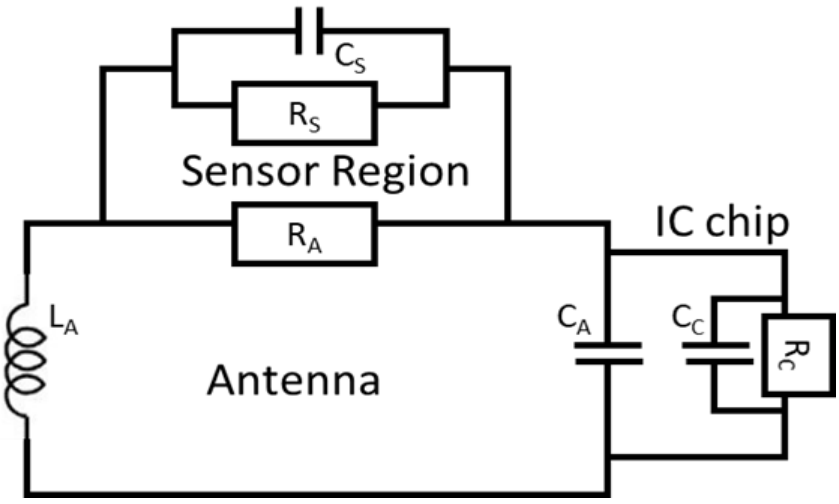

Figure 2 Basic RFID sensor design. Composed of an antenna, sensor region and the IC chip impedance matching network.

A basic RFID sensor forms an inductor-capacitor-resistor (LCR) circuit with the sensing antenna and integrated circuit chip inductance, capacitance and resistance (Fig. 2). [155] For near field coupling (NFC tags), mutual inductance coupling between the RFID sensor antenna and pickup coil of a sensor reader perform impedance measurements of the RFID sensor antenna over a few centimetres. Modulated RF signals are transmitted to the tag using only RF energy harvesting to power an integrated circuit (IC) via an antenna in a passive RFID system. [156] In the case of UHF, a resonant RFID tag antenna receives a RF signal from the RFID reader causing voltage build-up on the antenna terminals activating the chip and allowing for a signal to be sent back to the RFID reader along with backscatter signal modulation over several metres (Fig. 3). [157]

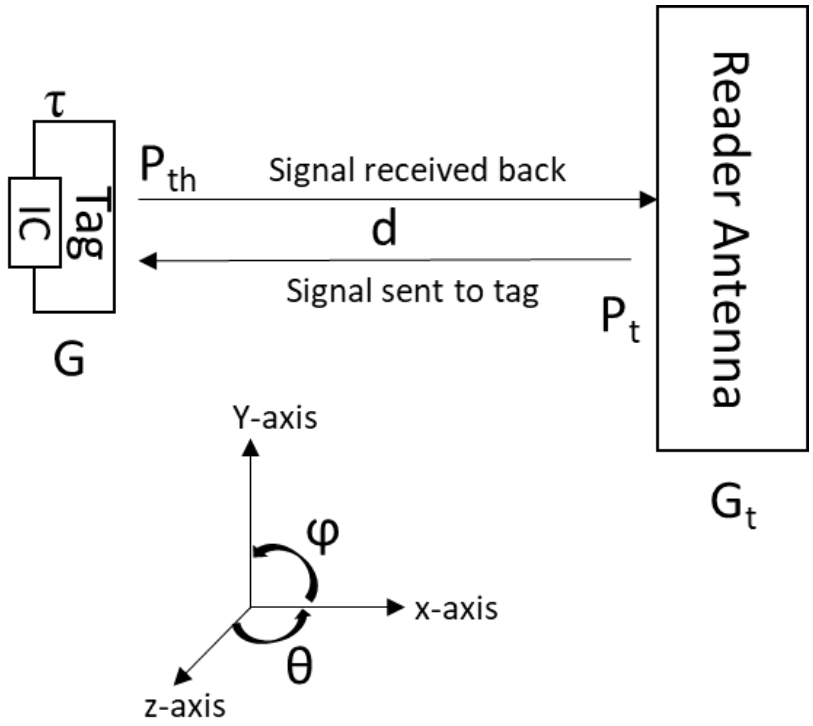

Figure 3 Schematic of antenna reader and antenna tag interaction and calculation components involved in the signal modulation.

The backscattered signal is controlled by the IC chip which modulates between two states ("high, power collecting, and low, close to short circuit"). A 50Ω impedance is standard in RF systems but RFID transponder chips have low resistance and significant capacitive impedance.

RFID chip sensitivity and impedance match to antenna define maximum forward tag range (r_{tag}) and power sensitivity. For example, the maximum forward tag read range in free space is determined by [157]:

$$r_{tag} = \frac{\lambda}{4\pi}\sqrt{\frac{P_t G_t G p \tau}{P_{th}}} \quad (1)$$

where wavelength is λ, RFID reader transmitter output power is P_t, reader antenna gain is G_t and effective isotropic radiated power (EIRP) is P_tG_t, tag antenna gain is G, tag and reader antenna polarisation mismatch is ρ, and power transmission coefficient is τ (an impedance-matching coefficient between the antenna tag and chip). [157] Gain is always given in dB while power and EIRP is usually calculated in Watts and read distance in meters. The coefficient τ is described by the equation:

$$\tau = \frac{4R_c R_a}{|Z_c + Z_a|^2} \quad (2)$$

where antenna impedance is $Z_a=R_a + jX_a$ and chip impedance (high power collection) is $Z_c= R_c + jX_c$. [3] It also characterises the antenna and chip impedance match. A given RFID tag antenna and chip are usually matched allowing for impedance normalisation which can be accomplished by using R_c^2 to go from the above formula to [156, 157]:

$$\tau = \frac{4r_a}{|1 + r_a + jQ(1 + x_a)|^2} \quad (3)$$

where normalized antenna reactance is $x_a =X_a/X_c$, normalized antenna resistance is $r_a = R_a/R_c$, and $Q = X_c/R_c$ is the resonant chip factor for a particular frequency and absorbed power. [156] The ambient environment can affect the electrical field generated by an RFID sensor because of its extension away from the sensor. This can provide an opportunity for sensing the external environment. [139, 154] The external sensed environment can be anything from a sample of food within the tag electrode's electric field or even an entire tag sensor antenna but in both, the impedance presented to the tag transponder chip depends on the capacitance and resistance

changes of the sensing region. [154, 158] Also, in RF applications using the real and imaginary impedance components in calculation can help improve the accuracy and precision of the sensor; calculating several other spectral parameters such as frequency position, real impedance magnitude, resonate and anti-resonate frequencies of imaginary impedance can also improve the sensor accuracy. [154] A resonant frequency is reached when the circuit is purely resistive (the imaginary portion of impedance (Z) is zero) and can be simply calculated by the resonant frequency (f_o) formula:

$$f_0 = \frac{1}{2\pi\sqrt{LC}} \quad (4)$$

with inductance (L) and capacitance (C) of the circuit included.

2.4.2.2 *RFID Current Applications:*

Current applications for RFID technology as microbial sensing systems are within the agriculture space. This is mostly as the current use of barcodes relies on a system with a limited data storage capacity for food labelling whereas RFID technology could provide real-time updates of food through the supply chain. Also, RFID labels have better traceability throughout all stages of production and delivery allowing for easy identification and location of arising issues such as contamination or incorrect storage practices (using humidity or temperature sensors). Currently the cost of passive RFID tags (the most affordable option) approximately $0.3 each when less than 1 million orders are placed; costlier than barcodes but with time this could be decreased. It is expected that the RFID label market will be worth around $30 billion by 2024 and the majority of the market will be utilised for retail sale (27%), individual transport (21%), logistics (6%) and medical applications (5%). Some of the current available RFID labels are used for the detection of food freshness (milk and fish) and microbial growth; there is also an interest in RFID labels coupled with biosensors. [159] Many of these systems are utilised as time temperature indicators for dairy [160], fish [161], fruits [162] or a combination of all [163]; However, most of these only monitored the temperature changes within the supply chain

rather than any contamination within the food product. It should be noted that there is research being done to detect microbial growth and contamination of food products or for use within medical fields. The following sections describe some reported RFID sensing systems.

2.4.2.2.1 Food Freshness:

Milk and fish represent two of the main categories within the agricultural space with available RFID devices. As some of these devices not only rely on time temperature indicators for spoilage but rather growth of microbial organisms, it is important to understand the current market for future development of any microbial sensors. Often, microbial growth can be liked with change in the dielectric properties of the food item or the detection volatile vapours produced during spoilage. Therefore, such milk and fish sensors will be discussed in more detail within this section.

2.4.2.2.1.1 Milk:

Microbial growth accounts for milk spoilage by modifying the composition of media due to metabolic by product release causing a change in the overall conductivity and ionic content of the milk. It is possible to use NFC RFID sensor technology to monitor milk freshness. Potyrailo *et al.* were able to use 23 × 38 mm RFID tags from Texas Instruments for monitoring milk freshness wirelessly. These RFID sensors were attached to the outside of a milk carton using an adhesive backing to monitor dielectric changes in the milk composition. Milk spoilage affects the dielectric properties of milk and can be used to determine the spoilage rate using a non-invasive RFID sensor through the milk carton walls because of the electromagnetic field penetration depth. This experiment was used for determining the spoilage rate for both fat-free and whole milk as well as a water control which exhibited that both milk samples caused impedance changes with increased storage time while the water control did not. The water control consisted of the same container and RFID sensors as the two milk samples. [154]

The spoilage rate was determined based on a function of storage time and change in dielectric solution constant and correlated to control measurements taken of fresh milk and negative controls. [154] Also, Ribeiro *et al*. showed that when different microbial specimens are introduced into a milk sample to induce milk spoilage, the microbial response to frequency over time is affected. They hypothesised that this was due to changes in the milk pH caused by lactose digestion into lactic acid and when a pH of around 6.5 is reached, then milk proteins (casein) start aggregating leading to milk spoilage and change in frequency of the NFC tag. Therefore, they stated that a change in tag frequency response accounts for a change in milk pH. [164]

2.4.2.2.1.2 Fish:

RFID sensor technology is capable of monitoring fish freshness. Potyrailo *et al.* constructed an RFID fish freshness monitor using 47 × 47 mm, NFC RFID tags from Avery Dennison (model AD 709, Flowery Branch, Georgia) and a polyaniline polymer sensing film deposited on the antenna. Polyaniline is an intrinsically conducting polymer (conjugated polymers). Gas recognition via changes in density, charge carrier mobility, and swelling of the polymer and polymer chain conformational transition are all mechanisms exhibited by conjugated polymers. [154] Fish odour is caused by bacterial metabolism realising volatile nitrogen compounds such as ammonia and volatile amines. [165]

Polyaniline and volatile nitrogen compounds exhibit strong acid-base interactions resulting in strong changes in the conductivity of the polyaniline film and thus realize a highly sensitive RFID sensor with a 500 part-per-trillion (ppt) detection limit of ammonia gas. To monitor fish freshness, Potyrailo *et al*. placed five RFID sensors in separate petri dishes with a fish sample plus a set of controls. The monitoring of the conductivity changes for all samples occurred congruently and over time, the deprotonation of the polyaniline film resulted in increased sensor impedance within 2 hours. [154] Other fish freshness detection methods studied mostly

utilise the detection in the change of the environmental temperature rather than detecting any chemical changes within the fish. [161] These types of non-specific designs can only determine fish spoilage based on the estimation of spoilage in regard to temperature changes over time.

2.4.2.2.2 **Microbial Growth Sensing:**

Antibodies, nucleic acids, bacteriophages, and lectins can all be immobilised on an electrode surface and used as bioreceptors in impedimetric sensors. These immobilised bindings then can be detected by a change in capacitance, impedance, or admittance on the electrode interface. A lipid bilayer (polar groups facing outward towards the aqueous environment and hydrophobic groups pointing inward forming the membrane interior) form most bacterial cell membranes. A capacitance of 0.5-1.3 $\mu F/cm^2$ and resistance of 10^2–10^5 $\Omega \cdot cm^2$ is naturally occurring in most bacterial cell membranes. When the electrode surface has attached bacterial cells, the electrode surface area where the current can reach is reduced, increasing the interface impedance. [154] However, natural cell wall capacitance and resistance has never been determined for fungal species such as *Candida*.

It is known that morphologically distinct cell walls have low conductivity (1/resistance) (0.02 to 0.2 S/m). A previous experiment showed that when a *Micrococcus spp*. cell wall is removed, the low frequency conductivity reduced further from 0.1 to 0.001 S/m. Surface conductance (related to surface fixed charge) is affected when there is a change in the cell wall structure (such as enzymatic removal) leading to a change in the conductivity magnitude. [166] Therefore, it is possible that the natural conductivity of *Candida spp.* will be low but any disruption caused in the cell wall such as due to antifungal use can be still visualised.

Potyrailo *et al*. also studied bacterial growth and impedance using a 23 × 38 mm NFC RFID tags from Texas Instruments by measuring antenna circuit resonance impedance. A food wrap film was deposited on the RFID sensors. The RFID sensor was attached via adhesive to one side of the film while a solution was exposed to the other side. Two solutions were used: one

solution containing *E. coli* and the other a sterile control solution. A pick-up coil was used to read the resonance impedance changes from the bottom of the sensor and petri dish. It was shown that accumulation of bacteria on the food wrap film over time was associated with dielectric change detected by the sensor. There was no dielectric change within the sterile solution. [154]

Yuan *et al.* were able to detect antibody response to pathogen presence using self-assembly of metal nanoparticles within a UHF RFID dipole antenna. Their self assembly system functioned as an immunoassay using metal nanoparticles attached to immunoglobulins to fill in gaps within the dipole antenna causing better matching and a longer read distance for the antenna once in the presence of the pathogen is detected. Also, because the length of the dipole is based on the nanoparticle adhesion, the developed system can correlate the concentration of the pathogen presence based on the nanoparticle adhesion which shares an ultimately linear relationship with the read distance of the antenna design. There was also an inclusion of a calibration antenna to normalise the nanoparticle adhesion to a known quantity. The signal-to-noise threshold levels of the system permitted a minimum value of 26.9 ng to be detected. [167]

Karuppuswami *et al.* also developed a milk freshness NFC RFID system based on microbial detection; this design utilised a hydrophobic surface to detect *E. coli* attachment contained in a sensor (LC 'tank'). The design exhibited an inverse relationship between the *E. coli* concentration and resonant frequency. As the concentration increased, resonant frequency decreased. With this design, the detection method was able to determine contamination within an hour for bacterial counts of 5 log CFU/ ml. Spectrophotometry verified the sensitivity of the RFID system. This system was utilised at NFC but as it is primarily a sensor technique that could be adjusted to function for different RFID frequency bands. [168]

2.4.2.2.2.1 Graphene-based Wireless Bacteria Detection:

Graphene material has good electrical, mechanical, and sensing properties and is an ideal material for sensor development. It has a high intrinsic strength (42 N m^{-1} and Young's modulus of ~1 TPa) and interfacial adhesion. Graphene has not been manufactured large scale because it must be grown using chemical vapour methods of deposition on supporting metallic films such as nickel and copper. Graphene, with interlinked electrode contact, can be printed on silk for easy transfer and used as a sensitive chemical and biological receptor. Mannoor *et al* demonstrated that graphene detection limits can be as low a single bacterium with wireless readout and power of a biotransferrable graphene nanosensor. AMP-graphene peptides can undergo self-assembly onto a graphene monolayer to achieve a high biological specificity without degrading the sensing, electronic components. [169]

Mannoor *et al* produced a hybrid biosensor which was not only able to be transferred onto small structures such as bovine teeth but also showed a wireless and battery free sensing proficiency. The conductivity of bacterial growth targets is monitored wirelessly following a binding of specific immobilised peptides on the graphene film using a radio frequency (RF) reader. An LRC resonant circuit, wireless transmission planar meander line gold inductive coil and resistance sensing capacitive electrodes comprise the architecture of the Mannoor *et al* passive wireless graphene nanosensor. [169]

Mannoor *et al* biotransferred the graphene nanosensor onto the enamel of a bovine tooth in order to investigate how sensor integration with biological tissue affects the sensor's performance. [169] Breath and saliva, a rich biological medium, are in continuous contact with teeth providing the possible source to identify disease, pathogens and any other changes in metabolism. [170-172] This tooth/ sensor combination allowed for sensing the effect of breath on the tooth in regard to conductance. It showed that there is a prompt response to breath which terminates quickly after exhalation in real-time change in conductance. [169]

When the nanosensor on the bovine tooth was exposed to a Gram-negative stomach pathogen responsible for most (~90% of) stomach and duodenal ulcers, *Helicobacter pylori*, the graphene-antimicrobial peptides (AMP) on the sensing region were able to selectively recognise human saliva containing *H. pylori* cells. [169, 173] Saliva alone was not able to produce a change in resistance upon exposure to 1 µl of sample whereas saliva containing around 100 *H. pylori* cells produced a noticeable decrease. The AMPs were able to bind and recognise *H. pylori* cells after a 15-minute incubation with the infected saliva. [169] As *H. pylori* concentration increased, the percentage change in resistance and frequency was calculated by the wireless RF reader recording at resonance after 10 minutes. [169, 174, 175]

Mannoor *et al* were also able to functionalise the graphene nanosensors with chemically synthesised peptides: dodecapeptide graphene binding peptide (GBP), a triglycine linker and an AMP odorranin-HP (OHP). [169] GBP-OHP has specificity towards Gram-negative bacteria (*Escherichia coli* and *Helicobacter pylori)* and a Gram-positive bacterium (*Staphylococcus aureus).* [176] Graphene sensor detection of the three strains of bacteria along with erythrocytes (40% haematocrit) were compared to fluorescent assay results. Binding of peptides to bacterial cells was higher than binding to DI water control. Elution with GBP-OHP with *S. aureus* exhibited the highest change in resistance over the tested time point. [169]

Fluorescently labelled *E. coli* cell binding a bare graphene sensor exhibited an electrical resistance change which correspond with the single bacterium binding and unbinding from the graphene surface. [169] This can be explained by the fact that Gram-negative bacteria contain a negatively charged membrane composed of lipopolysaccharides suggesting that the graphene transducer is processing resistance with a p-type behaviour as previously studied. [169, 177] Immobilised AMP on a graphene sensor can affect the resistance when a single bacterium is binding. When AMP is present, there is no visualisation of cell unbinding as seen with the bare graphene sensor. Fluorescein isothiocyanate-labelled GBP–OHP was able to coat the entire

sensing area of the graphene sensor uniformly, which allowed for selective binding of the bacterium with the graphene sensor. This suggests that the bacterium has a strong interaction with the immobilised peptides. [169]

Mannoor *et al* tested hospital sanitation and monitoring on intravenous (IV) bags by transferring a graphene nanosensor onto an IV bag to detect *S. aureus* growth which is responsible for more than 500,000 infections per year. *S. aureus* is a dangerous pathogen due to many cases of its antibiotic resistance such as with methicillin (MRSA) as well as its ability to survive in dry environments and on plastic for up to 9 weeks. Graphene transmittance and sheet resistance change in the IV bag were measured by drying various solutions with bacterial concentrations on the sensor for 30 minutes. The bacterial growth effect on the graphene resistance was monitored wirelessly as a change in the resonance curve of the sensor's bandwidth. The effect of bacterial concentration on the bandwidth of the sensor showed that as bacterial concentration increases, bandwidth also increases and change in percent resistance decreases. This showed an overall accurate system for microbial growth detection. [169]

2.4.2.2.2.2 RFID Spore Sensing:

To adjust and RFID tag for spore sensing, either the resonant antenna must become the impedance sensor itself or include a secondary sensor attached to the antenna and an integrated circuit memory chip which contains the sensor ID and calibrations. Electromagnetic field generated extending outside the sensor plane becomes affected by changes in the dielectric constant of the antenna biosensing component. This occurs by causing changes in the capacitance and resistance of the sensor affecting impedance of the antenna circuit. Real Zre(*f*) and imaginary Zim(*f*) impedance and four other spectral parameters, such as frequency position Fp and magnitude Zp of Zre(*f*) and the resonant F1 and antiresonant F2 frequencies of Zim(*f*) are all measured. To reduce impedance response, a multivariate analysis is needed for every single data point in the multidimensional space.[178]

A 2 µL of a lyophilised *Bacillus spp*. spore solution containing around 100 spores in water was deposited onto the surface of an RFID tag. The sensor detected a decrease in position frequency between the sterile water control and the spore containing solution. This exhibited the cheaper alternative to graphene-gold sensors as described previously.[178]

2.4.3 Body Mounted RFID Applications:

Often body mounted applications are utilised in hospital environments to help with tracking and patient monitoring. [179, 180] Human body interaction with RFID devices must be understood when developing any wearable or implantable passive RFID UHF device. It is known that when a UHF RFID tag is placed on or near the body, the antenna shows reduced efficiency and radiation pattern fragmentation. [179, 181, 182] Also, it has been shown that there is also variability in tag function on different individuals or even for a single individual but with different body part attachment of the tag. [181] This is due to having variability for electrical properties within human tissue; muscle versus skin have very different dielectric properties. [183-185] Even skin thickness due to ethnicity [186] or sunlight exposure [187] can effect the dielectric properties of the body. It was found that human tissue conductivity affects antenna efficiency while changes in permitivity affect the resonant frequency tuning. [181] Therefore, it is important to understand how to design any RFID antenna that will need to be mounted on or within the human body.

2.4.3.1 *Antenna Placement on Human Tissue:*

When developing antennas for attachment to highly conductive surfaces, an issue of image current formation around the dipole degrading the radiation efficiency and fragmentation of the radiation pattern needs consideration. Most importantly for UHF applications, this issue leads to short read ranges of less than even 0.4 m when appropriate tuning is not followed. However, most of the traditional approaches do not limit ohmic loses by inductive path

reduction. Input reactance can be adjusted by changing the antenna geometry however the input resistance is unlikely to see any large change in tag geometry adjustments. [188] Two approaches that can overcome these issues are a shunt scaling [188] approach for impedance matching and electric density centralisation. [189] Both approaches are just novel takes of loop based matching networks previously reviewed [190] for impedance matching.

2.4.3.1.1 Shunt Scaling Based Impedance Matching:

A shunt scaling approach utilises two elements for impedance matching such as seen in L-matching networks [191]; however, as reactance can be more easily adjusted by antenna geometry Zuffanelli *et al.* suggested focusing on the shunt reactive element to simply the network. [188] This approach is based on scaling the resistance of the antenna impedance to match the resistive part of the RFID ASIC impedance first described by [188]. Analytically this assumes that the overall generic impedance Z = R+jX of the antenna is adjusted with a reactance (X_p) shunt. This leads to a reactance (X_p) in parallel combination with impedance (Z_C) of the ASIC to match the antenna impedance (Z_A). This led to an overall matching impedance equation of:

$$Z_{\mathrm{A}} = \frac{R_C \cdot {X_p}^2}{{R_C}^2 + (XC + X_p)^2} + \mathrm{j}\,\frac{X_p \cdot [{R_C}^2 + X_C \cdot (X_C + X_p)]}{({R_C}^2 + [X_C + X_p]^2)} \tag{5}$$

To determine the exact reactance needed to match the antenna impedance, a scalar ($\alpha = R_A/R_C$) can be calculated by determining the resistive part of the antenna versus the resistive part of the ASIC. This then can be combined to give an equation of:

$$\left(1 - \frac{1}{\alpha}\right) X_P^2 + 2X_c X_p + (X_C^2 + R_C^2) = 0 \tag{6}$$

This ultimately provides a limit on the α maximum for the scalar as:

$$\alpha \leq 1 + \left(\frac{X_C}{R_C}\right)^2 \tag{7}$$

This provides an ultimate possibility for two solutions for the shunt needed to adjust the antenna impedance and match the IC. Giving a solution which is capacitive (X_{P1}) or inductive (X_{P2}) for

a resistance decrease (α<1) or for resistance increase (α>1) giving either both inductive (X_C < 0) or capacitive (X_C > 0) solution.

$$X_{P_{1,2}} = \frac{-\alpha X_c \pm \sqrt{\alpha\left[X_c^2 + (1-\alpha)R_c^2\right]}}{\alpha - 1} \quad (8)$$

As most ASIC reactance for UHF RFID applications tends to be strongly capacitive, Zuffanelli *et al.* suggested that (7) could be simplified to be:

$$X_{P_{1,2}} \approx \pm\left(\frac{\sqrt{\alpha}}{1 \mp \sqrt{\alpha}}\right) X_c \qquad \text{for } X_C < 0 \quad (9)$$

The resulting reactance (X_P plus X_C) of (4) can also be calculated from this when X_C is negative with the equation:

$$X_{A_{1,2}} \approx \pm\sqrt{\alpha} X_C \quad (10)$$

What should be not overlooked is that when a tag antenna is placed on any conductive or lossy surface, the antenna properties rely not only on the antenna properties itself but also on the antenna placement properties. What this means is that when an antenna is placed on a metallic surface or (on the human body), the antenna impedance characteristics cannot be calculated in air but rather when placed on or in the material.

For example, in [192] the antenna impedance was actually calculated as Z= R+jX where $R = R_{tag} + R_{glass} + R_{mylar}$ and $X = X_{tag} + X_{glass} + X_{mylar}$ as the antenna design was placed on a glass container and etched on mylar. This is important to remember because if the antenna impedance is calculated in air only without accounting for any attachment adjustment then the scaler (α) used will not be accurate and the shunt (X_p) needed will not allow for proper matching between the antenna and ASIC. The proper utilisation of this shunting process can be seen in [188] as this was the first publication to present the calculations necessary for this type of impedance real part adjustment. Whereas this approach directly adjusted the resistance of the antenna impedance by utilising an extra component, electric density centralisation instead suggests

altering the geometry of the design itself to reduce the proximity effect from lossy materials on antenna function.

2.4.3.1.2 Electric Density Centralisation as Impedance Adjustment:

Adjusted the geometry of the antenna itself can alter the antenna impedance to better match the ASIC impedance. However, normally resistance of an antenna cannot be changed easily by adjusting the antenna geometry due to space constraints for antenna placement. However, [189] found that if a design allowed for the electric density to be centralised away from the antenna borders, the design could isolate itself from any lossy substrate that the antenna is attached to. This removed the necessity of a ground plane to shield the antenna design from the proximity effect of lossy substrates. It is especially necessary for any antenna placement on high value dielectric substrates such as the human body. Radiation efficiency can be completely lost when any tag is placed directly on top of human tissue due to the body-proximity effect. By utilising this insulating approach by focusing the electric density away from any antenna borders, it can help overcome this proximity effect. This ultimately can increase the antenna robustness and antenna radiation efficiency while remaining frequency independent as this approach can be utilised at any UHF frequency. [189]

Both approaches were utilised in the design of all presented antenna UHF RFID sensors within this work as they allowed for simple adjustments to improve impedance matching between the antenna and ASIC. All tags utilised a circular design to the dipole geometry as this allowed for easier electric density centralisation away from the antenna borders while limiting the necessary size of the antenna. Also, as all of the presented design were attached to highly lossy materials (such as the human body) not only was it necessary in increase the self-insulating effect of the tag itself but to also scale the resulting antenna resistance to better match the ASIC impedance; It is known that human tissue conductivity has a great effect on radiation efficiency while tissue permittivity mostly affects tuned frequency. [179] Therefore, it is important that

both tag insulation from the proximity effect of tissue and impedance scaling should be utilised for any tissue or tissue like tag placement.

2.4.4 RFID Considerations:

The current limitation to widespread RFID use is the cost factor as even $0.3 per tag can be considered expensive for manufacturers in comparison to barcodes. The price changes dependent on volume bought, storage space, tag packaging as well as type of tag (passive or active). Environmental issues can also arise from disposal of RFID tags and their components especially for active tags (battery recycling issues in the case of battery assisted tags) even conductive inks could increase environmental problems as most cannot be recycled easily. [167] There is a need for future low-impact designs for environmental considerations.

A technical issue that can arise with increased RFID use is interference occurring when an RFID reader cannot detect an RFID tag because it is in a multi-tag and multi-reader environment. Collisions and correlations between the various RFID readers and tags usually cause the missing data. It is possible to apply a Self-adaptive Bacterial Foraging Optimization (SABFO) algorithm to try to limit this issue. When this communication is breached, the need to properly read all the information saved on each tag in a multi-tag system might become difficult therefore it is possible to apply the SABFO algorithm to help network scheduling of each RFID tag and reader identification. [193] The algorithm might be able to help solve any network RFID multi-tag reader issues based on tag and reader coverage. [193] Another possible choice for better tag identification and readout could be to use adaptive n-Resolution and k-Collision Arbitration which improves the efficiency of tag identification with *k*-splitting collision arbitration by at least 48.85 % identification delay and 23.87 % communication overhead. [194] All these issues must be addressed to make RFID technology viable for wider implementation in society; However, microbial growth detection passive RFID must first be developed and proven to be viable before multi-tag considerations need occur. Yet this is an

important future consideration for any implementation and/ or commercialisation of sensor technology.

2.5 Summary:

Although there is extensive information on *Candida albicans* colonisation and infection utilising multiple detection systems, there is no information or research on real-time detection. Also, there is a lack of information available on *C. albicans* formation in terms of electrical properties such as what occurs in the biofilm when forming on top of a sensor. Any amperometric or potentiometric-based technologies that do exist for microbial growth detection rely on changes to the culture media rather than due to the organism itself, in the most part, as the majority published work are within the food industry. No technology (based on the current literature review) even exist to detect *C. albicans* formation while within a mammalian host. All methods of detection rely on the appearance of symptoms to underline a need for species identification initiated by a clinician. Furthermore, most current detection methods employed within medical sector are laborious and require organism inoculation on or within some form of growth media with no direct identification within a host. This underlines the need for not only *C. albicans* electrical property quantification to develop future sensor technology but, also, systems able to detect *C. albicans* biofilm formation in real-time within a host and prior to symptoms occurrence and, ultimately, fungal disease.

3 Chapter 3: Project Aims and Publications

The overall project was to develop an RFID UHF based system that can detect *Candida albicans* biofilm growth on a medical device (voice prosthesis) while inside the body. It was important to understanding how *C. albicans* colonises medical devices to recognise what properties during this colonisation could be targeted as the detection method for the RFID sensor. This objective ultimately allowed for the design of four very similar RFID UHF sensing approaches:

1) A design able to determine *C. albicans* biofilm growth effect on sensor impedance (necessary to understand if *C. albicans* biofilm growth is even able to be detected).
    - Paper title: "Monitoring *Candida albicans* Biofilm Formation by Impedance Using Passive RFID"
        - Published: Not yet
        - Developed to understand how *C. albicans* biofilm grows in terms of electrical properties by utilising standard impedance-based *in vitro* equipment and prior published RFID systems.
        - Contribution of authors: Viktorija Makarovaite did all the research, writing and experimentation; Aaron Hillier provided the PDMS coating for sensor region. Remaining authors provided guidance.
2) A design able to detect minute dielectric changes with a closed liquid solution (something necessary if needing to design for the oral cavity containing saliva).
    - Paper title: "Passive Wireless UHF RFID Antenna Label for Sensing Dielectric Properties of Aqueous and Organic Liquids"
        - Published: in IEEE Sensors Journal
            - doi: 10.1109/JSEN.2019.2896481.

- Allowed to understand the sensitivity of the developed sensor in detecting dielectric changes within a closed liquid medium. Originally developed to be used as an indirect method for microbial growth detection within a culture media but expanded (and published) as a general liquid sensor.
- Contribution of authors: Viktorija Makarovaite did all the research, writing, experimentation and sensor design; Aaron Hillier provided the polymer coating for sensor region. Remaining authors provided guidance.

3) A design able to ignore human tissue conductivity and/ or permittivity changes while detecting an external variable (necessary for any design placement on / in the human body).
    - Paper title: "Adjustable Passive RFID Skin Sticker for Medical Dressings"
        - Published: Shorter version published in:
            - doi: 10.1109/BSN.2019.8771069.
        - Developed from trying to understand how the proposed indirect sensing of media could be utilised on the human body. A sensor designed without the body characteristics (particularly, capacitive loading of human tissue) accounted for would likely not function once placed within/ upon human tissue. This paper corresponds to this work which was expanded upon to include a smart medical dressing.
        - Contribution of authors: Viktorija Makarovaite did all the research, writing, experimentation and sensor design; Aaron Hillier provided the polymer coating for sensor region. Remaining authors provided guidance.

It was necessary to develop all these approaches first to have a full understanding of what is needed to:

4) develop a single system able to detect *C. albicans* biofilm growth on a voice prosthesis while within the body.

- Published: Shorter version published in:
    - doi: 10.1109/RFID-TA.2019.8891963
    - Recently accepted for publication with IEEE Journal of Radio Frequency Identification. [reviewer requested corrections currently in process]
- This paper corresponds to the accumulation of all the previous papers and research which concluded in a functional RFID sensor capable of detecting microbial growth within the body. Without this work, which led to the previous papers, it would have been difficult to complete a working sensor of this type as many issues would not have been addressed such human tissue capacitive loading or the electrical properties of *C. albicans* biofilm growth.
- Contribution of authors: Viktorija Makarovaite did all the research, writing, experimentation and sensor design. Remaining authors provided guidance.

This work includes all four papers which tried to answer all the presented objectives utilising similar methodology for tag design or were developed from the original project aims.

Passive Wireless UHF RFID Antenna Label for Sensing Dielectric Properties of Aqueous and Organic Liquids

V. Makarovaite, *Student Member, IEEE,* A. J. R. Hillier, S. J. Holder, C. W. Gourlay, J. C. Batchelor, *Senior Member, IEEE*

***Abstract*—The *in situ* wireless sensing of dielectric properties for organic aqueous solutions with a wide range of relative permittivities is presented. The use of a UHF passive label antenna design attached to either clear borosilicate glass bottle or petri plate is proposed and which allows for the unobtrusive, safe monitoring of the liquid solutions. The meandered dipole antenna (with a parasitic loop matching component) frequency is highly reliant on the chosen container as well as on the liquid present within, and adjusts with shifting dielectric properties. Tested solutions of high relative permittivity (such as water) along with low permittivity, lossy liquids (such as xylene) presented distinctive frequency characteristics with read distances of up to 7 meters for each type of container tested. The sensor was also able to detect 'unknown' solutions and determine the dielectric properties by utilizing standard curve analysis with an accuracy of ± 0.834 relative permittivity and ± 0.050 S·m^{-1} conductivity (compared to a standard dielectric measurement system available on the market). With the accuracy known, tuning the design to fit any necessary frequency is possible as a means to detect specific changes in any one liquid system. This sensor is a possible candidate for discreet real-time monitoring of liquid storage containers and an alternative for low-cost bulk liquid dielectric property identification which could be implemented in areas requiring, constant, or remote monitoring as needed.**

***Index Terms*—Antenna, battery-free, passive sensing, radio frequency identification (RFID), ultra-high frequency (UHF), wireless sensing.**

I. Introduction

There are many industrial chemicals such as butanol and methanol, which produce dangerous vapors equivalent to a category 4 hazard, when opened in enclosed spaces without adequate ventilation [1, 2]. This vapor inhalation can cause common symptoms such as drowsiness, dizziness and respiratory irritation, or with continued exposure can even lead to electrolyte imbalance and kidney failure [1, 2]. Therefore, identifying unknown solutions without the need to open containers and allow vapor formation could be an advantageous application for RFID sensor technology, as well as the capability to determine liquid contamination (or purity) within a closed container autonomously without user interference.

To address these issues, the sensor proposed here is a low-cost, low-complexity and unobtrusive design, useful for real-time monitoring and *in situ* assessment of liquid solutions such as seen within chemical research and healthcare.

II. Material Sensing Characterization

Material characterization via sensing techniques has rapidly grown within the last decade particularly in the area of low-cost, accurate material analysis and real-time monitoring of samples. Also, polar solutions (molecules with permanent dipole movements) within biomedical applications have been shown to have complex permittivity matching with biological tissues (including medical grade solutions) over the frequency ranges of 300 MHz to 6 GHz [3]. It is known that complex relative permittivity $\varepsilon^* = \varepsilon' - j\varepsilon''$, (where ε' is its real part, ε'' is the imaginary part and $\tan\delta = \varepsilon''/\varepsilon'$ is the loss tangent) has a strong frequency dependence due to molecular dielectric relaxation behavior [3]. In biomedical measurements such as Specific Absorption Rate (SAR), material loss can be expressed in terms of equivalent conductivity, σ; where $\sigma = 2\pi f\varepsilon''\varepsilon_0$ with f being frequency and ε_0 free space permittivity [3].

The high dependence of these organic solutions on frequency provides a mechanism for dielectric liquid identification when using electrically small antenna designs, which can be easily tuned to a lower frequency range via a high dielectric backing [4, 5]. However, this frequency shift is highly dependent on not only the dielectric properties but also the thickness of the backing. Therefore, it is possible to normalize solutions to reduce the effect of conductivity and permittivity for liquid differentiation [6]. This can be seen in the use of (1) for determining effective permittivity:

$$\varepsilon_{eff} = \varepsilon_0(f_0^2 \,/\, f_{over}^2) \quad (1)$$

where f_0 was the starting frequency and f_{over} is the resulting changed frequency after the addition of the polar solution [6, 7]. However, this equation is not applicable if dielectric thickness is not maintained at a constant level, meaning that thickness variation in the walls of each container (or reservoir) will skew the results [6, 7].

Organic solution identification and antenna design has been previously reviewed, and sensors exist to detect these solutions [3, 5, 8-11]. However, a single chipped design capable of identifying both polar and non-polar (no-dipole moment, low relative permittivity (ε_r' = 2 - 11) and low loss ($\tan\delta < 0.001$)) organic solutions, and spanning a range of relative permittivities, is not available due to the large variability in solution dielectric properties. Additionally, most of the current published designs for any RFID based dielectric sensing are not only incapable of testing both low and high dielectric solutions but, also, are all chipless systems functioning above 1 GHz with most requiring a minimum frequency span of 500 MHz to differentiate their limited solution dielectric ranges [3, 5, 8-11]. The present approach attempts to provide such a sensor capable of detecting and differentiating an assortment of organic liquids with dielectric constants ranging from 2 to 80 within a single design and within less than 200 MHz frequency span for research use.

III. METHODS

The basic principle of operation requires the excitation of a resonant mode within a known container, where the resonant frequency is dependent on the liquid present within the chosen container [3, 5]. The sensor is excited wirelessly via a reader antenna, and a calibrated Voyantic TagformancePro system [12] detects the resonant frequency. Specifically, the TagformancePro system ramps power up to a set max (30dBm) and stops transmission once a signal is received back to the system (correlating output to the transmitted power levels); the links for this type of system are forward power limited.

The proposed antenna label assumes a full chosen container filled to a known level (100 mL in an 80 mm diameter borosilicate glass bottle and 20 mL in a 100 mm diameter borosilicate glass petri dish) rather than a very minute sample as seen with other systems [3]. Presenting a highly lossy environment, allowing the polarity of the system to correlate with the shift in the frequency for a known thickness (fill level) of the dielectric used. This easy attachment and reading of the liquid can be affected by a change in the dielectric properties of the solution in question allowing for identification of the dielectric properties (once plotted) against known solutions of the same quantity.

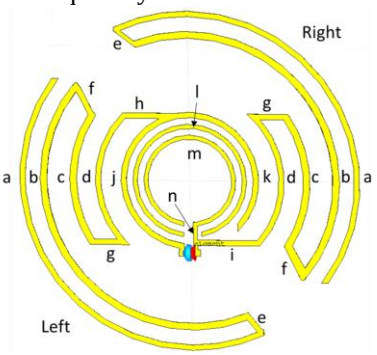

	Length (mm)		Length (mm)
a	36	**h**	5
b	33	**i**	6
c	12	**j**	13
d	12.5	**k**	13.5
e	3.3	**l**	23
f	3.7	**m**	20
g	3.5	**n**	2

Fig. 1 Liquid sensing UHF RFID half wave dipole antenna design with a 29 mm diameter and a parasitic loop matching system with three conductor widths: 1) 0.5 mm for lengths a - c and e - g; 2) 0.4 mm for lengths d, h - k; and 3) 0.3 mm for l - n.

A. Antenna Design

A Higgs-3 Electronic Product Code Class 1 Gen 2 RFID integrated circuit (IC) (Z_C = 23 – j192 Ω at 920 MHz) [13] was matched to a copper etched meandered dipole antenna (Fig. 1), by utilizing a matching resonating loop system.

In any RFID design, the impedance of the antenna (Z_A) must be conjugate matched to Z_C. Antenna placement on any material other than air will require either compensation or antenna retuning. When compensating for this change in antenna impedance, shunt scaling [14] can be utilized as an impedance matching network.

Shunt scaling uses the approach that if a reactance (X_p) is placed in parallel (shunt) with a known antenna impedance (Z_A), then Z_A can be expressed as:

$$Z_A = \frac{R_C X_p^2}{R_C^2 + (X_C + X_p)^2} + j\frac{X_p \cdot [R_C^2 + X_C \cdot (X_C + X_p)]}{(R_C^2 + [X_C + X_p]^2)} \quad (2)$$

where R_C and X_C are respectively the real and imaginary parts of Z_C. Given that $Z_A = R_A + jX_A$, shunt scaling for resistance [14] was used to develop a matching loop system with an alpha scalar ($\alpha = R_A/R_C$) of 0.29 when the antenna, Mylar and petri glass container have a combined impedance of Z_A = 6.74 – j131.9 Ω such that $R_A = R_{tag} + R_{glass} + R_{mylar}$ and $X_A = X_{tag} + X_{glass} + X_{mylar}$). It was shown in [14] that when the reactance of the IC is negative ($X_C < 0$), either a shunt capacitance 0.81 pF or a shunt inductance of 1.3 nH will satisfy (3) for α = 0.29.

$$X_p = \mp \frac{\sqrt{\alpha}}{1 \pm \sqrt{\alpha}} \cdot X_C \quad (3)$$

A shunt capacitance was chosen due to its linear frequency dependence. This led to a highly meandered half-wave dipole and a 1 pF capacitive loop system of about 29 mm in diameter (Fig. 1). Altogether, the two meandered dipole sides had lengths of 122 mm (left) and 110 mm (right), more than enough to account for the needed length for a half-wave dipole at 920 MHz.

B. Antenna Placement

The antenna label was attached to achieve the optimal matching with the container(s) chosen [12]. For the petri dish attachment, the sensor was placed on the underside of the 100 mm diameter borosilicate glass petri dish, Fig. 2 (A). It is important to note that the borosilicate glass had a 2 mm thickness and a glass height of 12 mm. A 500 mL borosilicate glass bottle (80 mm diameter) with a 5 mm glass thickness was also tested to determine the role of glass and liquid thickness on the sensor sensitivity, Fig. 2 (A).

The TagformancePro system was arranged as indicated in Fig. 2 (C) with a calibrated 30 cm space between the reader antenna and the sensor tag attached to the solution container. The configuration was set to a 'transmitted power' sweep between 750 MHz to 1000 MHz (for the petri dish) and 800 MHz to 1000 MHz (for the bottle) with 5 MHz frequency and 0.1 dBm power steps (up to 30 dBm) to identify any shifts in resonance to allow for effective permittivity calculation in (1).

C. Simulation

CST software suite is a time domain based electromagnetic simulator able to model material parameters in three dimensions [15]. For CST simulation purposes, the borosilicate glass properties were set as 7 for permittivity and 1×10^{-11} S·m^{-1} conductivity. Mylar thickness was calculated as 0.13 mm with a permittivity of 3.6 and conductivity of 0.0004 S·m^{-1}. As previously stated, the petri dish was modelled with a 100 mm diameter and 2 mm glass thickness with a liquid layer of 4 mm in height (equivalent to 20 mL of solution) (Fig. 2 (A)). The glass bottle was modelled as a cylinder with an 80 mm diameter and 5 mm wall thickness. For the liquid level equal to 100 mL of solution, a layer of 25 mm was simulated within the 115mm cylinder (Fig. 2 (A)). The simulated read distances (using built in CST capabilities) were calculated at the peak resonant frequency for each organic liquid tested, the receiver sensitivity was set at -20 dBm with a chip capacitance and impedance based on the Higgs-3 SOT IC [13] for the needed resonant frequency. This simulation sensitivity was chosen as (based on empiral experimentation) this provided a good working minimium read distance estimation without over estimation. All the simulated organic solution dielectric properties were taken from Table I and Table II. The simulated resonant frequency

responses for each liquid type and estimated read distance are shown in Fig. 3 (A) for the pertri dish and (B) for the bottle, and compared to the measured results.

It should be noted that there is no air gap between the glass and the RFID tag as the tag is directly attached onto borosilicate glass by very thin (< 5 micron) adhesive layer when measured (this adhesive layer was not included in simulation as the layer thickness was not electrically significant). As tag placement variability is possible even on the standard laboratory bottles and petri dishes utilized here, a future standard procedure must be defined for sensor placement.

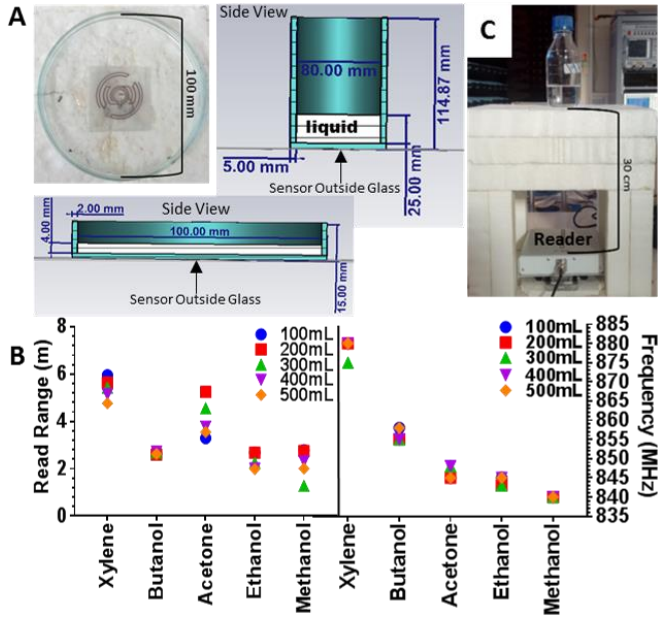

Fig. 2 Experimental setup. (A) Top view of antenna sensor placement on a borosilicate glass petri plate, and diagram of antenna placement of petri and bottle in side view (from CST simulation software). (B) Read range and frequency affect with change in volume within bottle. (C) Voyantic TagformancePro system arrangement with a 30 cm space between the reader antenna and the sensor on the bottom of either the borosilicate bottle or petri plate (bottle procedure shown).

D. Liquids

Six common organic liquids with relative permittivities ranging from 2 to 80 were chosen for determining the effectiveness of the antenna label sensor as a liquid identification system. These liquids have been studied within the antenna sensor field and their dielectric information is readily available [3, 5]. The six tested liquids were methanol, ethanol, butanol, acetone, xylene and deionized (DI) water. From experimentation, it was determined that 100 mL of solution in the 500 mL bottle presented the optimal results for differentiating various liquid chemicals. However any chemical amount up to 500 mL can be utilized for differentiation showing a discreet effective permittivity for each type of chemical.

Finally, to get a standard calibration curve for a permittivity range of 2 to 80, varying percentages of ethanol to DI water, as well as xylene to ethanol were used (Figs. 5 to 8). This allowed for a more accurate representation of how a standardized level change in permittivity affects the solution resonance frequency and effective permittivity. These standardized DI solutions were 100%, 75%, 50% and 25% percent ethanol (and the same percentages were used for xylene solutions mixed with ethanol). The liquid solutions were named as to reflect the percentage of ethanol in each solution, for example: 25% ethanol = 25% ethanol to 75% DI water, while 25% xylene = 25% xylene to 75% ethanol. The same naming trend was utilized for all the solutions. All liquid dielectric properties were measured at 865 MHz using a SPEAG Dak 3.5 probe [16] with a Rohde and Schwarz ZVL 6 GHz network analyzer using the standard manufacturer recommended procedure [15]. The measured values are given in Table I.

TABLE I
DIELECTRIC PROPERTIES OF THE SIX POLAR LIQUIDS USED WITHIN THE EXPERIMENT

Liquid	*Permittivity (294.13K)*	*Conductivity S/m*	*Petri Effective Permittivity*	*Bottle Effective Permittivity*
DI Water	78.20±0.20	0.09	1.462	1.196
Methanol	30.88±0.27	0.38	1.317	1.140
Ethanol	14.53±0.47	0.54	1.227	1.126
Acetone	21.10±0.30	0.07	1.227	1.126
1-Butanol	4.75±0.34	0.22	1.118	1.087
Xylene	2.57±0.15	0.07	1.080	1.027
Air	1	0	1	1

Calculated effective permittivity for both the borosilicate glass petri plate and 500 mL bottle. Read with the Dak system at 860 MHz frequency.

E. Single Frequency

After determining the sensitivity of the presented sensor, the sensors design can be tuned within any licensed EPC band to allow for easy UHF RFID liquid identification utilizing a single RFID reader without the requirement of any research quality wideband readers (as needed in previous sections). This would involve a simple adjustment to the dipole lengths. The design was tuned using parameter sweeps with CST software to determine the ideal dipole lengths for each frequency tested; calculated for 867 MHz and 920 MHz for both petri and bottle (Table IV). The results are given as left and right dipole lengths based on Fig. 1 overall side lengths.

F. Repeatability

To check the repeatability and accuracy of each liquid resonant frequency reading, an empty 'air' standard was run between each new replicate for every liquid tested as well as when switching between the different types of organic liquids. No noticeable resonant frequency drifts occurred throughout the experiment as each organic liquid readings were repeated in triplicate within multiple days. However, as the measurements were completed within a few weeks, it is possible that a frequency drift could occur with continued use. Therefore, all readings should be verified by the inclusion and tracking of an 'air' standard for any system utilizing this passive UHF liquid sensing system.

IV. Results and Discussion

When measured with the Voyantic system, each organic liquid demonstrated a distinct resonant frequency in both the 2 mm thick walled petri dish, Fig. 4 (A) and the 500 mL borosilicate glass 5 mm thick walled bottle, Fig. 4 (B). There was a wider resonance separation in accordance with the effective permittivity for the thinner petri plate than the thicker bottle yet the overall trends remained the same. Empty

containers had the highest resonance frequency whereas ethanol, acetone, and methanol showed a downward shift. Both container types had more difficulty differentiating between the alcohol solutions as these had very similar dielectric properties. However, as previously seen with the resonant frequencies, the overall trend in effective permittivity is identical between the two systems (Table I). Also, it should be noted that testing volume levels from 100 mL to 500 mL produced at most a 5 MHz resonant frequency shift for each organic liquid tested, Fig. 2 (B). Specifically, acetone produced a resonant frequency range from 845 MHz to 850 MHz (Fig. 2 (B)). Butanol and xylene also had resonant frequency shifts of 5 MHz; butanol ranged from 860 MHz to 865 MHz while xylene ranged from 880 MHz to 885 MHz (Fig. 2 (B)). Ethanol, methanol and DI water, however, remained unchanged and produced a constant resonant frequency from 100 mL to 500 mL volume of liquid (Fig. 2 (B)). However, it should be noted that with the increase above 100 mL, there was a change in read range for most of the organic liquids at their resonant frequency (Fig. 2 (B)). Though all read distances remained above 1 meter (at a minimum) throughout all the volumes tested (Fig. 2 (B)). For the petri dish, 20 mL of solution was used as the standard amount as this provided optimal repeatable results.

Finally, to verify the modulated signal resonance (S11), a loop coupling method with a network analyzer was utilized for both air readings Figs. 4 (C) and (D). This showed that both the TagformancePro and ZVL Rohde & Schwarz 6 GHz network analyzer produced the same resonant frequency for the air standards at 897 MHz (bottle) and 925 MHz (petri). Overall, the results exhibited the expected trends for increasing permittivity leading to a downward shift in resonance frequency.

A. Measured Resonance Shifts

The sensor match on the petri dish was achieved at a resonant frequency for air from 920 to 925 MHz with a bandwidth of about 100 MHz (transmitted power equal to or smaller than 15 dBm) equivalent to read range of 6.1 m when measured on the TagformancePro reader. For the bottle, the same resonance shift trend was seen. These results were as expected based on simulations as seen within Figs. 3 (A) and (B). The measured resonant frequency of the empty bottle also matched the desired frequency band at 915 to 925 MHz, resonating at 900 MHz with an acceptable bandwidth of about 100 MHz.

The loss in sensor sensitivity for the increased glass thickness in the bottle suggests that the material effect of the glass was overestimated by CST simulation when matched to air (Figs. 3 (A) and (B)). Due to the circular and parasitic nature of the antenna design, the electric fields add in phase rather than cancel leading to increased material penetration by the fields than modeled. This would also explain why the simulated read ranges were a fraction of the distances measured by the TagformancePro reader, Figs. 3 (A) and (B). When looking at directivity, the sensor design had a unidirectional appearance, with theta at both 0° and 180° representing the vertical main beam directions.

B. Measured Resonance Shifts

The sensor match on the petri dish was achieved at a resonant frequency for air from 920 to 925 MHz with a bandwidth of about 100 MHz (transmitted power equal to or smaller than 15 dBm) equivalent to read range of 6.1 m when measured on the TagformancePro reader. For the bottle, the same resonance shift trend was seen. These results were as expected based on simulations as seen within Figs. 3 (A) and (B). The measured resonant frequency of the empty bottle also matched the desired frequency band at 915 to 925 MHz, resonating at 900 MHz with an acceptable bandwidth of about 100 MHz.

The loss in sensor sensitivity for the increased glass thickness in the bottle suggests that the material effect of the glass was overestimated by CST simulation when matched to air (Figs. 3 (A) and (B)). Due to the circular and parasitic nature of the antenna design, the electric fields add in phase rather than cancel leading to increased material penetration by the fields than modeled. This would also explain why the simulated read ranges were a fraction of the distances measured by the TagformancePro reader, Figs. 3 (A) and (B).

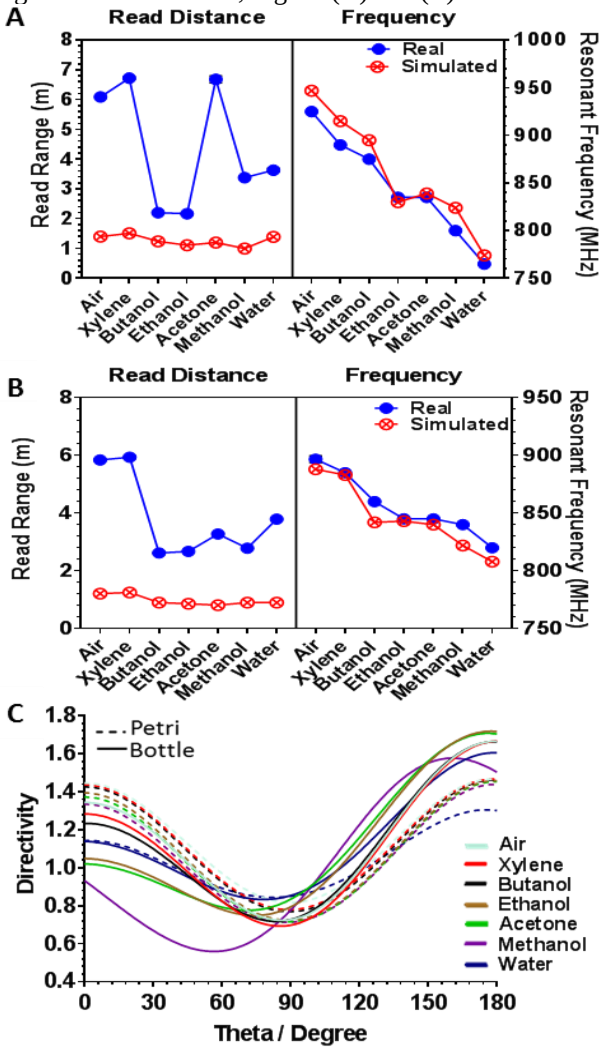

Fig. 3 Resonant frequency for the tested polar solutions within a borosilicate glass (A) petri dish and (B) bottle. Simulated and real resonant frequency readings had a good match for the chemicals tested; however, the read distance was underestimated for the simulated results compared to the real results. Real results showed no deviation between repeats with the highest read distances presenting for air, xylene and acetone in the petri setup and only air and xylene for the bottle setup (n = 3). Simulated results for water were averaged between the two observed resonant peaks in bottle (B) simulation only as all other simulations produced the same single resonance peak with multiple repeats. C) Simulated farfield directivity cut at phi 90° for each liquid tested at resonance with linear scaling for both petri and bottle settings. Theta 0° and 180° represent main vertical beam.

The resonance frequencies of each organic solution encompassed read ranges between 7 to 2 m for the petri dish, Fig. 3 (A), and 6 to 3 m for the bottle, Fig. 3 (B), dependent on the chemical used. This suggests that this sensor design is suited for use on glass containers. Air and xylene provided the longest read ranges for both glass containers (around 6 m for both in the bottle, and 6.1 and 6.7 m respectively for air and xylene in the petri dish). Xylene is a low polarity viscous fluid with a low conductivity (400 $pS \cdot m^{-1}$) and relative permittivity (2.6) [17], and able to cause a 35 MHz downward shift compared to air (permittivity 1 and conductivity 0.008 $pS \cdot m^{-1}$) while increasing the read distance of the tag, Figs. 4 (A) and 3 (A). Also, for the petri measurement, acetone showed a read range above 6.5 m.

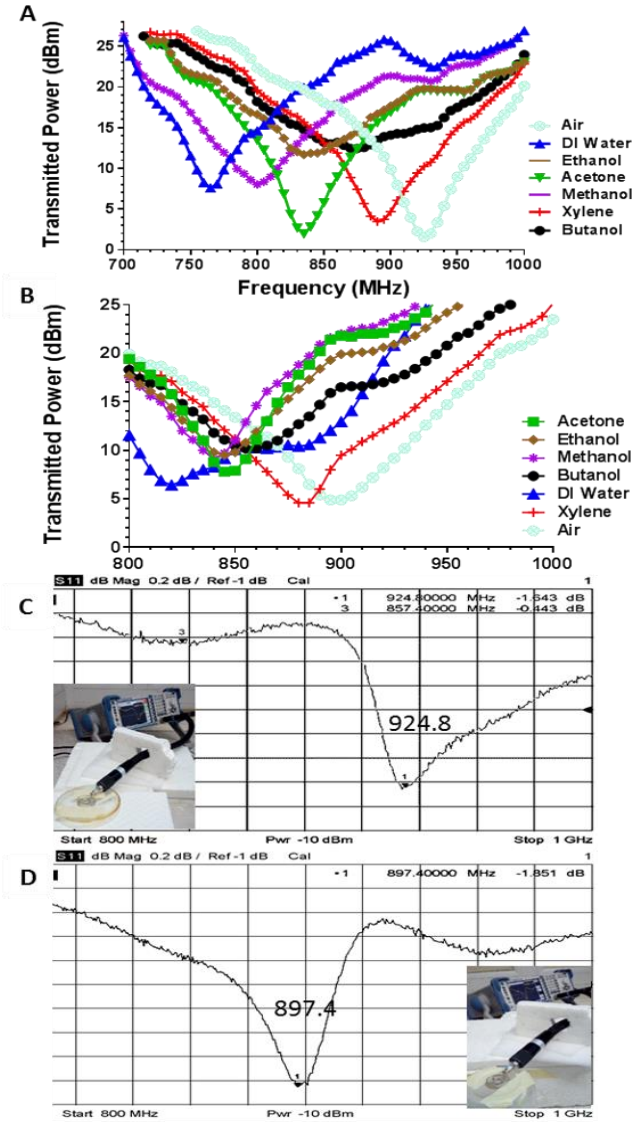

Fig. 4 Transmitted power for the tested polar solutions within A) 2 mm thick borosilicate glass petri dish and B) 5 mm thick borosilicate glass bottle. As permittivity increases, a downward shift in resonance occurs as expected. The three replicates for each chemical had no deviation (n = 3). (C) Petri and (D) bottle: S11 check for resonance without a modulated signal (in air) using a 2 cm loop coupled system with a ZVL Rhode & Schwarz network analyzer.

The overall trends between the calculated effective permittivities were identical between both sensor tag applications with a slight increase in sensitivity within the petri plate system allowing for a more distinct chemical identification when only using effective permittivity (Table I). Based on the results, increased glass thickness seems to decouple the liquid from the sensor enough to reduce the sensitivity of the sensor. This is most noticeable between the alcohols as there is a much smaller resonance difference between butanol, ethanol/acetone and methanol within the glass bottle, than for the petri dish. For example, the tag on butanol resonates at 875 MHz while methanol resonates at 800 MHz within the petri dish, whereas in the bottle the same solutions resonate at 860 MHz and 840 MHz respectively, Figs. 3 (A) and (B). That is a difference of 75 MHz versus 20 MHz for the same solutions.

C. Standardization of Ethanol Solutions

Ethanol solutions were utilized to achieve a standard curve for identifying solution properties based on the effective permittivity and to determine the relationship between the standard dielectric properties and effective permittivity. The petri dish set-up was utilized as it exhibited more sensitivity as seen in Section IV (A). There is a large difference between the air, 100% ethanol and DI water measurements (Fig. 5); however, the measurements between 75% ethanol and 25% ethanol become more difficult to differentiate as the values clustered around an effective permittivity of 1.3 (Table II). The resonance frequencies showed sensor tag read distances between 2 and 4 m with most of the samples giving around 3 m (Fig. 6).

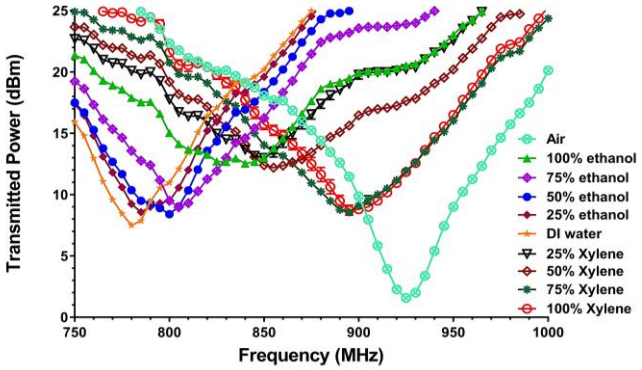

Fig. 5 Measurement of ethanol calibration solutions within a 2 mm thick borosilicate glass petri dish (three replicates each). There was some deviation within the replicates seen with 100% xylene and 25% xylene; however, the variance did not change the resonant frequencies just affected the transmitted power levels. There was a downward shift with increasing permittivity and less variance between solutions of close conductivity. Only 75% xylene and 100% xylene were indistinguishable from each other, all other solution mixes had unique resonance points.

There is an adequate variability between the permittivities within these close values but the conductivity does not show such a high variability (Table II and Fig. 7). It should be noted that conductivity affects resonance; however, it is primarily dependent on relative permittivity as it cannot affect a change alone within an acceptable correlation margin. Excluding air, the highest conductivity variance (with a relative low change in permittivity) stepwise is seen between DI water and 25% ethanol with a change of 0.114 S·m-1 causing only 10 MHz shift, whereas, a conductivity change of 0.053 S·m-1 between 100% and 75% ethanol showed a shift of 35 MHz. For the same calibration steps, even if conductivity only decreases by 0.053

S·m-1, the permittivity doubles leading to a more substantial downward frequency shift.

In order to make a complete permittivity curve, xylene was also mixed with ethanol (rather than DI water) to reduce the relative permittivity below that of absolute ethanol. Permittivity ranged from 2.4 to around 16, whereas conductivity varied from around 0.02 to 0.5 $S \cdot m^{-1}$ (Fig. 6). This further indicates that relative permittivity plays a primary role in frequency shifts than conductivity alone as 50% ethanol and 25% xylene both have similar conductivities (0.35 and 0.37 $S \cdot m^{-1}$, respectively), yet had a resonant frequency shift of 50 MHz owing to a relative permittivity difference of more than 30.

TABLE II
EXPERIMENTAL EFFECTIVE PERMITTIVITY FOR A RANGE OF ETHANOL SOLUTIONS

	Permittivity (297.45K)	*Conductivity (S/m)*	*Petri Effective Permittivity*
Water	77.8	0.169	1.426
25% Ethanol	64.6	0.283	1.389
50% Ethanol	48.9	0.35	1.337
75% Ethanol	33.6	0.427	1.320
100% Ethanol	16.2	0.483	1.213
	Permittivity (299.15K)	*Conductivity (S/m)*	*Petri Effective Permittivity*
100% Xylene	2.4	0.023	1.068
75% Xylene	4.9	0.096	1.068
50% Xylene	7.8	0.225	1.17
25% Xylene	11.1	0.372	1.18

The permittivity was varied from 2.4 to 78 by mixing ethanol with either DI water or xylene. Only 100% xylene and 75% xylene showed no difference within the calculated effective permittivity with both exhibiting at 1.068. Read with the Dak system at 860 MHz frequency.

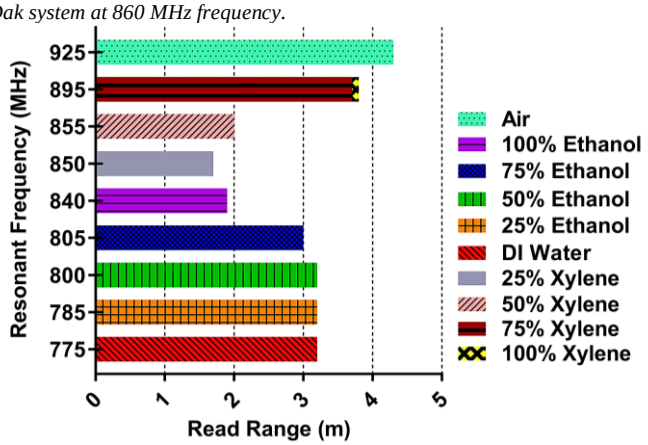

Fig. 6 Measure resonant frequency for the tested ethanol mixtures within a borosilicate glass petri dish. The read range showed between 2 m to about 4 m. The highest read distances were seen with 'air' at 4.3 m and both 100% and 75% xylene solutions about 3.8 m.

Also, comparing effective permittivity only against measured conductivities with simple linear regression for all the ethanol standardization solutions, they produced no significant differences (p value > 0.05 and $R^2 = 0.168$). However, when conductivity was included in the calculations alongside relative permittivity, a strong relationship was noted with effective permittivity, Fig. 7. This led to the creation of an equation for ε_{eff} relating ε' and σ obtained from a multivariate regression analysis and shown in Fig. 7.

As noted, relative permittivity and conductivity both simultaneously affect tag resonance on chemical solutions (as these values are known to be frequency dependent) especially when using a single type of sensor design. Thus, effective permittivity could be a better (or equivalent) identifier for chemical solutions than dielectric constant alone as it normalizes all the outside factors other than the chemical composition allowing for a single measurement using a UHF RFID reader only.

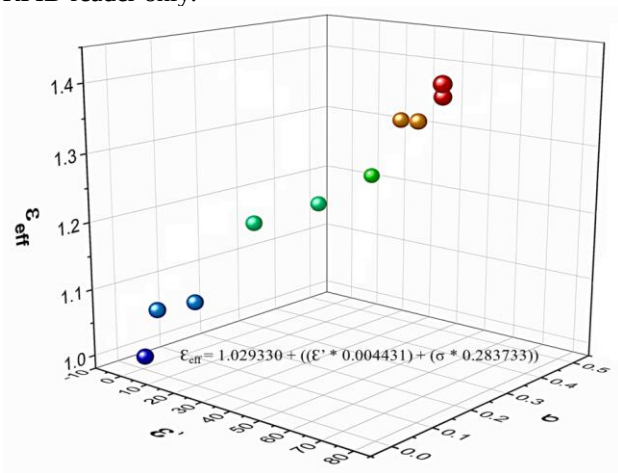

Fig. 7 XYZ plot of dielectric properties of the ethanol calibration solutions used within the experiment for the glass petri plate with 20 mL of each solutions from Table II. Comparison of calculated effective permittivity and measured standard permittivity and conductivity of solutions. A multivariate regression was used to determine the relationship between the effective permittivity and the relative permittivity and conductivity. Both conductivity (σ) and relative permittivity (ε') affect effective permittivity (ε_{eff}). The adjusted R-square value showed a correlation of 0.97 with a high significance (2.24e-6).

D. Interpolation of "Unknowns"

There is a clear differentiation between the standardization mixtures (Fig. 6) particularly when comparing relative permittivity or effective permittivity against resonant frequency (Fig. 8). In this instance, relative permittivity with linear regression produces an R^2 value of 0.825 while effective permittivity gives an R^2 value of 0.994 (Fig. 8). This shows that resonant frequency only has an acceptable correlation with effective permittivity and not relative permittivity on its own. All three curve fit equations plotted in Figs. 7 and 8 allow for the determination of dielectric properties of a solution from only the calculated effective permittivity without the need for additional equipment other than a UHF RFID reader.

It is possible to estimate an unknown solution's dielectric properties and resonant frequency by using the effective permittivity standard curve presented in this paper, (Figs. 7 and 8 (A)). To examine this, all the solutions in Table I were re-measured due to the increase in ambient temperature (294.13K to 297.45K) as temperature is known to affect dielectric properties [18]. This led to a slight shift in the effective permittivities for solutions in Table I (referred to as the "unknowns" for comparison reasons). The values in Table III indicate that the system was affected by the change in temperature between the two reading sets as expected. However, the correlation between the standard dielectric testing

system (SPEAG Dak 3.5 probe system) and the presented sensor design showed high accuracy. It is expected that dielectric properties would change with temperature that is why all dielectric measuring equipment (such as the SPEAG Dak system) available on the market require a calibration step for temperature.

For example, butanol shows an effective permittivity (ε_{eff}) of 1.131, making the dielectric properties between 75% and 50% xylene (Table II). By utilizing the equations plotted in Figs. 7 and 8, it is possible to produce a calculated relative permittivity of 6.55 and calculated conductivity of 0.26 $S \cdot m^{-1}$. This is within 0.26 of the measured permittivity (ε'_m) and 0.04 $S \cdot m^{-1}$ of the measured conductivity (σ_m) of the butanol values measured at 297.45K (Table III). Also, it should be noted that with the change in temperature, acetone (ε_{eff} = 1.253) and ethanol (ε_{eff} = 1.238) were distinguishable from each other. By repeating this for all the other measured liquid dielectric and resonance values within Table I, it is possible to determine that the current system (when using only effective permittivity) has a calculated accuracy of ± 0.834 relative permittivity and ± 0.050 $S \cdot m^{-1}$ conductivity when looking at the correlation between the standard Dak dielectric measurement probe system and the presented sensor design.

It should be noted that acetone values were excluded for the conductivity calculation of the mean absolute deviation (MAD) as the proposed system cannot differentiation below a conductivity of 0.096 $S \cdot m^{-1}$ as seen with the lack of differentiation between 75% and 100% xylene standards. The same was done for permittivity values where methanol was excluded due to being an outlier but if methanol values were included then the average deviation would still only be within ± 2.2 relative permittivity; this is equivalent to an R^2 value difference of 0.9997 versus 0.986 (respectively) with linear regression analysis.

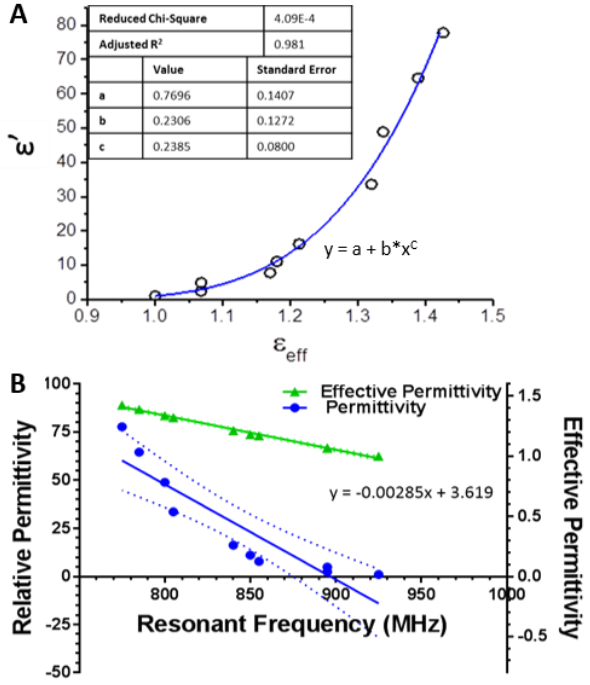

Fig. 8 (A) The relationship between effective permittivity and relative permittivity. No linear relationship exists, but by using an allometric model, there exist a power relationship where 'x' (relative permittivity) is proportional to 'y' (effective permittivity), when 'x' is set to a power 'c' multiplied by 'b' and combined with 'a'; a significant R^2 value of 0.981 is shown. (B) Standard curve of effective permittivity and relative permittivity against resonant frequency. Calculated effective permittivity exhibits a clear linear relationship with resonant frequency (p value < 0.05; R^2 = 0.994) while the relationship between measured relative permittivity and resonant frequency alone is not significant (p value > 0.05; R^2 = 0.825). Included equation corresponds with a linear regression for effective permittivity to help interpolate unknown samples.

TABLE III
DIELECTRIC PROPERTIES OF THE SIX "UNKNOWN" LIQUIDS USED WITHIN THE EXPERIMENT (297.45K)

Liquid	ε'_m	σ_m *(S/m)*	ε_{eff}	*Calc. ε'*	*Calc. σ (S/m)*	*Error ε'*	*Error σ (S/m)*
DI Water	77.8 ± 0.09	0.169	1.426	80.44	0.142	+2.64	-0.027
Methanol	31.5 ± 0.24	0.38 ± 0.02	1.327	40.43	0.418	+8.93[a]	+0.038
Ethanol	16.2 ± 0.19	0.483 ± 0.001	1.213	15.52	0.405	-0.680	-0.078
Acetone	22.39 ± 0.05	0.055 ± 0.001	1.253	22.30	0.440	-0.090	+0.385[a]
1-Butanol	6.29 ± 0.007	0.218 ± 0.001	1.131	6.55	0.255	-0.260	+0.037
Xylene	3.5 ± 0.23	0.16 ± 0.001	1.068	3.00	0.094	-0.500	-0.066
Air	1	0	1	x	x	x	x
Mean Absolute Deviation (MAD)	x	x	x	x	x	0.834	0.05

Calculated dielectric properties from effective permittivity in comparison to SPEAG Dak system measured values. Read with the Dak system at 860 MHz frequency. Symbol 'a' shows outliers excluded from MAD calculation.

TABLE IV
CST SOFTWARE SIMULATED DIPOLE TUNING

Type	**Bottle**				**Petri**			
	ETSI 865.6 - 867.6 MHz		**FCC 902 – 928 MHz**		**ETSI 865.6 -867.6 MHz**		**FCC 902 – 928 MHz**	
	Right	*Left*	*Right*	*Left*	*Right*	*Left*	*Right*	*Left*
Air	108	120	X	X	110	122	X	X
Acetone Ethanol	94	106	82	94	93	105	85	97
Methanol	92	104	80	92	90	102	80	92
Butanol	X	X	85	97	X	X	90	102
Xylene	102	114	94	106	105	117	95	107
Water	78	90	70	82	72	84	66	78

CST simulation adjusted lengths (mm) of each dipole side to fit a single UHF RFID reader within the EPC 18000-6C RFID regulations. The 'X' notes chemicals that do not require any additional tag tuning to fit suggested frequency band.

E. Single Frequency

As this design is ultimately a dipole antenna, it is easily tunable to fit any chemical by a simple tuning approach. Also, due to this design's sensitivity to minute changes in dielectric properties, it could potentially be used to detect chemical contamination within these closed glass systems as in Fig. 5 (ethanol was diluted with DI water). Therefore, it should be possible to utilize a single UHF frequency by adjusting the dipole lengths of this design to fit any regional frequency regulations for UHF antennas. Table IV shows just such

changes needed to match the frequencies within either the ETSI or FCC EPC Class 1 Gen 2 ISO18000-6C RFID requirements. In the future this could allow for any chemical to be tested for contamination or purity within a closed bottled system as long as the tested dielectric properties fall within the known sensing parameters (seen in Sections IV (A) through (C)).

CONCLUSION

A concept for liquid chemical identification was proposed and evaluated based on the shift in the resonant frequency of an applied UHF RFID chipped tag. There was a good correlation between the measured results with the presented sensor design in comparison to a standard dielectric identification system (SPEAG Dak 3.5 probe system) currently available on the market. To our best knowledge this is the first chipped passive UHF RFID sensor design for liquid identification and dielectric measurement capable of being utilized with a minimum of a 2 meter read range for both low and high permittivity liquid solutions.

If all values within an identification system are kept stable, effective permittivity can be calculated from the observed resonance frequency shift, and used to differentiate between chemical liquids within both 2 mm and 5 mm borosilicate glass containers at an accuracy of ± 0.834 relative permittivity and ± 0.050 $S \cdot m^{-1}$ conductivity when compared to a standard dielectric measurement system available on the market.

When used within a closed bottle system, this design can differentiate between hazardous chemicals without the need to open the bottle and experience exposure to hazardous vapors. Utilizing a single passive sensor design as well as a single UHF wideband RFID reader (to differentiate all organic liquids as tested); it is possible to determine the dielectric properties of liquid solutions (within the parameters of the calibration curve) without the need of bespoke equipment. It should be noted that the full range of liquid differentiation is aimed at laboratory utilization not for the general market as to detect the full range of dielectric constants (2 to 80 permittivity as shown here) would be outside of the allowable regional frequency regulations for EPC class 1 Gen 2 ISO18000-6C RFID. This is proposed as a cost effective and quick alternative for chemical identification without the need to invest in expensive dielectric testing systems in addition to expensive wideband readers.

For more practical use, this design could be easily tuned in the future to function at a single frequency for any specific liquid chemical as long as that chemical falls within the 2 to 80 permittivity range as described here. Therefore, this design could potentially be used to detect contamination within closed vessels as long as the dielectric changes are above the sensitivity of the described system. This sensor tag would be ideal for future 'smart' storage system integration within research facilities or hospitals requiring automatic chemical tracking, easy contamination and/ or chemical identification within large autonomous storage rooms requiring both hand-off and continuous readings via an integrated reader antenna. The tag could also be utilized in a tracking system for closed liquid containers (such as during manufacturing/ shipping of hazardous chemicals) as the presented design is a compact antenna label with good read distances on glass (6 meters in air).

As previously stated, this design is not intended to replace what is currently available on the market, in terms of dielectric property measurements, but rather to present a cheap, easy to manufacture sensor alternative for liquid bulk identification within known parameters using only a single wideband UHF RFID reader antenna or for the detection of dielectric changes (such as contamination) within a liquid by utilizing a tuned version of this design to fit any ETSI band as needed.

REFERENCES

[1] *CDC Emergency Response Card*. Accessed: June 06, 2018. [Online]. Available: https://www.cdc.gov/niosh/ershdb/emergencyresponsecard_29750029.html.

[2] *Thermo Fisher Scientific Butanol Safety Data Sheet*. Accessed: June 06, 2018. [Online]. Available: https://www.fishersci.com/shop. Accessed: 06-June-2018.

[3] A. P. Gregory, R. N. Clarke, "A review of RF and microwave techniques for dielectric measurements on polar liquids", *IEEE Trans. Dielectrics Electr. Insul.*, vol. 13, no. 4, pp. 727-743, Aug. 2006.

[4] V. S. Pranavsesh and P. Jain, "Study of effect of dielectric superstrate on resonance frequency of patch antenna and measurement of dielectric constant of superstrate", Proc. of International Conference on Computational Techniques in Information and Communication Technologies (ICCTICT), New Delhi, 2016, pp. 575-579.

[5] A. J. Cole, P.R. Young, "Chipless liquid sensing using a slotted cylindrical resonator", IEEE Sensors Journal, vol. 18, no. 1, pp. 149-156, Jan. 2018.

[6] P. S. Bansode, K. Makhija, S. A. Gangal and R. C. Aiyer, "Non-destructive measurement of dielectric constant using a 2.4 GHz microstrip patch antenna," Proc. of International Symposium on Physics and Technology of Sensors (ISPTS), Pune, 2015, pp. 219-223.

[7] D. Mathur, S. K. Bhatnagar and V. Sahula, "Nondestructive method for measuring dielectric constant of sheet materials," Proc. of IEEE Region 10 Conference TENCON 2011, Bali, Indonesia, pp.1105-1109, 2011

[8] Costa, F., Gentile, A., Genovesi, S., Buoncristiani, L., Lazaro, A., Villarino, R., & Girbau, D. (2018). A Depolarizing Chipless RF Label for Dielectric Permittivity Sensing. IEEE Microwave and Wireless Components Letters, 28(5), 371-373.

[9] H. Lobato-Morales, A. Corona-Chávez, J. L. Olvera-Cervantes, R. A. Chávez-Pérez, José Luis, "Wireless Sensing of Complex Dielectric Permittivity of Liquids Based on the RFID," IEEE Transactions on Microwave Theory and Techniques, vol. 62, no. 9, pp. 2160–2167, Sep. 2014.A. Lazaro et al., "Chipless Dielectric Constant Sensor for Structural Health Testing," IEEE Sensors Journal, pp. 1–1, 2018

[10] Lazaro, A., Villarino, R., Costa, F., Genovesi, S., Gentile, A., Buoncristiani, L., & Girbau, D. (2018). Chipless Dielectric Constant Sensor for Structural Health Testing. IEEE Sensors Journal.

[11] M. Abdolrazzaghi, M. Daneshmand, and A. K. Iyer, "Strongly Enhanced Sensitivity in Planar Microwave Sensors Based on Metamaterial Coupling," IEEE Transactions on Microwave Theory and Techniques, vol. PP, no. 99, pp. 1–13, 2018.

[12] *Voyantic Tagformance Pro*. Accessed: June 06, 2018. [Online]. Available: https://voyantic.com/tagformance.

[13] *Higgs-3 product overview*. Accessed: May 25, 2017. [Online]. Available: http://www.alientechnology.com/products/ic/higgs-3.

[14] S. Zuffanelli, P. Aguilà, G. Zamora, F. Paredes, F. Martín and J. Bonache, "An impedance matching method for optical disc-based UHF-RFID tags," 2014 IEEE International Conference on RFID (IEEE RFID), Orlando, FL, 2014, pp. 15-22.

[15] CST-Dassault Systemes. Accessed: October 10, 2018. [Online]. Available: https://www.cst.com/

[16] SPEAG *Dak 3.5*. Accessed: June 06, 2018. [Online]. Available: https://www.speag.com/products/dak/dak-dielectric-probe-systems/dak-3-5-200-mhz-20-ghz.

[17] *Shell Chemicals Xylene Data Sheet*. Accessed: June 06, 2018. [Online]. Available: https://www.shell.com/business-customers/chemicals/our-products/solvents-hydrocarbon/aromatic-solvents.

[18] B. Abedian and K. N. Baker, "Temperature Effect on the Electrical Conductivity of Dielectric Liquids", *IEEE Trans. Dielectrics Electr. Insul.*, vol. 15, no. 3, pp. 888-892, June 2008.

Adjustable Passive RFID Skin Sticker for Medical Smart Dressings

V. Makarovaite, *Student Member, IEEE*, A. J. R. Hillier, S. J. Holder, C. W. Gourlay, J. C. Batchelor, *Senior Member, IEEE*

***Abstract*— Passive Radio Frequency Identification (RFID) can be limited by such aspects as size that make overcoming the capacitive loading introduced by human tissue difficult when intending to produce an efficient antenna with a high read range. It is still possible to design a small and thin RFID tag with a read range above half a meter. Here we present such a design with a diameter of less than 3 cm. By utilizing a breathable polyurethane polymer with two thicknesses, it is possible to use a single tag design for human tissue (dielectric constants ranging from a 22 to 40) with only a slight loss in antenna read range. It is more cost effective to just adjust the polyurethane thickness for a single design than to tune the antenna design itself. Volunteers one and two had read ranges above one meter while volunteer three (with permittivity of 40) caused the largest shift in antenna resonance from 865 MHz (EU band) and required an increase in polyurethane thickness from 1.1 mm to 1.5 mm. However, both designs still produced read ranges above 0.5 m. By utilizing this design with the Higgs-4 UHD RFID IC adjustment, it can be possible to develop a thin (0.2 mm for 915 MHz or 0.1 mm for 865 MHz) moisture sensor tag capable of read ranges at minimum of 0.5 meters with a minimum detection capability of 10 to 30 µL at 865 MHz and 20 to 50 µL at 915 MHz. Also, this design can function while embedded within near 5 cm of gauze ideal for medical settings as a smart dressing. Ultimately, this led to a passive RFID designs that can be worn by most people with a simple thickness adjustment if needed.**

Keywords— UHF, RFID, Wearable, Antenna, Design

I. Introduction

The use of passive RFID (battery free) antenna designs in such diverse fields as security, warehousing, pharmaceutical, medicine and *etc.* are primarily due to ease of 'install' compared to tethered systems (less obstruction and wiring components). A passive RFID tag functions by receiving a command (a continuous wave) from a reading antenna and then sending back the received data via a backscattered modulation. Passive RFID sensor designs can utilize sensors that function based on techniques such as thickness shear mode, magnetic acoustic resonance, and resonant inductor-capacitor-resistor (LCR) transducers [1]. Also, by understanding the basic idea that a target's appearance (mostly physical and geometrical) can impact the overall antenna impedance matching to the chosen IC chip, most of these designs can be manufactured in a way to become self-sensing systems [2]. A 'self-sensing' approach is appealing as it removes the need for additional sensors or electronic components producing a more cost-effective tag design [2].

Utilizing an etched LRC circuit UHF RFID tag can further reduce the cost (no need for extra components as all components are implemented in the antenna structure) while showing great potential for wearable applications due to the ability to overcome human tissue capacitive loading [3,4]. Compared to HF RFID, the UHF alternative allows for higher efficiency antennas as well as higher data-rates [3] making it the more suitable choice for a sensing design as it allows reader placement to be further away from the wearable tag. The present paper features the matching methods for developing a wearable dipole antenna that could be utilized smart medical dressings. This is because of the sensitivity to any dielectric change upon the attached target as this sensor design was based on a 865 MHz and 915 MHz tuned versions of the design from [5]. This was chosen as it was able to produce read ranges above 4 m even when mounted on liquids with permittivities ranging from 2 to 80 (encompassing most human tissues).

II. Methods

An arm phantom was modelled with CST Microwave Studio ® software [6] and a SPEAG® Dak-3.5 probe system [7] provided dielectric properties of volunteer forearms for any necessary body models. This led to a simplified body phantom design that consisted of a single block of tissue (60 x 60 x 50 mm) with permittivities ranging from 22 to 40 and conductivity ranging from 0.2 to 0.7 S/m at 865 MHz (Table 1). This accounted for bone, muscle, fat and skin [3, 8] in a single block (based on dielectric probe readings) to predict the detuning effect with variable human tissue while reducing simulation meshing with this simplified body phantom design. An RFID wearable tag should be co-designed with the body in mind; the near body effects, mainly capacitive loading, must be accounted for within the calculations for the transponder chip and tag impedance matching as this will cause a large frequency shift and gain drop leading to reduced read ranges and antenna attenuation [3]. This can be accomplished as described in [5] by 'shunting' the system to produce better impedance matching between the IC and the antenna. However, as [5] had already accounted for the need of a shunt when working within the dielectric range of human tissue, this paper only determines what layer of polyurethane or gauze is needed to allow for this design to function when mounted on the human body while providing a respectable read range.

Antenna read range determines RFID system performance quality and minimum 'wake-up' power needed to activate an RFID IC. The maximum read range is determined by:

$$r_{\max} = \frac{\lambda}{4\pi}\sqrt{\frac{QG_{rd}G_{tg}P_{rd}}{P_{th}}} \quad (1)$$

where G_{rd} is the reader antenna gain; G_{tg} is the gain of the tag; Q is impedance mismatch factor between the tag and IC; λ is the reader transmitted frequency; P_{rd} is the reader transmitted power; and P_{tg} is the received power by the tag [9]. Only changes to G_{tg} or Q can be made as all other system aspects

are pre-set and cannot be adjusted due to the antenna reader limitations and RFID frequency band regulations within countries [8].

TABLE I. DIELECTRIC PROPERTIED OF VOLUNTEER FOREARMS INCOMPARISON TO BMI

Volunteer	SPEAG Dak Probe Measured Dielectric Properties (865 MHz) [a]		
	Relative Permittivity, ε_r (294.25 K)	***Conductivity, σ (S/m)***	***BMI***
1	22	0.27	20.6
2	30	0.42	27.2
3	41	0.67	24.6

[a.] No variability was seen within three replicates for each volunteer

A. Antenna Design:

The copper etched dipole antenna was matched to a Higgs-3 Gen 2 RFID IC with an impedance of 27-j216 Ω [10] by utilising a matching resonating loop and an adjustable polyurethane layer for resonance within the EU UHF range (865 MHz) (as described in [5]). The final design was around 30 mm in (Fig. 1) [5]; sides had total lengths of 88.6 mm and 80.6 mm, with a total dipole length slightly above (adjusted for meandering) the 160 mm needed for half-wave dipole resonance at 865 MHz. Polyurethane was attached with a negligible layer of glue onto the mylar layer (glue thickness less than 5µm).

B. Polyurethane Design Read Distance:

Three volunteers were chosen for testing as they represented an appearance of normal to muscular body types covering a wide tissue dielectric range (ε_r of 22, 30 and 40) (Table 1). In order to reduce the need for tag tuning for each volunteer, two polyurethane thicknesses were tested to provide a minimum of 0.5 m read range (for all volunteers) at 865 MHz for both simulation and measurement; this provides a minimum read range necessary for design to be read from the bedside or door reader and *etc*. This decision was based on the effect of tag decoupling from the skin with increased polyurethane thickness (simulated as lossy silicone within CST) [11]. A balance between read range and tag thickness (*i.e.* how cumbersome the design was) had to be struck; it was decided that sacrificing read range to produce the thinnest possible design was preferable for a wearable tag.

All measurements were conducted in triplicates using the Voyantic TagformancePro RFID antenna measurement system [12]. The antenna reader was set to frequency sweeps (between 800MHz to 1000MHz) with 5 MHz intervals and power (from 0dBm to 30dBm) sweeps with 0.1 dBm intervals. The system was calibrated for a 30 cm distance between the reader and tag which was maintained between all readings.

TABLE II. DIELECTRIC PROPERTIED OF VOLUNTEER FOREARMS FOR MOISTURE SENSING

Volunteer	SPEAG Probe Measured Dielectric Properties					
	Relative Permittivity, ε' (294.25 K)		***Conductivity, σ (S/m)***		***tan(δ)***	
	915 MHz	865 MHz	915 MHz	8655 MHz	915 MHz	865 MHz
1	20.3	22.2	0.18	0.22	0.19	0.20
2	31.4	26.2	0.42	0.30	0.28	0.23
3	36.6	37.4	0.56	0.57	0.32	0.32
4	27.7	25.8	0.30	0.26	0.23	0.21
5	34.0	34.4	0.42	0.43	0.26	0.26
6	31.8	31.9	0.43	0.43	0.28	0.28
7	22.0	24.2	0.27	0.27	0.21	0.22

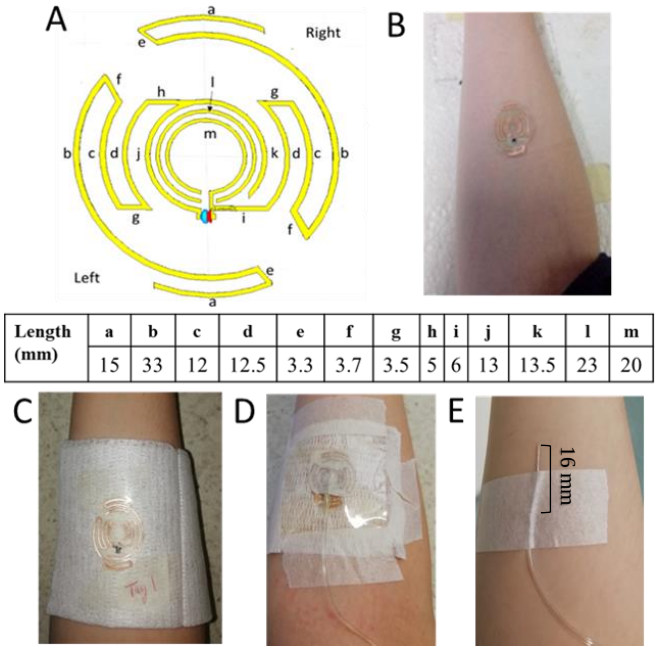

Length (mm)	a	b	c	d	e	f	g	h	i	j	k	l	m
	15	33	12	12.5	3.3	3.7	3.5	5	6	13	13.5	23	20

Figure 1. A) Dimensions (mm) of an on-skin antenna sticker design with the Higgs-3 IC; B) Copper etched tag on mylar with a polyurethane layer and skin; C) Copper etched tag on mylar with a cotton gauze layer and skin; D) Saline IV line with a 16 mm 'needle' through center of design and medical paper tape; E) View of 'needle' and saline IV line which was adjusted to penetrate through sensor and gauze center.

C. Moisture Sensing Adjustment:

In order to add moisture sensing capability to the skin tag and to increase the IC sensitivity, the presented design was matched to the Higgs-4 IC chip (23Ω -j120) [13] at 915 MHz (Fig. 1C). With a change to a more sensitive IC, it allowed the substrate material to be adjusted to cotton gauze (dielectric constant near 2.2) [14]. This involved selecting a gauze thickness of 0.2 mm (915 MHz) or 0.1 mm (865 MHz) between the skin and tag to achieve good matching. However, the overall antenna design remained the same as Fig. 1A. To properly determine the function of the tag, volunteer numbers were increased in order to assess a wider range of tissue dielectric properties (Table 2). Pure water was used for the moisture sensing with the cotton gauze as the absorbent material. The same body location (forearm) was used for moisture sensing as indicated in Fig.1. When an IV line was included, the liquid was switched to a medical grade (0.9% sodium chloride) saline solution (Fig.1 D). A steel wire (equivalent to an 18-gauge needle) was used to mimic an IV line inserted through the open center of the sensor to detect IV leaks and the effect of the IV line and steel metal 'needle' (Fig.1 D and E). Finally, porcine blood was added to understand the moisture sensing capabilities for human analogue bodily fluids.

III. RESULTS

It was expected that with increasing permittivity of body tissues (as seen between the volunteers), there would be a downward shift in resonant frequency (*i.e.* increase in permittivity leads to decrease in resonant frequency) if no adjustments were made to reduce the capacitive loading effect of the body [4]. Tuning adjustments can be easily

achieved by adjusting either the polyurethane or cotton gauze thickness.

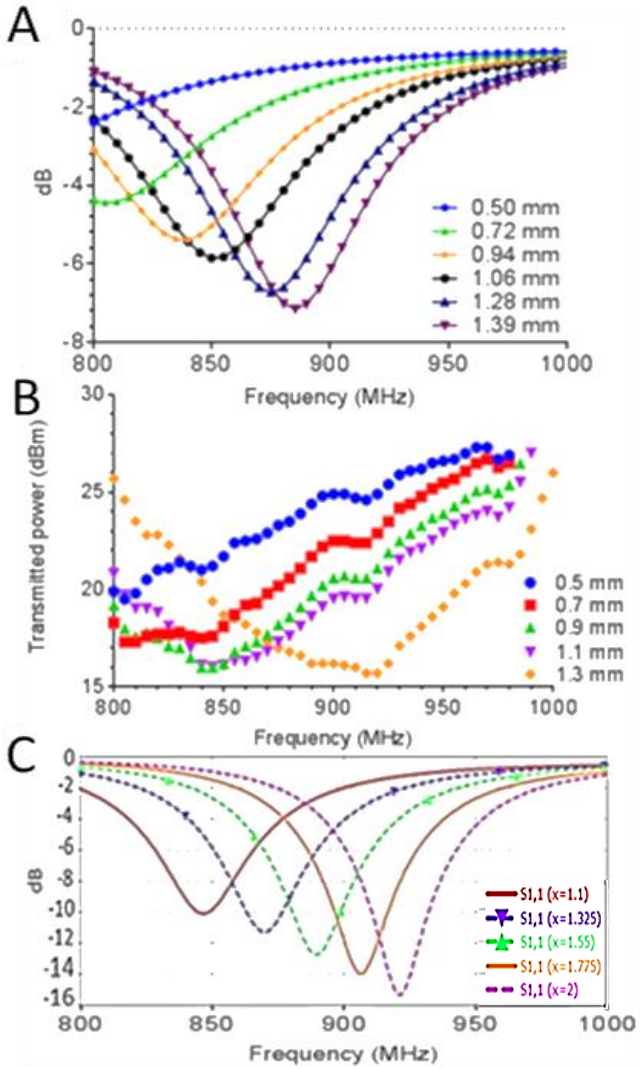

Figure 2. Effect of polyurethane thickness on RFID tag preformance for: (A) Volunteer 1 S_{11} simulation, (B) Volunteer 1 measured resonant frequency for comparison to simulation, and (C) CST simulated S_{11} for Volunteer 3 to determine the necessary thickness of polyurethane to match 865 MHz. Value 'x' represents the polyurethane thickness in milimeters for the simulated design.

A. Necessary Polyurethane Thickness Adjustment:

Increasing the polyurethane thickness is a simple solution for reducing the tag and skin coupling effect in order to bring the read range above 0.5 m (corresponding to a measured transmitted power below 22 dBm), Fig. 2. The required polyurethane thickness values were 1.1 mm for Volunteers 1 and 2, and 1.5 mm for Volunteer 3 (Fig. 3); The permittivity of Volunteer 3 indicated a need for a polymer thickness between 1.3 and 1.6 mm to achieve a match at 865 MHz while Volunteer 1 needed 1.1.mm thickness. Simulation indicated a directivity of 1.89 dBi at 166° main lobe direction (Fig. 3) suggesting a unidirectional appearance with a slight center offset and a 1.43 m CST simulated read range with a total efficiency of near -7 dBi. It was expected to see power dissipation within human tissues leading to reduced antenna total efficiency and in practice, values better than -20dB total efficiency can be considered usable for body mounted RFID wearables with read ranges of 0.5 m or more. However, it should be noted that the total efficiency seen within all designs did not fall below -14 dB.

The measured read range at 865 MHz for Volunteer 1 was 1.49 m suggesting that the simulated tag sensitivity of -17 dBm slightly underestimated the actual tag sensitivity when body mounted (Fig. 4). Overall, there was a good correlation between the simulated resonant frequencies and measured resonant frequencies for each volunteer (Fig. 4). At 865 MHz, the read range for each permittivity was 1.49, 1.23m and 0.63 m (ε_r = 22, 30 and 40, respectively), Fig. 4 (B). Volunteer 1 with the lowest permittivity and BMI, had the highest read range with Volunteer 3 having the lowest read range.

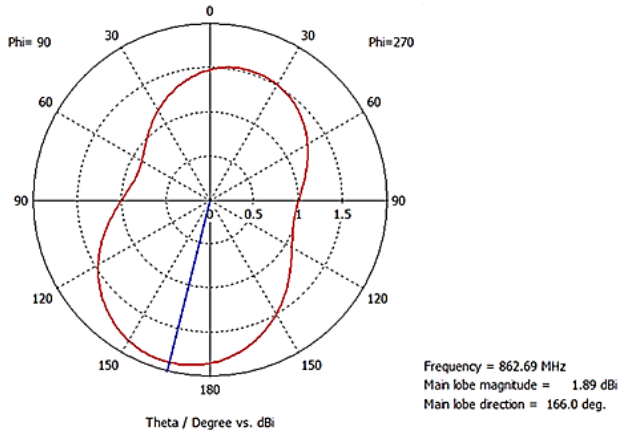

Figure 3. Simulated polar plot for antenna directivity cut at phi 90° when mounted on body of volunteer one with a unidirectional appearance at a main lobe directivity of 166°.

The data in [4] showed that an increase in muscle content corresponds to increased dielectric properties (permittivity and conductivity) causing increased attenuation and reduced read ranges for RFID systems. Increased conductivity reduces antenna-IC matching and efficiency while permittivity effects the resonant frequency rather than efficiency [4]. This is understandable as pure muscle has a dielectric constant near 60 [11] causing Volunteer 3 to exhibit the largest frequency shift (without a polyurethane thickness adjustment) (Fig. 2 C).

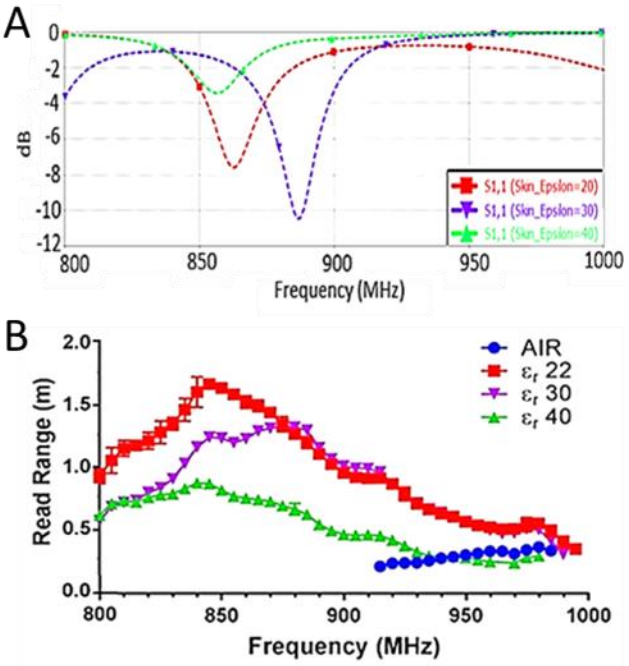

Figure 4. A) Simulated S_{11} (tag input reflection coefficient) mounted on body model. Simulation accounted for both permittivity and conductivity of each volunteer. B) Measured read range for tag mounted on volunteers.

Polyurethane thickness of 1.1mm (ε_r = 22 and 30) or 1.5mm (ε_r = 40) in both A and B. Measured data represents three replicates each.

The present data correlates with [4] as there was a noticeable decrease in read range between Volunteer 1 and 2, and then 3 as the dielectric constant increased. Therefore, as tissue dielectric properties increase, so should the polyurethane thickness in order to reduce the antenna detuning by the increased tissue capacitive loading. Decoupling an RFID tag from skin is a priority if attempting to achieve a higher read range. To exhibit the medical practicality of this sensor design as it was shown to produce read ranges above 0.5 m on all volunteers, the design was adjusted to function on medical gauze (cotton) and within both the EU and US frequency bands.

B. Moisture Sensing:

In total seven volunteers were used to determine the function of the moisture sensor with the addition of a more sensitive IC (change from -17dBm to -18.5dBm) [13]. Within the US UHF frequency band (near 920 MHz), all volunteers with a dry tag of 0.2 mm thickness were able to achieve a minimum of 1 m read range (Fig. 5A). When looking at EU UHF frequency, the gauze layer needed to be reduced to 0.1 mm in order to tune the tag resonance towards 865 MHz. Even with the reduction in the gauze layer thickness, the tag was still able to achieve a minimum of 0.5 m read range for all volunteers (Fig. 5B). It should be noted that the thinner gauze layer showed a greater variability in read range for all volunteers (Fig. 5 C).

Volunteers 7 and 5 were chosen to assess the effect of an increase in moisture amount as they represented maximum and minimum read ranges at both 865 MHz and 915 MHz, Fig. 6; volunteer 7 showed the best-read range for both the EU and US frequency bands. The detection moisture level for the design with 0.2 mm gauze layer was 20 µl to 100 µl for volunteer 7; the 10 µl did not show any measurable change in read range at 915 MHz for volunteer 7 while there was a detectable change for volunteer 5 (Fig. 6B). For the 0.1 mm thickness at 865 MHz, the detection sensitivity increased to 10 µl; however, the minimum read range for volunteer 5 could only be detected till 30 µl. Based on Volunteer 5 readings at 915 MHz, the moisture detection level could only be able to detect an increase within the first 50 µl as a decrease in read range of 0.2 m might be outside of the usable detection range. Therefore, it would be advisable to utilize this system with the US frequency band or limit the detection with the first 30 µl for utilization within both the EU and US frequency bands. Nevertheless, the results show usable read ranges for both extremes of body type.

When the tag was allowed to fully dry after the addition of the 100 µl of fluid, the tag returned to the original read range for all frequency adjustments. This suggests that the design could be reusable. When a standard IV line was inserted with a steel 'needle' through the open center of the sensor design, there was a small loss in the read range of the design however there was no noticeable change in the peak resonant frequency (Fig. 6 A and B). When the addition of saline was repeated from 10 µl to 50 µl and 100 µl at the point of IV-line insertion (Fig. 6), the exact same trends were seen as with the previous addition of DI water with a slight loss in read range for both frequency bands. This suggests that both the metal needle and polymer IV line had a limited effect on the function of the smart dressing. This would allow the sensor to detect IV-line leaks with as little as 10 µl of spillage within the EU band and 20 µl with US band. Also, as there was no noticeable variability between saline and DI water, suggest that this smart dressing could be usable with a variety of medical solutions. With the addition of porcine blood, similiar results to saline were seen. Detection below 30 µl at 865 MHz and below 50 µl at 915 MHz showed best results with an interpolated best fit line having an R squared value of less than 0.9 at 865 MHz for Volunteer 7 (Max) (Fig. 6D). If the 100 µl value is excluded then the R square value is adjusted to 0.8, suggesting improved fit.

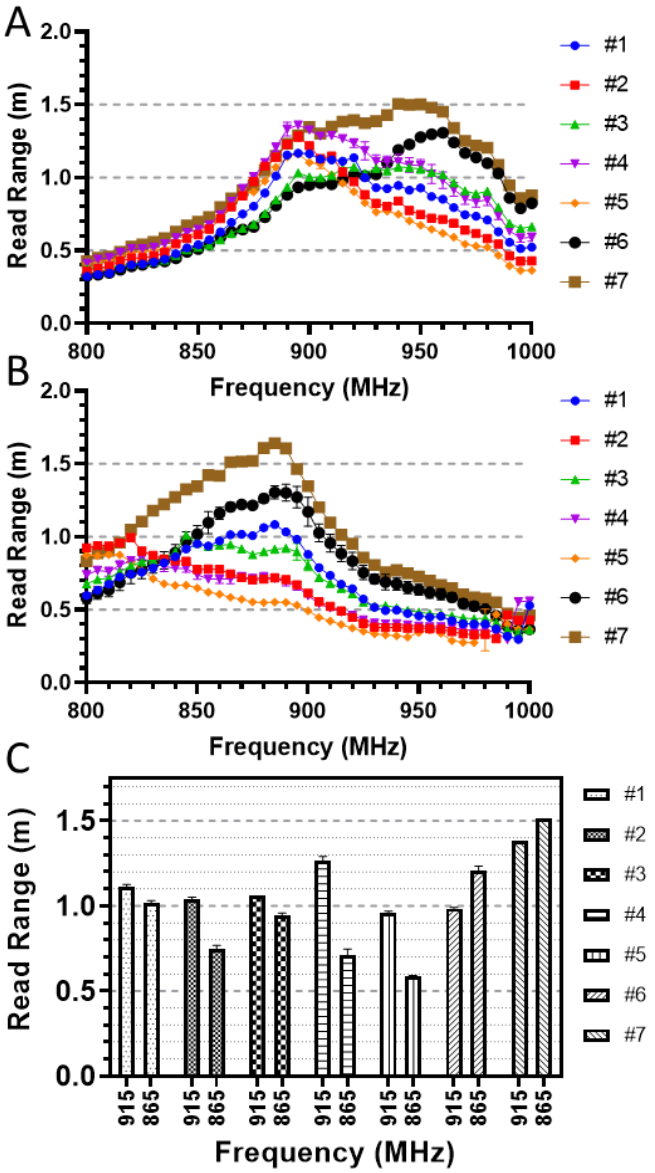

Figure 5 Measured read ranges for moisture tag mounted on seven volunteers with: A) 0.2 mm cotton gauze backing, B) 0.1 cotton gauze backing and C) difference between 865 MHZ and 915 MHz measurements of dry tag application. Measured data represents three replicates each with no noticeable variation present.

Finally, up to 4.8 mm of additional gauze can be placed over the tag (while the backing layer is kept at 0.1 mm between the skin and tag) before any noticeable loss in read range occurs (Fig. 7). This suggests the design could be used within medical gauze to determine changes in moisture within the enclosed area such as is seen with accidently opened stiches

or pulled out medical/ IV lines. Also, if incorporated into sanitary dressings, it should be possible to detect incontinence as soon as it occurs aiding with personal hygiene and care with continuous readings.

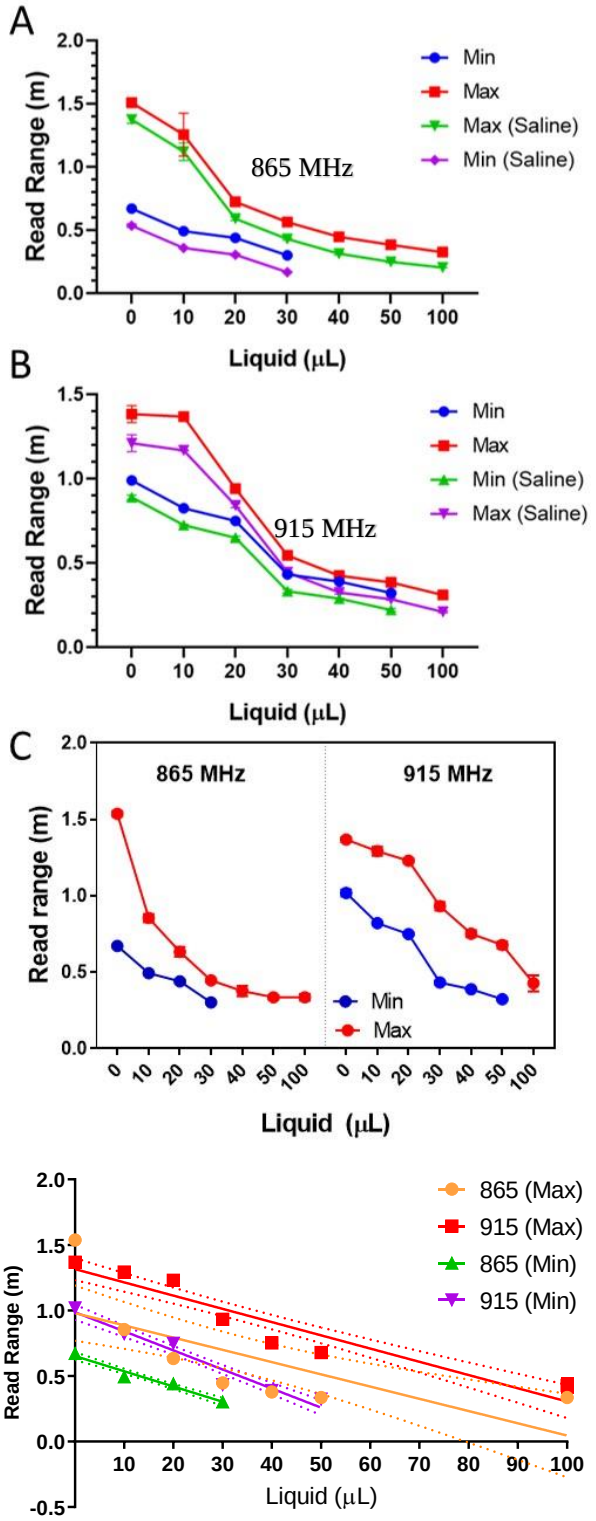

Figure 6 Measured read range of moisture sensing tag with increasing liquid amount with A) 0.1 mm (865 MHz) and B) 0.2 mm (915 MHz) cotton gauze backing (shown Volunteers #1 (max) and #5 (min)) while C) exhibited the addition of porcine blood. D) exhibits the interpolated line of best fit to determine the linearity of the detection capabilities for porcine blood. Moisture level was increased in 10 µl increments (from 0 to 50 µl and then 100 µl). All samples were allowed to dry and were re-read, they exhibited no difference to the original 0 µl readings. Measured data represents three replicates each with no noticeable variation.

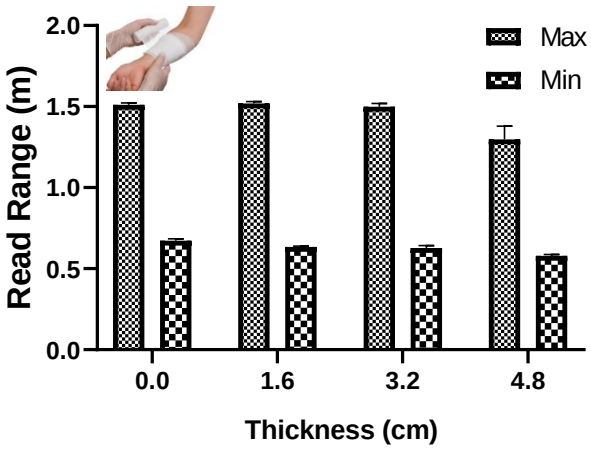

Figure 7 Measured effect on read range based on the addition of gauze placed over the tag for volunteer #1 (max) and #5 (min) of Table II at 865 MHz. Substrate gauze was set to 0.1 mm for a 865 MHz reading with the EU frequency band. Measured data represents three replicates each with no noticeable changes.

IV. CONCLUSION

The wearable skin-mounted tag designs were made to utilize the dielectric properties of human tissues to reduce size without detuning the tag due to loading from the skin's high dielectric properties. These small thin designs were able to produce read ranges above 0.5 m for all volunteers (with permittivities from 20 to 40). Although read range remained above 0.5 m, there was a decrease for the higher permittivity volunteers with polyurethane use; however, any permittivity below 30 produced a read range above 1.2 m. Also, once the tissue dielectric properties were above 30, there was a need to increase the polyurethane layer thickness to help decouple the tag from the skin. This means that highly muscular individuals tend to require thicker polyurethane substrate tags.

When applied to moisture sensing by changing to the Higgs-4 IC, the tag is able to function above 1 m read range for a wide range of volunteers at 915 MHz. It is able to detect a minimum of 20 µl of fluid useful as a medical dressing. When utilizing the same design for EU frequency band, there is a need to use a thinner gauze layer (0.1 mm) to achieve frequency resonance above 0.5 m at 865 MHz for all volunteers. When incorporated with an IV-line or the addition of porcine blood and saline, there was no significant variation to the function of the smart dressing. Also, multiple re-drying sessions should be a done in order to determine when a frequency shift or read range drop will occur. With the addition of the ability to function while embedded with almost 5 mm of cotton gauze, this current published design can be utilized for low cost, minimal signal outage and unobtrusive application for human mounted care needs. Further study of the effects of various body fluids would be advantages as a more universal smart medical dressing.

ACKNOWLEDGMENT

This work was funded by the UK Engineering and Physical Science Research Council (EPSRC). Conflict of interest: None declared.

REFERENCES

[1] R.A. Potyrailo, N. Nagraj, Z. Tang, F.J. Mondello, C. Surman, W. Morris. "Battery-free radio frequency identification (RFID) sensors for food quality and safety", Journal of agricultural and food chemistry, 60, pp. 8535-43, (2012).

[2] G. Marrocco 1, F. Amatoali. “Self-sensing Passive RFID: from Theory to Tag Design and Experimentation.” Proceedings of the 39th European Microwave Conference.

[3] M.A. Ziai, J. C. Batchelor, “Temporary On-Skin Passive UHF RFID Transfer Tag”, IEEE Transactions On Antennas And Propagation, Vol. 59, No. 10, October (2011).

[4] D. O. Oyeka, J. C. Batchelor and A. M. Ziai, "Effect of skin dielectric properties on the read range of epidermal ultra-high frequency radio-frequency identification tags," in Healthcare Technology Letters, vol. 4, no. 2, pp. 78-81, (2017).

[5] V. Makarovaite, A. J. R. Hillier, S. J. Holder, C. W. Gourlay and J. C. Batchelor, "Passive Wireless UHF RFID Antenna Label for Sensing Dielectric Properties of Aqueous and Organic Liquids," in IEEE Sensors Journal. [Online Early Access]

[6] Dassault Systemes, “CST- Computer Simulation technology”. Available at www.cst.com, accessed: March 06, 2019. [Online]

[7] SPEAG, “DAK - Dielectric Assessment Kit Product Line”. Available at speag.swiss/products/dak/dielectric-measurements, accessed: March 06, 2019. [Online]

[8] Q Duan, J H Duyn, N Gudino, J A de Zwart, P van Gelderen, “Characterization of a Dielectric Phantom for High-Field Magnetic Resonance Imaging Applications,” Medical Physics, 41 (10), pp.102303-6, (2014).

[9] B. D. Braaten and R. P. Scheeler, “Design of Passive UHF RFID Tag Antennas Using Metamaterial-Based Structures and Techniques,” Radio Frequency Identification Fundamentals and Applications, Design Methods and Solutions, February, pp. 51–68, (2010).

[10] Alien Technology, “Higgs-3 product overview”. Available at www.alientechnology.com, accessed: 25 May 2018. [Online]

[11] ItIs Foundation, “Dielectric Properties database”. Available at /www.itis.ethz.ch, accessed: 5 June 2018. [Online]

[12] Voyantic, “Tagformance Pro”. Available at http://voyantic.com/products/tagformance-pro, accessed: June 06, 2018. [Online]

[13] “Higgs 4 RFID IC.” Alien Technology, www.alientechnology.com/products/ic/higgs-4/.

[14] Sankaralingam S; Gupta B. Determination of Dielectric Constant of Fabric Materials and Their Use as Substrates for Design and Development of Antennas for Wearable Applications. IEEE Transactions on Instrumentation and Measurement. 2010; 59 (12); 3122 – 31

Monitoring *Candida albicans* Biofilm Formation by Impedance Using Passive RFID

V. Makarovaite, *Student Member, IEEE,* A. J. R. Hillier, S. J. Holder, C. W. Gourlay, J. C. Batchelor, *Senior Member, IEEE*

Keywords: RFID, Sensor, Yeast, Biofilm, Dielectric Properties.

Abstract

Medical implants are routinely colonized by microbial biofilms especially yeast biofilms such as those formed by *Candida albicans*. As medical implants move towards smart technology and IoT, it is more important than ever to understand the electrical properties of biofilm formation. Here we present an attempt at understanding how *C. albicans* biofilm formation effects sensor technology. We propose that *C. albicans* biofilm formation increases hydrophobicity causing a noticeable decrease in conductivity leading to impedance mismatch that can be detected by measuring impedance. We show that a *C. albicans* biofilm changes its dielectric properties during maturation and, once mature, can be equated to a thin polymer layer as it loses detectable conductivity. We demonstrate that these properties can be used to enable constant monitoring of a *C. albicans* biofilm using passive RFID, offering a new detection methodology that may be applied to surfaces known to be readily colonise.

I. INTRODUCTION

Surface colonisation of implant material account for 20-25% of primary complications [1], which with a 2023 projection for the global market in the medical implant sector exceeding US$140 billion with a US$3.9 billion increase on next generation implants alone [2, 3] could develop into a serious strain on the global healthcare system. Colonisation often leads to microorganism biofilm formation, where multiple (or singular) species adherence to a material surface causes extracellular matrix formation, which can even multiply to a 300 (or more)-micron thickness [4]. Bacterial and fungal organisms can be found within mixed biofilms that form on medical devices. The most common yeast species associated with biofilm formation and implant failures is *Candida albicans* [4]. *S. aureus* has been widely recognised as an implant coloniser, particularly on titanium surfaces [5] while *Candida albicans* biofilms prefer colonisation of medical polymers [6]. Biofilm formation is clinically relevant as it allows microorganism(s) to become resistant to most drug interventions and the host immune system further necessitating removal of implant [6].

C. albicans biofilms are known to evade reactive oxygen species triggering and neutrophil killing within the host [7], to secrete aspartic proteases to avoid human complement attack [8] and other evasion methods that have been previously reviewed [4, 9]. *C. albicans* biofilms are known to cause over 100,000 deaths annually within the United States alone, and are responsible for 40% of clinical blood infections and 15% of sepsis cases [10].

With the projected increase in next generation implants (or smart implants), it is becoming imperative to understand microbial biofilm formation in terms of electrical properties. Most of the biofilm growth detection systems rely on electrochemical impedance spectroscopy (EIS) which indirectly measure microbial growth by a change in the conductivity of the testing system [11]. There have been impedance studies of *S. aureus* biofilm growth [12-18], however non-EIS impedance methods have yet to be published for *C. albicans* biofilm formation. This paper will try to address this shortfall.

II. METHODS

A. *Candida albicans* Culture Conditions

The clinical isolate type strain SC5314 of *Candida albicans* was cultured on Yeast Extract Peptone Dextrose (YPD) agar (Sigma-Aldrich) with 2% glucose at 37°C for 48 hours. Then the cells were harvested and re-suspended in standard 2% glucose YPD liquid media (Sigma-Aldrich) followed by a 24-hour incubation at 37°C. This allowed for an overnight cell density growth of 10^7 CFU/ml (haemocytometer counted) for the biofilm studies. Cell density was adjusted as needed.

B. Biofilm Growth

For sterilisation, RFID wells were washed with a 70% ethanol solution and after drying, a 30-minute incubation with 50% Fetal Bovine Serum (FBS, Sigma-Aldrich) at 30°C allowed for cell adherence. FBS helps coat the biofilm surface and allows for increased yeast adherence. After the FBS incubation, each well was washed with sterile PBS twice followed with an adhesion phase of 90 minute at 37°C with 1 ml of *C. albicans* (10^7 CFU/ml) in 10% glucose YPD media. After cell adhesion, each well was lightly washed twice with sterile PBS to remove non-adherent yeast cells and refilled with 1 ml of fresh YPD liquid media for a 48-hour incubation at 37°C. The same process was used for xCELLigence detection of biofilm growth (detailed below) except for the sterilisation as all E-plate-units are shipped as sterile closed plates and the use 200 µl rather than 1 ml. xCELLigence standardized growth was then compared to two different RFID sensor designs for the ability to detect impedance changes with *C. albicans* biofilm formation.

C. Assessment of *C. albicans* biofilm growth using the xCELLigence System

The real time cell analyzer (RTCA) xCELLigence (ACEA Bioscience Inc., San Diego, CA) detects growth of eukaryotic

cells due to variations in impedance signals (stated as cell index (CI)) throughout the growth process upon the bottom of the gold-microelectrode E-plates [12]. This system has been previously utilized for biofilm growth detection of *Staphylococcus aureus* with repeatable results and a similar approach was taken for the presented *C. albicans* growth [13, 14]. The RTCA was placed in a 37°C incubator with 5% CO_2 without shaking during biofilm growth. However, due to the use of YPD growth media, the xCELLigence system was calibrated by the use of 200 µl of fresh media to have as the basal CI value of "0". Once the basal value was recorded, the biofilm growth protocol was followed as described. To determine the *C. albican*s biofilm hydrophobicity, 2 µL or 6 µL of zymolyase (100T) was added to the mature biofilm at 24 hours equivalent to 1T and 3T, respectively. Growth of the biofilm correlates to change in detected impedance of the system. It should be noted that in order to determine the accuracy of the change in protocol for biofilm growth and adherence presented, *S. aureus* was utilized along with *C. albicans* and compared to [14]. *S. aureus* was utilized in order to determine the accuracy of biofilm growth using the RTCA as *S. aureus* xCELLigence growth has been previously published [13, 14] while no known xCELLigence biofilm growth publication exists for *C. albicans*.

D. RFID Antenna Designs

Two main antenna designs were used to monitor biofilm growth (Fig. 1). The readily available RF-Micron RFM2100-AER [19] tag which utilises a Magnus-S3 chameleon IC able to adjust capacitance from 2pF to 3pF which can be read as a sensor code reading ranging from 32 to 0 (Fig. 1 A). While the interdigit sensor tag utilises an Alien Higgs-3 Electronic Product Code Class 1 Gen 2 RFID integrated circuit (IC) (31-j216 Ω) [20] mounted on FR4 (Fig. 1 B). To assist in biofilm formation, both tags had a PDMS overlay of 20 µm on the sensor regions and attachment of a square reservoir for the liquid growth media around the sensor region.

E. RFID Measurements and Simulation

CST Microwave Studio ® was used to simulate *C. albicans* growth on the RFID design. The CST antenna models were adjusted with data obtained from the xCELLigence experiments (Fig. 2 and 3) to simulate a nonconductive layer of as a mature biofilm. This was also used to determine transponder chip and tag matching (Table 1) as well as predict the maximum theoretical read range. Antenna read range is the primary judge of RFID system performance and it determines the maximum distance that an RFID IC can be activated by passing the threshold for 'wake-up' power. The maximum read range was calculated by the formula:

$$r_{max} = \frac{\lambda}{4\pi}\sqrt{\frac{qG_{rd}G_{tg}P_{rd}}{P_{th}}} \quad (1)$$

where G_{rd} is the reader antenna gain, G_{tg} is the gain of the tag, q is impedance mismatch factor between the tag and IC, λ is the reader transmitted frequency, P_{rd} is the reader transmitted power and P_{tg} is the received power by the tag [21]. The only flexibility in the system rests with changes to the G_{tg} or q of the system; all other aspects of the calculations are pre-set due to antenna reader limitations or manufacturer guidelines, and country laws dictating frequency use by RFID technology [21].

All RFID measurements were conducted using the Voyantic TagformancePro RFID measurement system in triplicates. The Voyantic system was set to sweep both the frequency (between 800MHz to 1000MHz) and power (from 0dBm to 30dBm) to determine the peak read range values. The *C. albicans* biofilm growth was measured after the removal of excess growth media using a pipette to reduce any stray conductivity not already present within the biofilm.

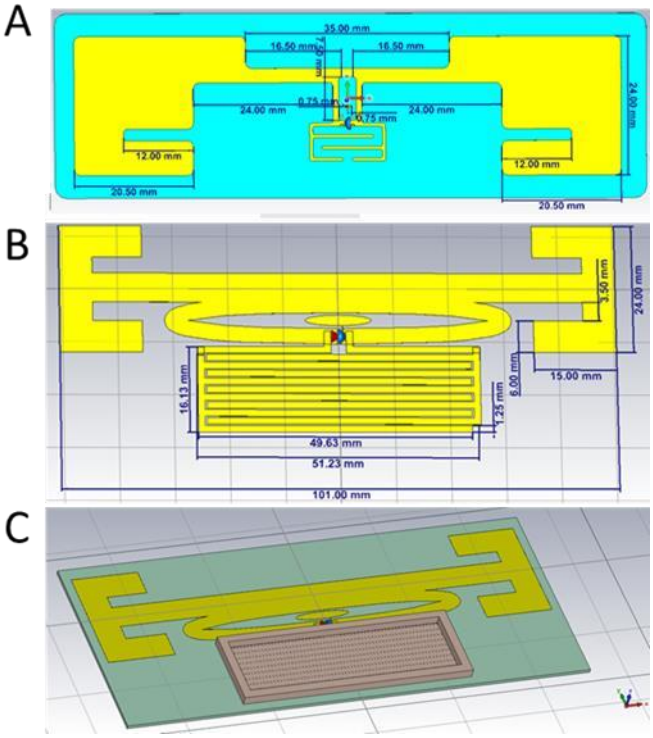

Figure 1 Antenna designs utilized within CST simulation: (A) RFMicron tag, (B) simple interdigit sensor for UHF antenna and (C) representation of the 5 mm height reservoir around the sensor region of (B) allowing for biofilm growth in liquid media.

III. RESULTS AND DISCUSSION

A correlation was observed between the results obtained with the xCELLigence system and the UHF RFID sensors, both of which suggest a link between mature biofilm hydrophobicity on the sensor surface and growth detection.

A. Measurement of biofilm growth using xCELLigence

S. aureus growth was employed to test if the applied biofilm growth protocol would result in the same trends seen for biofilm forming wildtype *S. aureus* strains in [13] and [14]. This current protocol produced repeatable results comparable to [14] as the 0 to 6-hour (min) growth compared to the 18 to 24-hour (max) growth had a similar 0.12 CI difference (same as previously published).

With the xCELLigence RTCA *C. albicans* growth showed a bell-curve appearance peaking at around 18 hours, where change in impedance plateaued before there was a decay of the impedance signal (Fig. 2 A and B). The reversal in impedance after 18h correlated with the formation of an intermediate to mature biofilm under these growth conditions [4-7]. This suggests that some property of the biofilm at this stage of its development leads to a change in capacitance (sensor

impedance) as disruption to the biofilm formation (Fig. 3 A) reverses this decay once the growth plateau is reached. This can be understood from the system calculation of CI values which are the highest capacitance (as well as most conductive) at a basal value of '0' [12]. As capacitance decreases, impedance at a set frequency increases leading to a higher CI value.

Table 1. Simulated changes in impedance on interdigit design with increasing *C. albicans* biofilm thickness at resonant frequency of 800 MHz

Thickness (µm)	Capacitance	Resistance
No growth	1.9e-10	34.9
35	1.2e-12	4.5
57	1.8e-12	0
80	2.0e-12	1.2

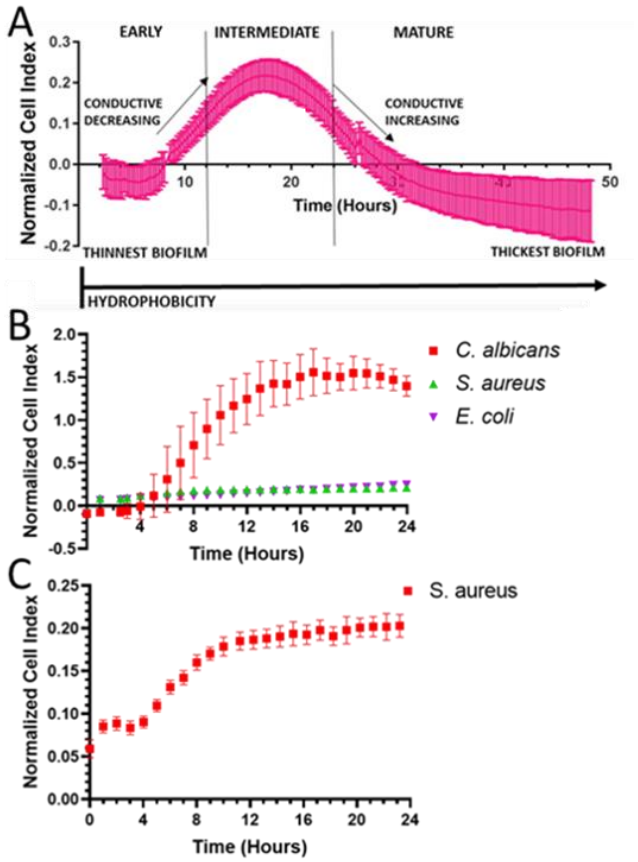

Figure 2 *C. albicans* biofilm growth with the xCELLigence system. (A) *C. albicans* 48-hour growth; the liquid media is represented as the 0 line on x-axis (N=3, n=18). The hours are broken down into early, intermediate, and mature biofilm hours where there is loss in conductivity which occurs starting at 18 hours. (B) 24-hour *C. albicans* growth in comparison to *S. aureus* (n=6). (C) *S. aureus* growth with a 0.10 cell index change (from minimum to maximum cell index values) (n=6). All data was normalized for evaporation and liquid media.

To test cell detachment as a possible cause for the decay seen after 20 hours of growth, zymolyase was utilized to breakdown the yeast cell wall of a biofilm during the maturation phase of growth (post 24h). If cell detachment from the sensor region caused the observed decrease in CI value post 18 hours as suggested in [13] then the addition of zymolyase should cause increased detachment and breakdown of the biofilm and, thus, even faster decay in CI values for zymolyase samples in comparison to the positive growth control. However, the opposite was observed (Fig. 3 A), as zymolyase was added we observed a noticeable increase in the CI value of the xCELLigence system. In comparison to the positive control, addition of zymolyase at 24 hours of growth caused a significant (p-value <0.05) change in biofilm detection starting with 39 hours (3T) and 41 hours (1T) onwards (Fig. 3B). The addition of zymolyase showed that the likely cause of the CI value decrease is due to the lack of interaction between the highly conductive liquid media and sensor region as cell adherence interrupts the sensor basal value leading to a loss in sensor capacitance (decreased impedance and increased admittance). This effect was also observed in growth measurements using UHF RFID (Fig. 6).

After 24h of growth the maturation of a *C. albicans* biofilm leads to deposition of dense matrix material and an increase in overall height [22]. It is possible that changes in electrical properties result from either the properties of the matrix or the size of the biofilm itself. Both may influence liquid conductivity and interaction between the E-plate microelectrodes and the growth media. In support of this, growth media is known to be more conductive than fungal cells themselves [23]; In addition, it is already known that as yeast cell density increases, conductance of growth media decreases [23]. We suggest that biofilm growth packs yeast cells upon the sensor over time causing decreased interaction of the liquid media and sensor leading to a loss in CI signal (change in impedance) which corresponds to change in sensor capacitance. At this point the impedance of the system is adjusted to maintain the system at the pre-set frequency causing a reversal in capacitance.

It is plausible that the removal of conductive growth media (as nutrients are absorbed by yeast cells [4-7]) from the available electrode surface may correspond to some part of the reverse in impedance seen near 20 hours of growth in xCELLigence. This can be seen with the negative controls (media only) as there is a clear decrease in CI value after 20 hours (without any contamination) due to slight media evaporation (Fig. 2 and 3). However, it is more likely that the matrix material deposited by *C. albicans* is responsible for the reversal in observed impedance and CI value. [13] suggested that the change in CI was due to number of adhered cells (increased adhered cells, increased CI value) on the microelectrodes rather than a loss in media conductivity and sensor basal capacitance. It is unlikely that a loss of cell contact with the E-plate sensor occurs at 20 hours as loss of surface contact is not reported at this time and "shedding" of biofilm material takes place following 48 hours of growth for *C. albicans* biofilms. It should be noted that the growth protocol in [13] and [14] used bacteria seeded media rather than only adhered cells, as we have presented, for the biofilm formation and so represent results obtained from a mixture of biofilm and planktonic growth.

Another explanation for the loss in signal may be loss of viability. However, *C. albicans* viability did not reduce over the period of biofilm growth examined as XTT assays performed (after the 48-hour growth in the xCELLigence E-plate) XTT near 2.2 ± 0.4 (Table 2).

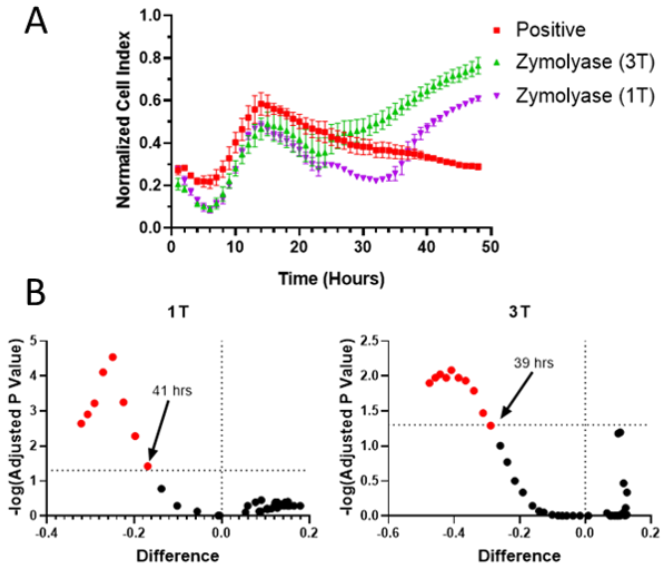

Figure 3 Zymolyase disruption of mature *C. albicans* biofilm growth within the xCELLigence system normalized against media control. A) *C. albicans* 48-hour growth with the addition of zymolyase at 24 hours; B) Volcanic plots showing first hour of significance (p-value < 0.05) with zymolyase (1T or 3T) addition at 24 hours during *C. albicans* biofilm growth in comparison to a positive control. Statistical significance determined using the Holm-Sidak method.

Table 2. XTT assay of *C. albicans* biofilm formation

Type	XTT assay (Average)	Repeats
Negative	0.03± 0.01	24
Positive	2.2 ± 0.4	24
1T Zymolyase	2.0 ± 0.1	5
3T Zymolyase	2.3 ± 0.2	4

B. Sensor Properties

Our simulations of the electric and magnetic fields show that there is an adequate response from the sensor designs to the biofilm growth (Fig. 4). The simulated surface current was able to produce 1731 A/m in current concentrated within the sensor region containing the biofilm at an 868 MHz frequency (Fig. 4 A). The electric field (Fig. 4 B) showed a maximum voltage produced of 879kV/m with the thickest *C. albicans* biofilm included in the simulation (89 µm). The magnetic density equated to 2312 A/ m concerted within the sensor region (Fig. 4 C). Similarly, the RFMicron design also had a good response for the magnetic field (383 A/m (Fig. 4 D)) and surface current (349 A/m (Fig. 4 E)). These suggest that the current design is able to produce good wave propagation.

The simulated antenna directivity and realized gain (Fig 5 A and B, respectively). The directivity of the main lobe for the interdigit sensor UHF antenna was simulated as 1.89 dBi at a phi 90° cut, suggesting that this design has a primarily wide unidirectional appearance; however, it should be noted that the directivity flows in both the x and z axis with the majority of the read range reaching in the z-axis (Fig. 5 A). As for the realized gain of the antenna, the simulation calculated a low gain comparable to an electrically small antenna; though this can allow the antenna to be read from any location within 2 meters (x-axis) to 5 meters (z-axis). A highly directed antenna is not necessary for this study.

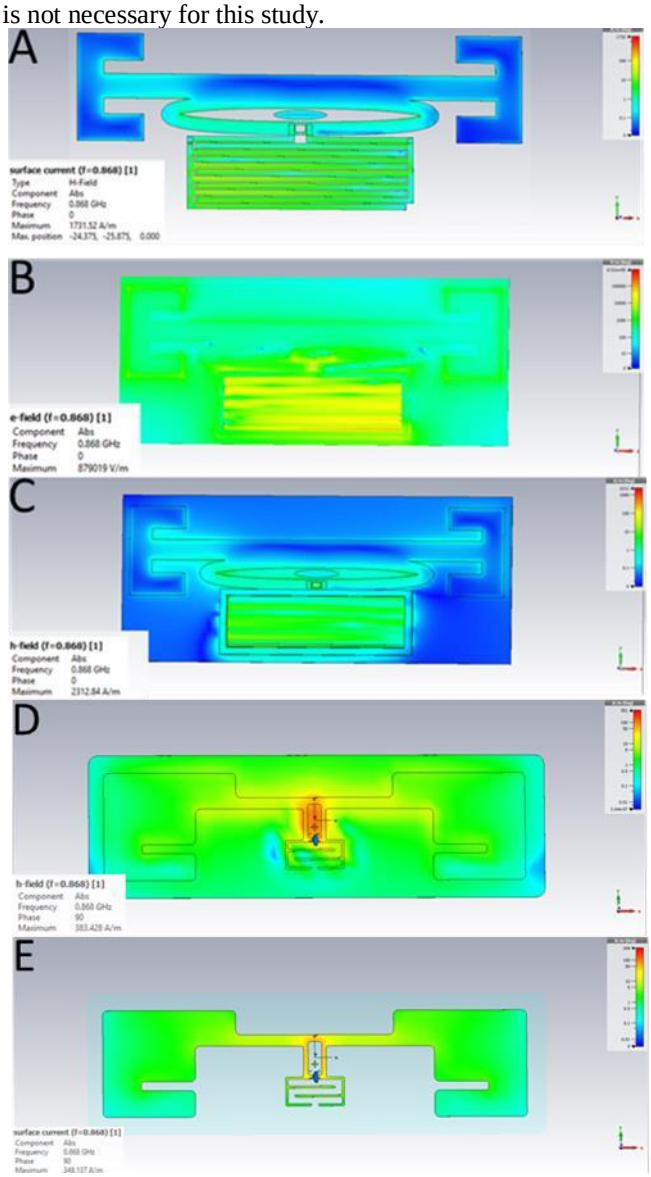

Figure 4 Simulated *C. albicans* biofilm growth effect on (A) surface current, (B) e-field and (C) h-field on the interdigit UHF sensor design. As well as the (D) h-field and (E) surface current for the RFMicron tag. Simulations exhibited are for the thickest biofilm growth studied (80 µm).

C. RFID Biofilm Growth of *C. albicans*

To begin to investigate the cause of loss of impedance we simulated mature *C. albicans* growth on biosensors as an increase in a lossy polymeric substance (simulated as increased layers of silicone (CST library) within this paper). The thickness was adjusted from 0 µm to 80 µm as the majority of *C. albicans* biofilms remain within this thickness level [4-7]. It was seen that increase in the biofilm thickness correlated with a change in capacitance that was seen as resonant frequency shifts with multiple resonance points (Fig. 8 and 6 A).

We observed a large shift (near 100 MHz) from a thickness with 0 growth to 35 µm); at the second resonance point, there was a decrease in resonant frequency of about 20 MHz (Fig. 6A). This trend continued up to 80 µm thickness. This dual resonance was also seen with the 'no growth' thickness which had the second resonance at 925 MHz (not shown). Depending

on resonance frequency used per thickness, this RFID sensor would produce a bell-curve (in regard to biofilm thickness) that is comparable to that obtained using the xCELLigence system (Fig. 4 A). If looking at capacitance (within the 0-hour growth resonant frequency bandwidth), our simulations suggested that an increase in biofilm thickness of 35 µm would result in a decreased capacitance and a near 30Ω resistance loss (Table 1). With further increase in size, our simulations suggested that the capacitance would increase while there was a continued decrease in resistance.

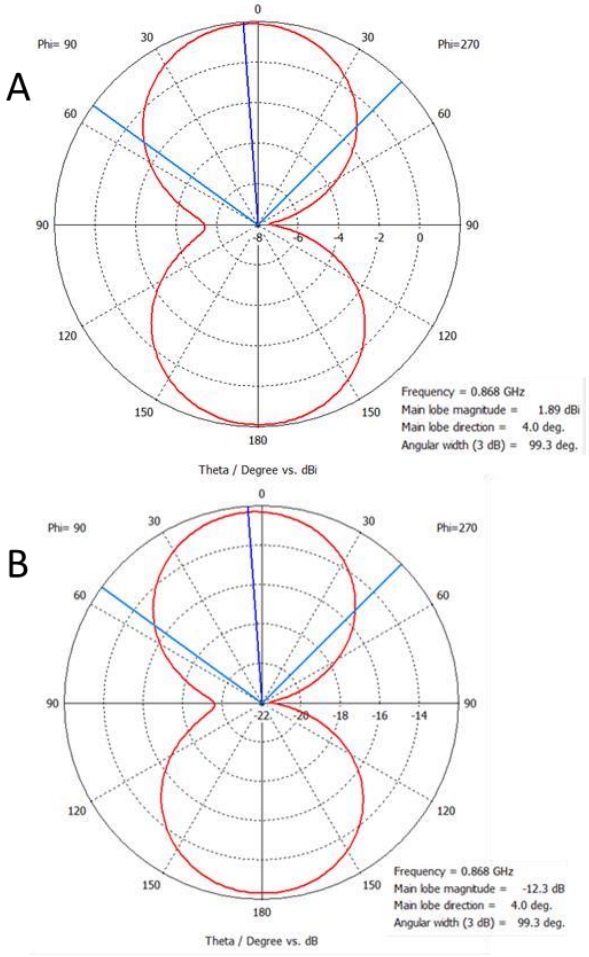

Figure 5 Simulated (A) directivity and (B) realized gain for *C. albicans* growth on the interdigit UHF sensor design. Both views were cut at phi 90°.

As Table 1 values were read at a constant 800 MHz to determine the effect of thickness on the sensor design, this does not consider the real changes that would occur when measuring the sensor. To achieve peak resonance matching, a shift in frequency to compensate for the IC impedance matching would occur as an increase in capacitance mathematically causes a decrease in resonant frequency. This correlates with the trends seen in all sensors (Fig. 8) as the 'no growth' and 48-hour growth had the highest capacitance simulated. It should be noted that in RF impedance calculations for antenna and IC matching, frequency and capacitance tend to have an inverse relationship; as capacitance increases in the system, the resonant frequency must decrease to stabilize the system at a certain impedance.

When looking at the measured values using the Voyantic antenna reader system, we observed a similar shift in resonant frequency with increase in biofilm growth where the biofilm thickness acts as an insulating polymer layer. This same shift was also seen in the RF-Micron sensor expressed as change in internal IC capacitance (sensor code) rather than resonant frequency. This can be seen in the simulation of the RF-Micron sensor (Fig. 7 A) with increased polymer thickness, there is the same shift in resonant frequency to compensate for the change in capacitance.

The RF-Micron tag, there was a significant difference between the 0 hour (no growth), 8 hours and 48-hour growth when the samples were air dried (Fig. 7 C). The same bell-curve response was noted as seen with the xCELLigence; the capacitance decreased from 0 hours to 24 hours before it reversed within 24 to 48 hours (Fig. 8 and 7 C). When the samples where fully dried with ethanol, there was less significant variation between the dry growth hours and the 0-hour growth control, yet, the change in sensor code corresponded to what was expected when there is only an increase in a polymer layer on top of the RF-Micron sensor (Fig. 7 C) [24]. This measured relationship was estimated with simulations (Fig. 7A) showing that if a decrease in dielectric properties (permittivity) occurs between 0 and 45µm and then again from 45 to 90 µm, there is a reversal in resonate frequency towards the resonance of 0 µm (Fig. 7 B). This trend correlates exactly to what was seen in real life measured values (Fig. 7 C).

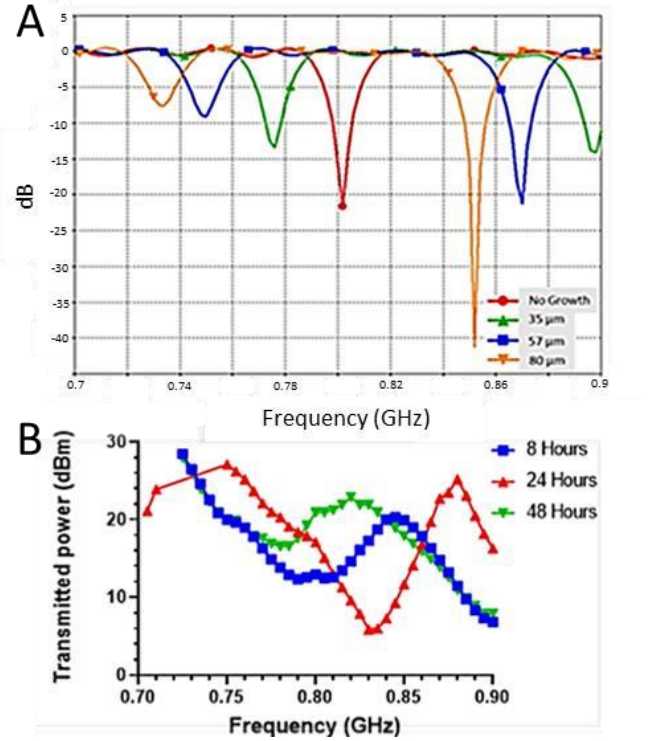

Figure 6 (A) S_{11} *C. albicans* growth simulation with increasing biofilm thickness on the interdigit UHF sensor design. (B) Measured *C. albicans* growth at 8, 24 and 48 hours; there was no noticeable change between clean media (0 hours) and 8 hours of growth. It can be seen that as biofilm growth thickness or hours increase, there is a noticeable shift in frequency and more than one resonance points per thickness (n= 10).

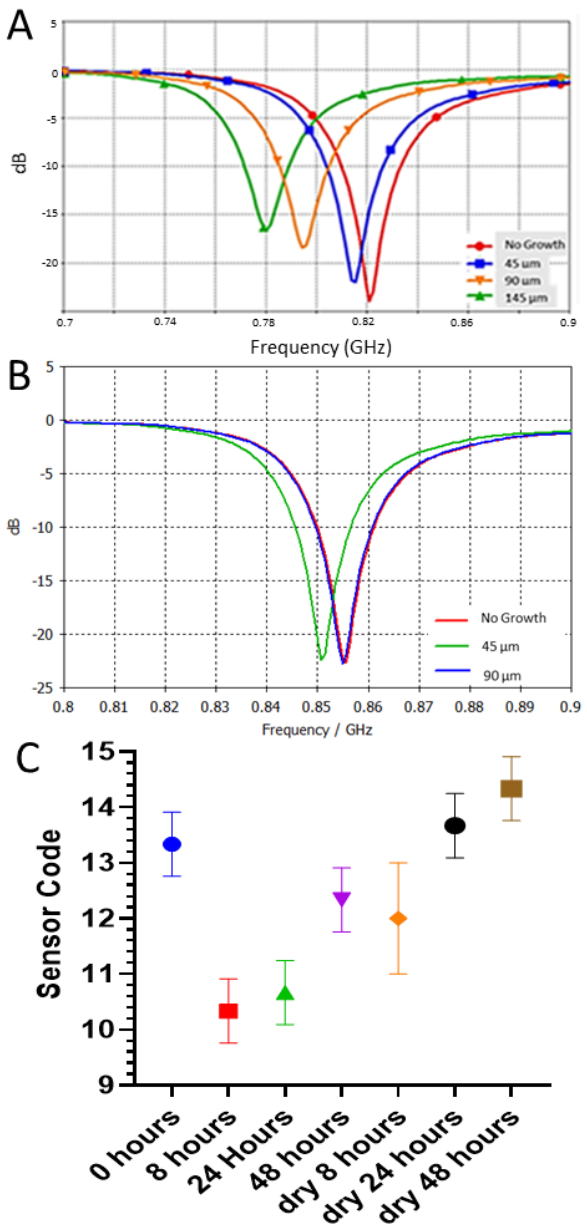

Figure 7 S_{11} *C. albicans* growth simulation for the RFMicron UHF sensor design. (A) Simulated increasing biofilm thickness without changing biofilm dielectric properties. (B) Simulated increasing biofilm thickness with changes in biofilm permittivity; no growth had permittivity equivalent to water, 45 µm decreased the permittivity to 47 and 90 µm had permittivity equivalent to polymer (2). (C) The RFMicron sensor tag measured detection of *C. albicans* biofilm growth.

Similar to the simulations (Fig. 6 A and 7A) as biofilm thickness increases, it acts as a non-conductive material such as silicone which displaces the conductive media with increased biofilm growth. Once growth occurs (increase in polymer (Table 1)) there is a noticeable drop in resistance which then needs to be compensated for with change in capacitance and/ or shift in resonant frequency. If no change in resonant frequency can occur, as possible with the interdigit sensor method (Fig. 6 B), then at a pre-set frequency capacitance must be adjusted to change the system impedance as seen with xCELLigence and RF-Micron sensors. This suggest, just as with the xCELLigence, that growth was more highly impacted by the fluid within the biofilm matrix as when the fluid is fully removed (Fig. 7 C) the dry thickness has a linear relationship with capacitance as predicted by simulations (Fig. 7A). Therefore, it is likely that as biofilm formation causes the matrix and cell density to increase, it becomes hydrophobic and insulating against the conductivity of the liquid media detected by all systems.

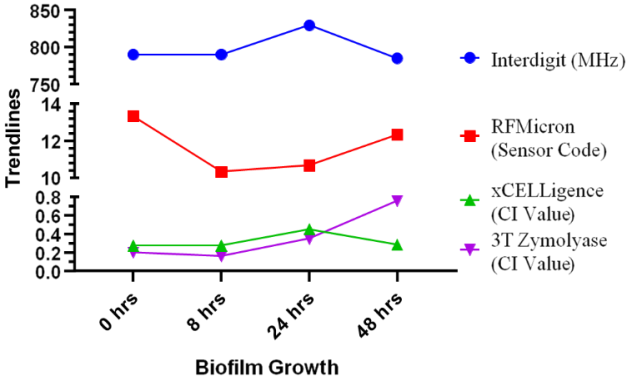

Figure 8 Measured data for all methods showing a change in capacitance corresponding to biofilm growth. All methods showed a decrease in sensor capacitance from 0 hours to 24 hours with a reversal from 24 to 48 hours. In all sensor types, 48-hour readings and 0 (and/ or 8 hour) readings had similar measured values. The only variation to this trend was seen with the zymolyase sample as growth from 24 to 48 hours continued with a noticeable decrease in capacitance (and equivalent to an increase in CI value).

IV. CONCLUSION

C. albicans biofilm growth detection is possible utilizing both RFID UHF antenna sensors and the purchased xCELLigence equipment. Both systems types were able to detect biofilm formation at intermediate and mature stages. The xCELLigence with the ability to do continuous (30-minute intervals) monitoring of growth was able to detect changes before the 24-hour mark. In theory, both the interdigit sensor and RFMicron UHF designs should, also, be able to detect early growth however some system tuning would be necessary especially if detection within growth media was necessary rather than taken as a snapshot monitoring. The RFID sensors, however, provide a cheap alternative to expensive manufactured microorganism growth sensor such as the xCELLigence machine.

Acknowledgements

This work was funded by the UK Engineering and Physical Science Research Council (EPSRC). Conflict of interest: None declared.

References

2. “Medical Implants Market - Forecasts from 2018 to 2023”. Available at: www.researchandmarkets.com/research. [Online]
3. “Global Next Generation Implants (NGI) Market –Analysis and Forecast (2017-2023) - Market Share Analysis and

Competitive Insights". Available at: www.researchandmarkets.com/reports. [Online]
1. Jakobsen, TH, Eickhardt, SR, Gheorghe, AG, Stenqvist, C, Sønderholm, M, Stavnsberg, C, Jensen, PØ, Odgaard, A, Whiteley, M, Moser, C, Hvolris, J, Hougen, HP, Bjarnsholt, T. Implants induce a new niche for microbiomes. APMIS 2018; 126: 685– 692.
4. Gulati, Megha, and Clarissa J Nobile. "Candida albicans biofilms: development, regulation, and molecular mechanisms." Microbes and infection vol. 18,5 (2016): 310-21.
5. Angélica de L. Rodríguez López, Myung-Ryul Lee, Benjamín J. Ortiz, Benjamin D. Gastfriend, Riley Whitehead, David M. Lynn, Sean P. Palecek. Preventing S. aureus biofilm formation on titanium surfaces by the release of antimicrobial β-peptides from polyelectrolyte multilayers, Acta Biomaterialia, 2019.
6. Kojic EM, Darouiche RO. Candida infections of medical devices. Clin Microbiol Rev. 2004; 17:255–267.
7. Xie Z, Thompson A, Sobue T, Kashleva H, Xu H, Vasilakos J, Dongari-Bagtzoglou A. Candida albicans biofilms do not trigger reactive oxygen species and evade neutrophil killing. J Infect Dis. 2012 Dec 15;206(12):1936-459.
8. Gropp K, Schild L, Schindler S, Hube B, Zipfel PF, Skerka C. The yeast Candida albicans evades human complement attack by secretion of aspartic proteases. Mol Immunol. 2009 Dec;47(2-3):465-75.
9. Cavalheiro, Mafalda, and Miguel Cacho Teixeira. "Candida Biofilms: Threats, Challenges, and Promising Strategies." Frontiers in medicine vol. 5 28. 13 Feb. 2018.
10. Nobile CJ, Johnson AD. Candida albicans biofilms and human disease. Annu Rev Microbiol. 2015; 69:71–92.
11. Randviira EP, Banks CE. Electrochemical impedance spectroscopy: an overview of bioanalytical applications. Anal. Methods, 2013,5, 1098-1115
12. "XCELLigence RTCA Systems." ACEA Biosciences Inc., www.aceabio.com/products/xcelligence-rtca.
13. Junka AF, Janczura A, Smutnicka D, Mączyńska B, Anna S, Nowicka J, Bartoszewicz M, Gościniak G. Use of the Real Time xCelligence System for Purposes of Medical Microbiology. Pol J Microbiol. 2012 Sep 28;61(3):191-197.
14. Gutiérrez D, Hidalgo-Cantabrana C, Rodríguez A, García P, Ruas-Madiedo P (2016) Monitoring in Real Time the Formation and Removal of Biofilms from Clinical Related Pathogens Using an Impedance-Based Technology. PLOS ONE 11(10): e0163966
15. Mannoor MS, Tao H, Clayton JD, Sengupta A, Kaplan DL, Naik RR, et al. Graphene-based wireless bacteria detection on tooth enamel. Nat Commun. 2012; 3:763.
16. Gomez-Sjoberg, R.; Morisette, D.T.; Bashir, R. Impedance microbiology-on-a-chip: Microfluidic bioprocessor for rapid detection of bacterial metabolism. J. Microelectromech. Syst. 2005, 14, 829-838.
17. Johnson N, Chang Z, Bravo Almeida C, Michel M, Iversen C, Callanan M. Evaluation of indirect impedance for measuring microbial growth in complex food matrices. Food microbiology. 2014; 42:8-13.
18. Hidalgo-Cantabrana C, Kekkonen R, de los Reyes-GavilaÂn CG, Salminen S, Korpela R, Gueimonde M, et al. (2014) Effect of bacteria used in food industry on the proliferation and cytokine production of epithelial intestinal cellular lines. J Funct Foods 6: 348±355.
19."RFM2100 Wireless Flexible Moisture Sensor." Axzon Website, axzon.com/rfm2100-wireless-flexible-moisture-sensor/. [Online]
20. "Higgs® 3." Alien Technology, www.alientechnology.com/products/ic/higgs-3. [Online]
21. B. D. Braaten and R. P. Scheeler, "Design of Passive UHF RFID Tag Antennas Using Metamaterial-Based Structures and Techniques," Radio Frequency Identification Fundamentals and Applications, Design Methods and Solutions, February, pp. 51–68, (2010).
22. Cuellar-Cruz, M., et al., The effect of biomaterials and antifungals on biofilm formation by Candida species: a review. (1435-4373 (Electronic)).
23. Ribeiro T, Romestant G, Depoortere J, Pauss A. Development, validation, and applications of a new laboratory-scale indirect impedancemeter for rapid microbial control. Applied microbiology and biotechnology. 2003;63(1):35-41.
24. Hillier, A.J.R., et al., *A Passive UHF RFID Dielectric Sensor for Aqueous Electrolytes.* IEEE Sensors Journal, 2019. 19(14): p. 5389-5395.

Voice Prosthesis Implantable UHF RFID Self-Sensing Tag for Microbial Growth Detection

V. Makarovaite, *Student Member, IEEE*, A. J. R. Hillier, S. J. Holder, C. W. Gourlay, J. C. Batchelor, *Senior Member, IEEE*

***Abstract*— Passive Radio Frequency Identification (RFID) implantable antennas experience low efficiency due to the capacitive loading of human tissue that the implantable design has to overcome. Here we present two passive UHF implantable voice prosthesis sensors able to produce a read range of 65 cm (EU frequency band) and 80 cm (US frequency band) from within the body as well as a smaller digital IC version able to produce a 11 cm read range. With a slight adjustment, prototype 1 (self-sensing tag) can be utilized to sense microbial growth due to shifts in resonant frequency while prototype 2 can self-tune and report impedance changes as a nominal value once mounted upon a voice prosthesis. Simulated *Candida albicans* biofilm growth can be detected within the body with these sensors from early and up to a mature biofilm thickness of 30 µm or 60 µm (0 to 48-hour growth *in vitro* equivalent); allowing for early detection of contamination of the voice prosthesis. These designs suggest that it is feasible to produce implantable UHF technology on small prosthetic devices, such as voice prostheses, that may facilitate cost-effective monitoring of microbial growth leading to more effective clinical care procedures and treatments.**

***Keywords*— UHF, RFID, Implantable, Design, Sensor**

I. Introduction

The medical implant market is projected to be worth around US$141 billion by 2023 with an increase of US$3.9 billion in the global market for next generation implants [1, 2]. However, this overall expected increase in medical implant utilisation also underlines the primary complication for implant surgery, (20-25%) colonisation by microorganisms of the implant surface or any adjacent tissue [3]. It should be noted that the average (for all implant types) infection rate is only around 2%; however, when looking at temporary medical devices (such as catheters) this infection rate could be as high as 50% [4]. More importantly when infection occurs it often necessitates the removal and/ or replacement of the implant adding unnecessary cost of already straining healthcare systems [3].

Infection is a common issue with voice prostheses that occur after a patient has had a laryngectomy and requires assistance for speaking [4]. One of the most common oral colonizers of voice prostheses tends to be the fungal species *C. albicans*, which can form a multi-layer biofilm upon the device [4-6]. Also, actual detection of *C. albicans* growth only occurs due to either device failure or infection symptoms of the patient [3-6]. Therefore, detecting microbial growth on an implantable device would be desirable and utilizing passive UHF RFID (radio frequency identification) technology could allow the development of an implantable sensor capable of detecting microbial growth while inside the body before the need for removal and any addition of unnecessary cost.

Passive RFID technology requires the receipt of a continuous wave from a reader antenna, which then returned including backscatter modulation on the signal. There are many different types of passive RFID sensors which function via methods including magnetic acoustic resonance, inductor-capacitor-resistor transducers (LRC), or thickness shear mode [7]. Alternatively, a 'self-sensing' approach to RFID sensor design removes the necessity for additional components as it functions on the idea that any physical or geometrical change in structure will directly affect signal modulation received by an antenna reader [8]. This is a cost-effective approach for any short-life system such a device that detects microbial colonization and indicates the need for removal before a patient exhibits medical symptoms of infection and requires treatment or hospitalization.

Etching a self-sensing resonant circuit reduces cost involved in the fabrication process and it can be tuned to compensate for the capacitive loading of human tissues [7, 8]. The present paper utilizes a tuned and smaller version of the design presented in [9] and is able to achieve a read range above 4 meters when mounted on high dielectric constant solutions similar to human tissue (2 to 80 permittivity range). This design was further improved (through adjustment to the transponder Integrated Circuit (IC) impedance matching) and by utilizing a digital sensing IC (Magnus® S chip [10]) which is able to self-tune the system capacitance and report impedance changes as a nominal value. Here it is shown how the antenna functions within a gelatine and salt phantom of the human neck, and simulation indicates the sensing of microbial growth with these designs.

II. Methods

UHF RFID performance is often determined based on the read range achieved by any proposed design. Passive systems depend on minimum 'wake-up' power necessary for integrated circuit (IC) activation that is provided by an antenna reader. The RFID maximum read range formula is:

$$r_{max} = \frac{\lambda}{4\pi}\sqrt{\frac{QG_{rd}G_{tg}P_{rd}}{P_{tg}}} \qquad (1)$$

where G_{rd} is the reader antenna gain, G_{tg} is tag gain, Q is impedance mismatch factor, λ is reader wavelength, P_{rd} is reader power, and P_{tg} is tag received power [8]. G_{tg} and Q are the only adjustable properties to improve read range as all others are determined by the manufacturers of the reader antenna, transponder IC and country RFID frequency regulations [8]. UHF RFID is able to provide higher gain and data rates for matched systems with an increased read range compared to HF [11].

For experimental measurement, a neck phantom was developed utilizing gelatine and salt [12] to produce a 10 cm in diameter and height structure. The body gelatine phantom

had measured dielectric properties equivalent to human muscle (permittivity of 59 and conductivity of 1 S/m). For simulation purposes, two extra muscle blocks were included (above and below the neck phantom) to simulate a more accurate tag directivity and efficiency. TagformancePro Voyantic RFID antenna measurement system was used to measure the performance of the design (all measurements done in triplicate) [13]. 5 MHz frequency and 0.1 dBm power (up to 30 dBm) sweeps were utilized between 800 MHz to 1000 MHz with a calibrated system at 30 cm distance between tag and antenna reader (Fig. 1 A). The Higg-3 Gen 2 RFID integrated circuit (31- j216 Ω at 865 MHz) was incorporated into an etched dipole antenna [9, 14] with a resonating loop shunt. The final design was a half-wave dipole sensor of 22 mm diameter (Fig.1 B).

To adjust for the sensing requirements in simulation, there was a need to shunt an extra component of 2.2 pF into the system to account for the resonance shift caused by the saliva, biofilm and an extra polymer layer on top of the sensor (prototype 1). The sensor faces towards the inside of the neck phantom as biofilm growth is more prevalent and damaging within this region. The movable phalange that allows a laryngectomy patient to speak after the removal of the 'voice box' is most commonly damaged as a result [7]. The overall design adjustments were accomplished as described in [9] except by the addition of a lumped capacitance (Fig. 1 B) in parallel with the IC. This led to a *C. albicans* growth simulation consisting of a single CST library silicone layer (with the same diameter as the voice prosthesis design) on top of the actual sensor (with thickness ranging from 0 µm to 65 µm) followed by an additional 10 µm layer of saliva on top, Table 1. In practice, it was necessary to add a 10 µm polymer layer over the sensor as *C. albicans* would not commonly grow on metal in real life. In the simulation, this was included in the biofilm layer which therefore had a thickness of 10 µm corresponding to zero growth.

The same biofilm and saliva layer structure was applied to the second prototype that utilized the Magnus S IC. In this case, the sensor region and antenna were adjusted as shown in Fig. 1 C. This enabled the simulation of *C. albicans* biofilm growth as it is known that once a biofilm forms, it becomes more hydrophobic [3-6]. This was validated in-house using a separate commercial system [15]. Silicone dielectric properties were chosen for the simulated biofilm material as empirical experimentation suggested that the hydrophobicity of the biofilm layer causes a loss in conductivity equivalent to a thin polymer. This causes a noticeable shift in either peak resonant frequency or system capacitance.

Table I. SPEAG Probe Dielectric Properties (865 MHz)[a]

	Permittivity (294.25 K)	***Conductivity (S/m)***	***BMI***
Volunteer 1	22	0.27	20.6
Volunteer 2	30	0.42	27.2
Volunteer 3	41	0.67	24.6
Saliva	40	0.3	x
Gelatine phantom	59	1	x

a. No variability was seen within three replicates for each volunteer

However, the antenna tag performance was measured without biofilm growth or saliva as it was necessary to determine the sensor function within the body before performing any necessary adjustments to account for the high dielectric of these layers directly upon the sensor. Also, the simulation was re-run using dielectric data gathered from volunteers using a SPEAG Dak Dielectric Probe [16] (Table 1). This allowed the effect of human tissue variability to be included in the simulations and to determine any additional adjustment needed to stay within the EU UHF frequency band for prototype 1. Prototype 2 was able to auto-tune and the tissue variability study was not necessary.

III. Results

The Prototype 1 design had a radiation efficiency of -20.57 dB (within human tissue an efficiency near -20 dB is expected due to power dissipation) (Fig. 2). The convoluted dipole antenna design offers a 90% power transfer to the transponder IC at 867 MHz. When mounted within a gelatine/salt human throat phantom (Fig. 1A), the tags read more than 65 cm outside the phantom (read distance) at 867 MHz (EU frequency band) or more than 80 cm at 915 MHz (US frequency band) using a 2 W beam power (EIRP) standard RFID reader (Fig. 1 B). Moreover, this measurement was repeated in triplicate without any noticeable variability in read range.

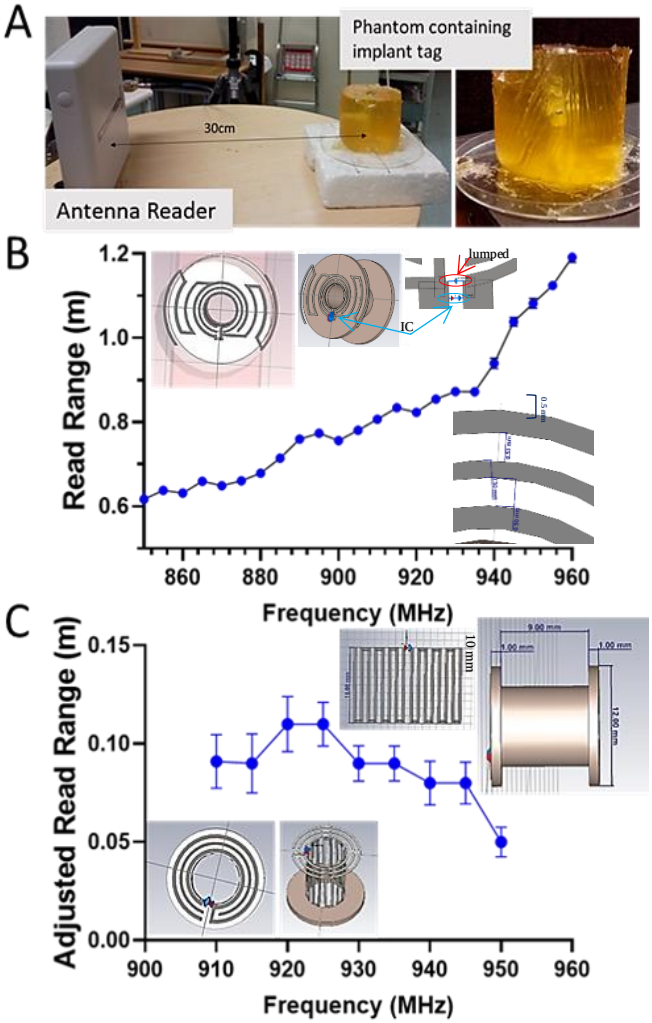

Figure 1 Measured read ranges of the passive UHF implantable tags mounted upon a voice prosthesis within a gelatine and salt neck phantom. A) Antenna and phantom calibration set-up. B) Prototype 1 tag was able to achieve a read range above 60 cm at both the UHF EU and US frequency bands. C) Prototype

2 tag was only able to achieve 11cm read range at the US frequency band (920 MHz).

Prototype 2 was only able to produce less than a 20 cm read range at 920 MHz (11 cm) (Fig. 1 B) when placed within a gelatine phantom with no reading below 910 Mhz. The read range was obtained by lowering the calibration by 20 cm which was then accounted for in the read range exhibited. However, it should be noted that read ranges of less than 20 cm are common for small passive UHF, implantable devices. As this was only testing the function of the antenna within the neck phantom, the sensor code was not utilized other than to get a dry reading which provided a sensor code of 15 once placed inside the neck phantom. This would suggest that a dry prototype 2 (without a biofilm or saliva) expresses a capacitance of near 2.5 pF as the system ranges from 3 pF to 2 pF when moving from a 32 to 0 sensor code readout. This is within the expected capacitance range without the additional capacitance loading of saliva (conductive liquid).

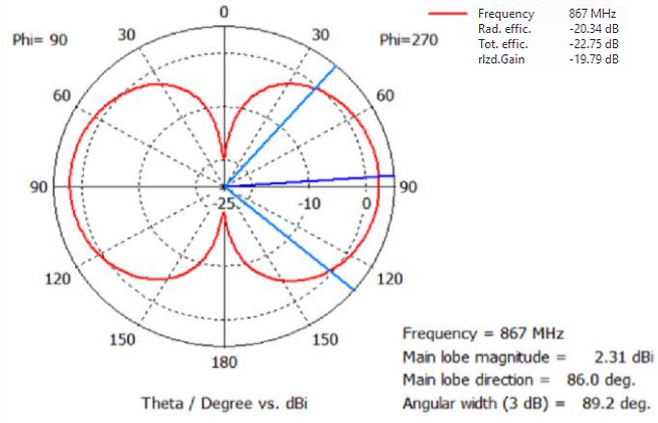

Figure 2 Antenna directivity polar plot cut at phi 90° when mounted on a voice prosthesis and implanted within a gelatine and salt neck phantom.

A. Simulation of Prototype 1 Adjustments for Biofilm Growth:

The simulations for Prototype 1 (after the necessary capacitance adjustments) showed that with the increase in *C. albicans* biofilm, there was a noticeable shift in frequency due to the decoupling of the saliva from the antenna. As the biofilm layer increases in thickness, the saliva layer is pushed further away from the parasitic loop sensor region mimicking the hydrophobic activity expected in biofilm growth on polymer material. Therefore, it is possible to detect biofilm growth from only a 5 µm thickness up to a mature biofilm (30 -35 µm [3-6]) by utilizing this adjusted sensor within the body. Also, an increase in the biofilm layer (on the micron scale) is enough to affect the sensor region of the etched design by changing the capacitance within the system and causing an increase in resonant frequency (Fig. 3B). This change in capacitance arises due to the decoupling of the saliva layer from the design for IC matching purposes.

It has been previously shown [17] that conductivity reduces antenna matching when increased; this can be seen when the biofilm layer is thinnest (0 µm) compared to thickest (30 µm)). A change in system permittivity will cause a resonant frequency shift rather than a change in efficiency [17]. Based on this the sensor function within this design suggests that the change in the biofilm thickness causes a larger change in the permittivity observed by the sensor than the conductivity as there is not much effect on matching, Fig. 3 B. Once the tag was mounted on a voice prosthesis and implanted, it showed a unidirectional appearance with an estimated directivity magnitude of 2.31 dBi and 86° main lobe direction towards the sides of the design, Fig. 2. As stated previously, the total efficiency for all different *C. albicans* growth thicknesses remained near the -20% range as expected for any implantable UHF passive tag.

A

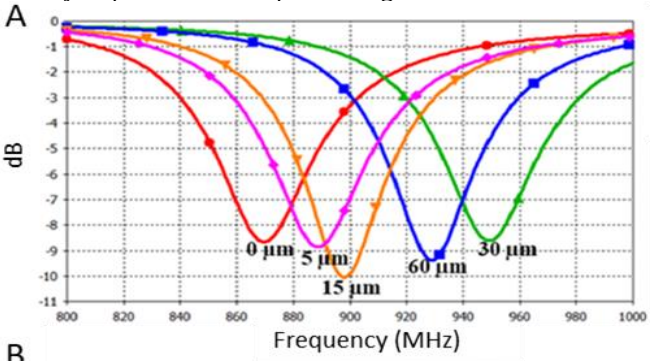

B

"Biofilm Thickness		No Growth	5 µm	15 µm	30 µm	60 µm
Resonant Frequency (MHz)		868	889	898	949	928
Capacitance at Resonance (x 10^{-11})		1.7	1.5	2.1	1.5	1.7
Impedance at Resonance	Real	56	53	50	55	52
	Imaginary	-10	-12	-8	-11	-9.9

C

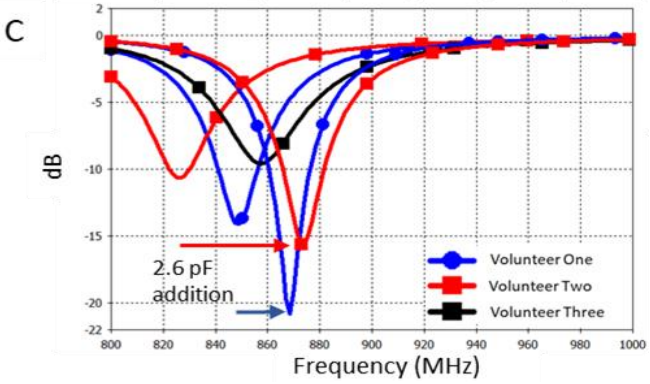

Figure 3 S_{11} of Prototype 1 simulating the increase of biofilm thickness on the (A) sensor design and (B) Effect of biofilm thickness on changes in simulated antenna matching parameters. As the biofilm thickens, there is an increase in resonant frequency till a 30 µm thickness is reached. (C) Phantom adjustments based on volunteer data from Table 1 to encompass a wider range of volunteer dielectric properties. When the phantom dielectric properties are changed to mimic volunteer data, there is a need for a 2.6 pF shunt to tune the design within the EU UHF frequency band for volunteers one and two (blue and red, respectively).

B. Adjustment for Neck Musculature:

When adjusting the simulated neck phantom to account for the dielectric properties collected from volunteers, there was a noticeable correlation with previously published [17] data. As the dielectric properties decreased from the gelatine and salt phantom (high dielectric), there was a shift in the resonant frequency towards a lower frequency. Also, as the conductivity was decreased of the simulated phantom (from the 1 S/m of the gelatine) to match volunteers (0.67 S/m or less), there was a noticeable decrease in the impedance This suggest that the tag would have better efficiency within real human tissue compared to the gelatine neck phantom which mimicked homogenous human muscle. Even though there was a noticeable shift for each volunteer, only volunteers one and two would require an adjustment to the lumped capacitance from 2.2 pF to 2.6 pF as the simulated resonance on the third volunteer was near 867 MHz, Fig. 3 C. This approach could be easily implemented by having two versions of design available dependent on user muscle to fat ratio

appearance; where muscular individuals could utilize the un-altered design (with 2.2 pF capacitance) while average appearing individuals could use the increased version with 2.6 pF. Volunteer BMI did not show a nice trend with the dielectric properties; therefore, musculature appearance should be used as differentiation between the need for a high or low device variable when tissue dielectric properties measuring equipment is not available.

However, it has been reported that neck musculature does not scale proportionally with body weight or height [18]. Our volunteer data in Table 1 was highly variable (between individuals) and was taken from an easy data collection site (the forearm) to help simulate the wide range of real human tissue dielectric properties. However, when only looking at neck dielectric data from additional volunteers (BMI range of 20.5 to 44.9), there was not much variability seen (Table 2). Average neck permittivity only varied by ± 2.31 while conductivity varied by 0.64±0.058 suggesting only a single optimally tuned design could be possible for real life implementation within the neck for *C. albicans* biofilm growth detection upon a voice prosthesis. Within simulation this allowed for the use of a more accurate single human model for the effect of biofilm growth on prototype 2 provided by CST Studio software. The model chosen was the 'Hugo' human tissue bio-model with all tissue layers included and set to average thickness values, Fig. 4 C.

Table II. SPEAG Probe Dielectric Properties of Volunteer Necks (865 MHz)

BMI	***Permittivity (293.75 K)***	***Conductivity (S/m)***	***tan(δ)***
20.8	40.30 ± 0.19	0.63± 0.007	0.33±0.003
44.9	40.29±0.68	0.60±0.20	0.31±0.005
26.1	42.70±0.77	0.72±0.017	0.35±0.003
20.5	36.75±1.14	0.58±0.03	0.33±0.007
Average	**40.1±2.31**	**0.64±0.058**	**0.33±0.015**

C. Adjustments for Biofilm Growth with Prototype 2:

Compared to Prototype 1 (Fig. 3 A), Prototype 2 (Fig. 4 A) was able to provide a more linear resonant frequency shift with increasing biofilm layer. However, this digital IC which would be utilized at a single frequency (915 MHz based on simulation) for detection of changes in internal capacitance with increasing biofilm thickness, there was a noticeable increase in capacitance (Fig. 4 B) between no growth and 0.02 mm of growth before the capacitance drops again and reaches a reading near the no growth output for a 0.065 mm layer thickness. In order to achieve a resonance within the EU UHF frequency band, a 3 pF shunt is necessary, Fig. 4 C [9]. This suggests to achieve resonance within multiple frequency bands, the use of multiple designs rather than a single design as seen with prototype 1 would be needed. However, the advantage of this design is the clear output of a sensor code which could be used with simple UHF readers without the need to understand antenna frequencies or polarisation allowing this to have a more practical use than prototype 1.

IV. CONCLUSION

An implantable design adjusted from [9] provides a starting performance (as a voice prosthesis sensor) able to produce a read range of 65 cm (EU UHF band) and 80 cm (US UHF band). Once slightly adjusted with a lumped capacitance, this design was able to detect (within simulation) up to 30 μm of biofilm growth (a known mature *C. albicans* biofilm growth thickness) [3-6]. When attempting to adjust the simulation based on volunteer tissue dielectric information, the designs were still able to function within the EU frequency band and only volunteers one and two required an increase in lumped capacitance from 2.2 pF to 2.6 pF. As the chosen location for this device would be within the neck, it is expected that there would be less variability in the dielectric properties (even for a high BMI) between patients.

This was further improved by implementing a digital sensing IC to reduce reliance on frequency shifts as a determinant for microbial growth while utilizing the same sensor region with an adjusted antenna design. This alternative prototype was able to produce a 11 cm read range at 915 MHz, which falls within the expected read ranges for an implantable design of less than 6 mm in diameter. In order to achieve resonance within the EU UHF frequency band, Prototype 2 would need an additional lumped capacitance of 3 pF. Therefore, for any new frequency band implementation, a lumped capacitance adjustment will be necessary. Both presented designs are able to produce adequate read ranges for an implantable system as a passive UHF RFID system suggested for utilization as a cost-effective alternative for implantable microbial detection.

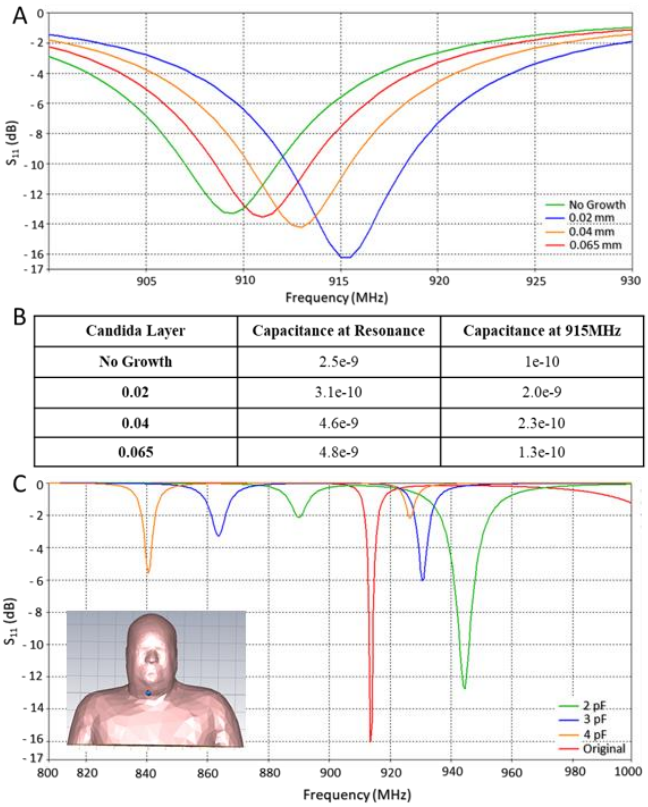

Candida Layer	Capacitance at Resonance	Capacitance at 915MHz
No Growth	2.5e-9	1e-10
0.02	3.1e-10	2.0e-9
0.04	4.6e-9	2.3e-10
0.065	4.8e-9	1.3e-10

Figure 4 S_{11} of Prototype 2 simulating the increase of biofilm thickness on the (A) sensor design and (B) Effect of biofilm thickness on simulated antenna capacitance measurements. As the biofilm thickens, there is a detectable capacitance change when read at a single frequency (915 MHz). (C) Necessary adjustment to tag design to achieve both EU and US frequency bands; there is a need for a 3-pF shunt to tune the design within the EU UHF band.

ACKNOWLEDGMENT

This work was funded by the UK Engineering and Physical Science Research Council (EPSRC). Conflict of interest: None declared.

REFERENCES

[1] Medical Implants Market - Forecasts from 2018 to 2023. Accessed: June 06, 2018. [Online]. Available at www.researchandmarkets.com/research.

[2] Global Next Generation Implants (NGI) Market –Analysis and Forecast (2017-2023) - Market Share Analysis and Competitive Insights. Accessed: June 06, 2018. [Online].

www.researchandmarkets.com/reports.

[3] Jakobsen, TH, Eickhardt, SR, Gheorghe, AG, Stenqvist, C, Sønderholm, M, Stavnsberg, C, Jensen, PØ, Odgaard, A, Whiteley, M, Moser, C, Hvolris, J, Hougen, HP, Bjarnsholt, T. Implants induce a new niche for microbiomes. APMIS 2018; 126: 685– 692.

[4] Fox EP, Nobile CJ. The role of *Candida albicans* biofilms in human disease. In: Dietrich LA, Friedmann TS, editors. Candida albicans symptoms, causes and treatment options. Nova Science Publishers; 2013. pp. 1–24.

[5] Gulati, Megha, and Clarissa J Nobile. "Candida albicans biofilms: development, regulation, and molecular mechanisms." Microbes and infection vol. 18,5 (2016): 310-21.

[6] Talpaert MJ, Balfour A, Stevens S, Baker M, Muhlschlegel FA, Gourlay CW (2015) Candida biofilm formation on voice prostheses. J Med Microbiol 64(Pt 3):199–208

[7] R.A. Potyrailo, N. Nagraj, Z. Tang, F.J. Mondello, C. Surman, W. Morris. "Battery-free radio frequency identification (RFID) sensors for food quality and safety", Journal of agricultural and food chemistry, 65, pp. 8535-43, (2012).

[8] B. D. Braaten and R. P. Scheeler, "Design of Passive UHF RFID Tag Antennas Using Metamaterial-Based Structures and Techniques," Radio Frequency Identification Fundamentals and Applications, Design Methods and Solutions, February, pp. 51–68, (2010).

[9] V. Makarovaite, A. J. R. Hillier, S. J. Holder, C. W. Gourlay and J. C. Batchelor, "Passive Wireless UHF RFID Antenna Label for Sensing Dielectric Properties of Aqueous and Organic Liquids," in IEEE Sensors Journal. [Online Early Access]

[10] Magnus® S Product Family. Accessed: July 06, 2019. [Online]. Available at www.rfmicron.com/magnus-family/

[11] M.A. Ziai, J. C. Batchelor, "Temporary On-Skin Passive UHF RFID Transfer Tag", IEEE Transactions On Antennas And Propagation, Vol. 59, No. 10, October (2011).

[12] Q Duan, J H Duyn, N Gudino, J A de Zwart, P van Gelderen, "Characterization of a Dielectric Phantom for High-Field Magnetic Resonance Imaging Applications," Medical Physics, 41 (10), pp.102303-6, (2014).

[13] Voyantic Tagformance Pro. Accessed: June 06, 2018. [Online]. Available at https://voyantic.com/tagformance.

[14] Alien Technology, "Higgs-3 product overview". Available at http://www.alientechnology.com/products/ic/higgs-3, accessed 25 May 2017.

[15] "xCELLigence RTCA Systems." ACEA Biosciences Inc. Accessed: June 06, 2018. [Online]. available at www.aceabio.com/products/xcelligence-rtca.

[16] SPEAG *Dak 3.5*. Accessed: June 06, 2019. [Online]. Available: https://www.speag.com/products/dak/dak-dielectric-probesystems/dak-3-5-200-mhz-20-ghz.

[17] D. O. Oyeka, J. C. Batchelor and A. M. Ziai, "Effect of skin dielectric properties on the read range of epidermal ultra-high frequency radiofrequency identification tags," in Healthcare Technology Letters, vol. 4, no. 2, pp. 78-81, (2017).

[18] Kamibayashi LK, Richmond FJ, "Morphometry of human neck muscles," in Spine (Phila Pa 1976). vol. 23, no. 12, pp. 1314-23 (1998).

4. Chapter 4: Concluding Thoughts:

We have demonstrated that the development of an RFID UHF based system for the detection of *Candida albicans* biofilm growth on voice prosthesis while inside the body is possible following characterisation of the electrical properties involved in *C. albicans* biofilm formation. This allowed for targeted device development against known (and tested herein) aspects of *C. albicans* biofilm development such as changes to system impedance (capacitance, resonant frequency and changes of environmental dielectric properties). This is the first work to investigate the electrical properties of *C. albicans* colonisation of materials used in the construction of medical devices. Progress required me to conduct four separate studies related to different aspects of *C. albicans* biofilm formation.

Our published paper [192] developed from a need to understand the electrical changes involved with microbial colonisation of liquid media as *C. albicans* is known to change the environmental pH during colonisation [25]. We found that it is possible to develop a passive RFID UHF antenna sensor able to detect minute changes utilizing standard curve analysis with an accuracy of ± 0.834 relative permittivity and ± 0.050 S·m-1 conductivity. We also found that with a capacitive sensor [197], we could also detect changes within a solution based on salt concentration and molarity (from 0 to 2 M). This allowed us to understand that even within an aqueous environment, a sensor can be developed to respond to system impedance variations; allowing utilisation for microbial detection particularly within a moist environment, a necessary consideration for any development of a sensor device that must be attached or embedded into a voice prosthesis as the implant location is within the throat.

The presented sensor, with accuracy for minute dielectric changes within liquid solutions, could be mass produced and easily implemented in the real world. One particular use would be application within a future smart cabinet for easy detection of fluid contamination within a

laboratory setting or even clinical settings if placed on medication vials. It is known that most medical mistakes occur due to human error, therefore any assistance with medication handling to prevent incorrect dose accruement would be useful, particular with this type of low-cost sensor. Ideally, this would be a safety check and not a primary dispensary for medication as, ultimately, the medical personnel should still verify the correct dosing once removed from the proposed smart cabinet. This should reduce the need for extensive clinical trials as this sensor would not be involved in the clinical care but rather act as a wireless management system to reduce error in terms of medical dosage. However, it should be noted that the system is currently adjusted for liquid amounts exceeding 50 mL, so medication utilising smaller quantities would need further testing.

Also, this system only functions optimally when the liquid amount is kept the same between reads; the effect of liquid removal from very small quantities of fluid (less than 10 ml) were never tested with this sensor. There might be an easy fix for this, requiring the medical personnel to recalibrate the sensor when returning any used liquid medication. This itself would pose a challenge as medical personnel would need to be trained to accomplish proper calibration to continue the use of the currently presented system. Therefore, the smart cabinet might need to include an automatic recalibration for any medication that is returned to the internal cabinet surface. However, this might reduce the sensors sensitivity to any contamination which might have occurred prior to the return. My suggestion would be that only unused and non-tampered liquid containers be kept inside these smart cabinets to prevent this type of sensitivity issue. If not possible, then the sensitivity and fringing field penetration, responsible for detecting these liquid changes, might need to be reduced if liquid removal has a much greater effect within smaller quantities of liquid once tested. Ultimately, based on current date literature review, there are no other passive UHF RFID sensor designs published

able to detect dielectric changes within a closed liquid system to such a sensitivity suggesting that this could further the field for RFID sensor technology.

Once we understood that a sensor could be developed to function within a wet environment, we had to understand the effect of human tissue dielectric variability on such a device. We knew from previous studies [179] that variability within human tissue can have a detrimental effect on the function of a passive UHF RFID device; skin conductivity affecting impedance matching between the IC and antenna while the skin permittivity shifts the frequency resonance of a wearable antenna based on tissue dielectric variation. To overcome this lossy effect, we had to find a way to either compensate for or negate the human tissue capacitive loading on RFID devices. With our previous paper [192], we developed a process of designing our sensor region to act as a capacitive shunt to overcome (or at least minimize) any capacitive loading from a high dielectric environment. We implemented the same process, with the addition of a layer adjustment between the high dielectric environment and antenna, which allowed us to develop a single wearable RFID design able to easily adjust to a range of human tissue properties.

Once a single function design was developed, we took it further by trying to see if it would possible to use the design as a self-sensing system to detect any additional changes to the surrounding environment. This interest led to the development of the ‘smart dressing’, which was able to detect as little as 10 µL of leakage from an inserted IV line. This work could be further expended upon by utilising body fluids and/ or different stocks of common medication to see if any changes can be caused within this stable smart dressing. As it is able to function embedded with a deep layer of gauze (up to almost 5 cm), it also might be of interest for continuous incontinence detection in hospitalised patients. Both the IV-line leakage and detection of incontinence were presented to us as serious issues dealt within the medical sector by clinicians suggesting that this design provides a clinical necessity not yet available on the

market. This could be ideally brought to market as a Class I device as it is unlikely to cause any risk or harm and, therefore, vary likely would not require any clinical trials to get FDA approval [195]. The main hurdle would be acquiring a commercial partner or possibly utilising a National Institute for Health Research product development awards [197] (or similar) to bring this to market within the EU. This obviously would come with its own hurdles therefore going through a commercial partner might be preferable.

Understanding that it was both possible to detect environmental changes surrounding a passive UHF RFID sensor while maintaining the capacitive loading effect of human tissue to a minimum, we had to understand the timed impedances changes caused by *C. albicans* biofilm growth specifically. We decided to utilise the readily available xCELLigence RCTA system along with our previously published liquid detection sensor [197] as well as a simple interdigit antenna sensor to do a timed study of *C. albicans* biofilm growth. We found a correlation between all three methods, as *C. albicans* biofilm develops there is an impedance imbalance that occurs which exhibits at a single frequency as a loss in capacitance or with a frequency sweep as a shift in resonance. However, this loss in capacitance only occurs till an intermediate biofilm layer develops (up to 24 hours) once the biofilm passes this stage, the dielectric properties of the layer become very hydrophobic changing the fringing field capacitance. This is most likely due to the basic concept of changing the dielectric constant between two parallel plates as *C. albicans* cells are less conductive than pure media, there is a decrease in the dielectric constant present between the sensor "fingers". Once the *C. albicans* layer fully settles over the sensor with an intermediate growth of 24 hours, it is no longer just the thin layer involved. At this point, more advances process are contributing as it is known that the dielectric constant of the film on top of a fringing field and the substrate below can change the measured capacitance for any isotropic fringing fields [198]. The calculation for such a fringing field is [198]:

$$C1 = \varepsilon_0(\varepsilon_r + \varepsilon_k)\frac{k\left(\sqrt{1+(a/b)^2}\right)}{k(a/b)} + 2\varepsilon_0\varepsilon_k\frac{t}{a} \quad (11)$$

where ε_0 is the dielectric constant in the free space ($\varepsilon_0 = 8.8542\times10^{-12}$ F/m); a and b (distance between two) are the electrodes widths; t is the thickness of the electrode; ε_r is the dielectric constant of the substrate; and k (·) the first kind complete elliptic integral; ε_k is the dielectric constant of the dielectric film. It can be clearly seen that decreasing the dielectric constant of the biofilm layer (as expected between 0 and 24 hours) would cause a decrease in capacitance. Once the 24-hour point is reached there is no longer any noticeable (by fringing fields) change in the biofilm dielectric constant but rather just an increase in the biofilm layer on top of the sensor which causes a reversal in the capacitance.

Simulations also suggested that an increase in only the dielectric layer thickness had a linear change in resonance and capacitance. The measured relationship was only seen (particularly for the RFMicron design) in simulation when a decrease in the dielectric properties was included from 0 hours (dielectric constant equivalent to water) to 24 hours (dielectric equivalent to silicone). Therefore, this is just a relationship between hydrophobicity of the *C. albicans* during biofilm formation and the detected dielectric properties by the sensor technology. For passive UHF RFID, it is also possible that a shift in frequency (due to the increase in biofilm layer thickness) causes the 2nd resonance to shift within the read bandwidth, increasing the system capacitance after 24 hours of growth. The interdigit antenna simulations also showed multiple resonant peaks which shifted based on the thickness of the film on top the sensor. However, this theory was tested by utilising zymolyase enzyme to disrupt the biofilm formation and increase the layer conductivity (and reducing hydrophobicity) by providing access to the media at the sensor surface without changing the biofilm layer thickness. Zymolyase was able to reverse the gain in capacitance after 24 hours of growth, suggesting that it is both the dielectric constant and layer thickness that play a role in the growth of *C. albicans* rather than just an appearance of the 2nd resonance.

To further prove this relationship, a zymolyase experiment would need to be repeated with both the RFMicron and the interdigit sensors. Possibly the use of a salt-gel layer could provide a time-dependent repeatable model, without reliance on the biology of a microorganism. As the salt-gel is allowed to dry and become less conductive with time, it would be possible to fully study the relationship between conductivity, sensor capacitance and layer thickness without reliance on simulation alone. Once these detection methods are perfected, then this approach could be implemented for other microorganisms allowing for the categorisation of their electrical properties for future sensor development.

These three main experiments (and papers) allowed the final development of voice prosthesis passive RFID microbial sensors able to function past 60 cm (prototype 1) or at 0.11 cm (prototype 2). Prototype 2 was developed to utilize a digital IC able to self-tune the internal capacitance and provide any changes as a nominal value; this reduced the reliance on resonant frequency shifts as a method for microbial detection. Also, there was a need to minimize the width of the device from prototype 1 as clinician feedback requested a smaller size for functional use. With a smaller size, there was a loss in read range; however, the read range remained within the boundaries of what was expected for an implantable device. As only the function of the antenna was measured within a body phantom with microbial growth simulation based on previous work presented, it is necessary that any future project test actual timed growth of *C. albicans* on top of the presented final designs. Also, it might be of interest to test for mixed biofilm colonisation as there are links with worse patient outcomes, particularly with implant lifespan. To our knowledge this is the first device able to detect *C. albicans* biofilm formation while within a human body (phantom).

Any interest in commercialisation of these devices would require safety testing and quality control if intended for implantation within a human patient as well as to validate the precision, sensitivity and robustness of the presented systems. However, all devices were kept below an

RFID reader signal of 30 dBm (safe level for human utilisation) and had no issues with wave propagation at these low values. Understanding the growth and detection of *C. albicans* could allow the application of this type of system, with slight adjustments, upon other implantable sensor for the detection of various organism. However, it should be noted that the current sensors rely on impedance mismatch (causing a resonance shift or capacitance adjustment) as methods of detection and, thus, are not species or organism specific. It is possible that other microorganism would not cause such a growth response or at least a large enough response to be detected as exhibited by *C. albicans*. We saw this using the xCELLigence, *S. aureus* produced a fractional change (CI value change of ~0.12) in comparison to *C. albicans* (CI value change of ~2). As we did not test *S. aureus* with any of our devices, we do not know if our sensors are robust enough to detect such minimal growth. Also, the device was not tested at varying temperatures nor at varying humidity. This could possibly have an effect as it is known that dielectric properties can be affected by temperature at a minimum. It should be also noted that in [169], the conductance of the graphene sensor was highly changed by the bovine breath and saliva. Therefore, it is possible that such simple things as increased saliva production or intake of breath could alter the sensitivity of the device as this was never tested. Therefore, there is still need for continued verification of this presented device. However, as the device is covered by a thin layer of polymer, it should in theory be less susceptible to breath and humidity unlike the published work. Therefore, it is possible that only an adjustment to the polymer layer thickness (or structure) would be necessary to minimise any unwanted effects other than growth detection of a *C. albicans* biofilm.

The most logical alteration might be to functionalise our sensors for more pathogen specific detection by changing the polymer film on top of the sensors. As we know that microorganism can cause environmental pH changes or increase inflammation surrounding a medical devices, the use of pH sensitive or temperature sensitive polymers [199] (as often utilised for drug-

delivery methods) might allow for a broader pathogen list for detection. Also, having polymers immobilised with aptamers [200, 201] might even permit species specific detection allowing the medical device to only detect species known to cause device failure, such as *C. albicans* and voice prosthesis. As medical device structure was taken into substantial considerations (the main limiting factor of the sensor design) when developing the voice prosthesis sensor, which was unobtrusive and could be easily embedded with the device, any alteration to the sensor must foremost not alter the medical device unnecessarily. Any polymeric changes should not weaken the device or increase rates of microbial colonisation such as seen with polymer surface roughness [202, 203] or contact angle [204] alterations. Therefore, any changes to the current design, in order to improve upon it, must first take into consideration any issues that might arise during patient use.

In general, for any of this to be taken to market the design must be adjusted as etching copper is time consuming and, as stated previously, not ideal for medical applications. This brings a technical challenge as silver might have a similar conductivity to copper (near 6e7) but a cheaper alternative preferred by medical companies, aluminium, has a conductivity half of this. This necessitates an adjustment to the design to account for any cheaper alternative chosen by a medical device company. Also, it is preferable to have conductivity near that of copper to reduce the changes to the device as the current device already has a read range below one meter, any reduction in conductivity could further reduce the read range by affecting the circuit resonance and might necessitate an extra matching network to match IC and antenna impedance at the desired frequency. This would add bulk (likely lumped capacitor) to the system and reduce the ability for implementation within a thin voice prosthesis. Any substantial changes would most likely require a clinical trial to prove device safety. In general, a clinical trial would be necessary to bring the voice prosthesis sensor to market as it would likely be classed above Class I at a minimum as “moderate risk”; if the sensor is implemented in device incorrectly, it

could alter function of the device affecting the breathing and speaking of the patient reliant on the voice prosthesis. Therefore, this would add expense and time needed to bring the device to market. Currently, this work is in the process of being commercialised with the help of Smiths Medical [205].

Chapter 5: References

1. Brown, G.D., et al., *Hidden killers: human fungal infections.* Sci Transl Med, 2012. **4**(165): p. 165rv13.
2. Romani, L., *Immunity to fungal infections.* Nat Rev Immunol, 2011. **11**(4): p. 275-88.
3. Blanco, J.L. and M.E. Garcia, *Immune response to fungal infections.* Veterinary Immunology and Immunopathology, 2008. **125**(1): p. 47-70.
4. Sanglard, D. and T.C. White, *Molecular Principles of Antifungal Drug Resistance*, in *Molecular Principles of Fungal Pathogenesis*. American Society of Microbiology, 2006.
5. Miceli, M.H. and S.A. Lee, *Emerging moulds: epidemiological trends and antifungal resistance.* Mycoses, 2011. **54**(6): p. e666-e678.
6. Moran, G., D. Coleman, and D. Sullivan, *An Introduction to the Medically Important Candida Species*, in *Candida and Candidiasis, Second Edition*. 2012, American Society of Microbiology.
7. Tsai, P.-W., et al., *Study of Candida albicans and its interactions with the host: A mini review.* BioMedicine, 2013. **3**(1): p. 51-64.
8. Lim, C.S.-Y., et al., *Candida and invasive candidiasis: back to basics.* European Journal of Clinical Microbiology & Infectious Diseases, 2012. **31**(1): p. 21-31.
9. Wisplinghoff, H., et al., *Nosocomial Bloodstream Infections in US Hospitals: Analysis of 24,179 Cases from a Prospective Nationwide Surveillance Study.* Clinical Infectious Diseases, 2004. **39**(3): p. 309-317.
10. Desai, J.V., *Candida albicans Hyphae: From Growth Initiation to Invasion.* Journal of fungi (Basel, Switzerland), 2018. **4**(1): p. 10.

11. Sudbery, P.E., *Growth of Candida albicans hyphae.* Nature Reviews Microbiology, 2011. **9**: p. 737.

12. Biswas, S., P. Van Dijck, and A. Datta, *Environmental sensing and signal transduction pathways regulating morphopathogenic determinants of Candida albicans.* Microbiology and molecular biology reviews : MMBR, 2007. **71**(2): p. 348-376.

13. Kadosh, D., *Morphogenesis in C. albicans.*, in *Candida albicans: Cellular and Molecular Biology*, P. R., Editor. 2017, Springer, Cham.

14. Shareck, J. and P. Belhumeur, *Modulation of Morphogenesis in Candida albicans by Various Small Molecules.* Eukaryotic Cell, 2011. **10**(8): p. 1004-1012.

15. Cottier, F. and F.A. Mühlschlegel, *Sensing the environment: Response of Candida albicans to the X factor.* FEMS Microbiology Letters, 2009. **295**(1): p. 1-9.

16. Sabine E. Eckert, C.C.S.a.F.A.M., *Regulation of Morphogenesis in Candida species*, in *Candida: Comparative and Functional Genomics,* C.d.E.a.B. Hube, Editor. 2007, Caister Academic Press: U.K.

17. Maidan, M.M., et al., *The G protein-coupled receptor Gpr1 and the Galpha protein Gpa2 act through the cAMP-protein kinase A pathway to induce morphogenesis in Candida albicans.* Molecular biology of the cell, 2005. **16**(4): p. 1971-1986.

18. Cloutier, M., et al., *The two isoforms of the cAMP-dependent protein kinase catalytic subunit are involved in the control of dimorphism in the human fungal pathogen Candida albicans.* Fungal Genetics and Biology, 2003. **38**(1): p. 133-141.

19. Liu, H., J. Kohler, and G. Fink, *Suppression of hyphal formation in Candida albicans by mutation of a STE12 homolog.* Science, 1994. **266**(5191): p. 1723-1726.

20. Morschhäuser, J., *Nitrogen regulation of morphogenesis and protease secretion in Candida albicans.* International Journal of Medical Microbiology, 2011. **301**(5): p. 390-394.

21. Flanagan, P.R., et al., *The Candida albicans TOR-Activating GTPases Gtr1 and Rhb1 Coregulate Starvation Responses and Biofilm Formation.* mSphere, 2017. **2**(6): p. e00477-17.

22. Davis, D., et al., *Candida albicans RIM101 pH response pathway is required for host-pathogen interactions.* Infect Immun, 2000. **68**(10): p. 5953-9.

23. Davis, D.A., *How human pathogenic fungi sense and adapt to pH: the link to virulence.* Current Opinion in Microbiology, 2009. **12**(4): p. 365-370.

24. Li, M., et al., *Candida albicans Rim13p, a protease required for Rim101p processing at acidic and alkaline pHs.* Eukaryotic cell, 2004. **3**(3): p. 741-751.

25. Vylkova, S., *Environmental pH modulation by pathogenic fungi as a strategy to conquer the host.* PLOS Pathogens, 2017. **13**(2): p. e1006149.

26. Setiadi, E.R., et al., *Transcriptional Response of Candida albicans to Hypoxia: Linkage of Oxygen Sensing and Efg1p-regulatory Networks.* Journal of Molecular Biology, 2006. **361**(3): p. 399-411.

27. Gil-Bona, A., et al., *The external face of Candida albicans: A proteomic view of the cell surface and the extracellular environment.* Journal of Proteomics, 2018. **180**: p. 70-79.

28. de Groot, P.W.J., et al., *Adhesins in Human Fungal Pathogens: Glue with Plenty of Stick.* Eukaryotic Cell, 2013. **12**(4): p. 470.

29. Kinneberg, K.M., et al., *Effect of INT1 Gene on Candida albicans Murine Intestinal Colonization.* Journal of Surgical Research, 1999. **87**(2): p. 245-251.

30. Schaller, M., et al., *Hydrolytic enzymes as virulence factors of Candida albicans.* Mycoses, 2005. **48**(6): p. 365-377.

31. Theiss, S., et al., *Inactivation of the phospholipase B gene PLB5 in wild-type Candida albicans reduces cell-associated phospholipase A2 activity and attenuates virulence.* International journal of medical microbiology : IJMM, 2006. **296**(6): p. 405-420.

32. Dos Santos, A.L.S., et al., *Secretion of serine peptidase by a clinical strain of Candida albicans: influence of growth conditions and cleavage of human serum proteins and extracellular matrix components.* FEMS Immunology & Medical Microbiology, 2006. **46**(2): p. 209-220.

33. Muszewska, A., et al., *Fungal lifestyle reflected in serine protease repertoire.* Scientific Reports, 2017. **7**(1): p. 9147.

34. Soll, D.R., *The role of phenotypic switching in the basic biology and pathogenesis of Candida albicans.* Journal of Oral Microbiology, 2014. **6**: p. 10.3402/jom.v6.22993.

35. Fourie, R., et al., *Iron at the Centre of Candida albicans Interactions.* Frontiers in Cellular and Infection Microbiology, 2018. **8**(185).

36. Okutomi, T., et al., *Augmented inhibition of growth of Candida albicans by neutrophils in the presence of lactoferrin.* FEMS Immunology & Medical Microbiology, 1997. **18**(2): p. 105-112.

37. Lee, R.E.B., et al., *Genome-wide expression profiling of the response to ciclopirox olamine in Candida albicans.* Journal of Antimicrobial Chemotherapy, 2005. **55**(5): p. 655-662.

38. Heymann, P., et al., *The siderophore iron transporter of Candida albicans (Sit1p/Arn1p) mediates uptake of ferrichrome-type siderophores and is required for epithelial invasion.* Infection and Immunity, 2002. **70**(9): p. 5246-5255.

39. Chen, C., et al., *An iron homeostasis regulatory circuit with reciprocal roles in Candida albicans commensalism and pathogenesis.* Cell host & microbe, 2011. **10**(2): p. 118-135.

40. Chen, C. and S.M. Noble, *Post-transcriptional regulation of the Sef1 transcription factor controls the virulence of Candida albicans in its mammalian host.* PLoS pathogens, 2012. **8**(11): p. e1002956-e1002956.

41. Hsu, P.-C., C.-Y. Yang, and C.-Y. Lan, *Candida albicans Hap43 is a repressor induced under low-iron conditions and is essential for iron-responsive transcriptional regulation and virulence.* Eukaryotic cell, 2011. **10**(2): p. 207-225.

42. BAILLIE, G.S. and L.J. DOUGLAS, *Role of dimorphism in the development of Candida albicans biofilms.* Journal of Medical Microbiology, 1999. **48**(7): p. 671-679.

43. Chandra, J., et al., *Biofilm formation by the fungal pathogen Candida albicans: development, architecture, and drug resistance.* Journal of bacteriology, 2001. **183**(18): p. 5385-5394.

44. Douglas, L.J., *Candida biofilms and their role in infection.* Trends in Microbiology, 2003. **11**(1): p. 30-36.

45. Hawser, S.P. and L.J. Douglas, *Biofilm formation by Candida species on the surface of catheter materials in vitro.* Infection and immunity, 1994. **62**(3): p. 915-921.

46. Nobile, C.J., et al., *Biofilm matrix regulation by Candida albicans Zap1*. PLoS biology, 2009. **7**(6): p. e1000133-e1000133.

47. Uppuluri, P., et al., *Dispersion as an important step in the Candida albicans biofilm developmental cycle.* PLoS pathogens, 2010. **6**(3): p. e1000828-e1000828.

48. Uppuluri, P., et al., *The transcriptional regulator Nrg1p controls Candida albicans biofilm formation and dispersion.* Eukaryotic cell, 2010. **9**(10): p. 1531-1537.

49. Nobile, C.J., et al., *A recently evolved transcriptional network controls biofilm development in Candida albicans.* Cell, 2012. **148**(1-2): p. 126-138.

50. Hogan, D.A. and F.A. Muhlschlegel, *Candida albicans developmental regulation: adenylyl cyclase as a coincidence detector of parallel signals.* Current Opinion in Microbiology, 2011. **14**(6): p. 682-686.

51. Yi, S., et al., *Alternative Mating Type Configurations (a/α versus a/a or α/α) of Candida albicans Result in Alternative Biofilms Regulated by Different Pathways.* PLOS Biology, 2011. **9**(8): p. e1001117.

52. Bockmühl, D.P. and J.F. Ernst, *A potential phosphorylation site for an A-type kinase in the Efg1 regulator protein contributes to hyphal morphogenesis of Candida albicans.* Genetics, 2001. **157**(4): p. 1523-1530.

53. Nett, J.E., et al., *Time course global gene expression analysis of an in vivo Candida biofilm.* The Journal of infectious diseases, 2009. **200**(2): p. 307-313.

54. Nobile, C.J., et al., *Critical role of Bcr1-dependent adhesins in C. albicans biofilm formation in vitro and in vivo.* PLoS pathogens, 2006. **2**(7): p. e63-e63.

55. Nobile, C.J., et al., *Complementary adhesin function in C. albicans biofilm formation.* Current biology : CB, 2008. **18**(14): p. 1017-1024.

56. Schweizer, A., et al., *The TEA/ATTS transcription factor CaTec1p regulates hyphal development and virulence in Candida albicans.* Molecular Microbiology, 2000. **38**(3): p. 435-445.

57. Donlan, R.M., *Biofilm Formation: A Clinically Relevant Microbiological Process.* Clinical Infectious Diseases, 2001. **33**(8): p. 1387-1392.

58. Khot, P.D., et al., *A small subpopulation of blastospores in candida albicans biofilms exhibit resistance to amphotericin B associated with differential regulation of ergosterol and beta-1,6-glucan pathway genes.* Antimicrobial agents and chemotherapy, 2006. **50**(11): p. 3708-3716.

59. Arendrup, M.C. and T.F. Patterson, *Multidrug-Resistant Candida: Epidemiology, Molecular Mechanisms, and Treatment.* The Journal of Infectious Diseases, 2017. **216**(suppl_3): p. S445-S451.

60. Mateus, C., S.A. Crow, Jr., and D.G. Ahearn, *Adherence of Candida albicans to silicone induces immediate enhanced tolerance to fluconazole.* Antimicrobial agents and chemotherapy, 2004. **48**(9): p. 3358-3366.

61. Herwald, S.E. and C.A. Kumamoto, *Candida albicans Niche Specialization: Features That Distinguish Biofilm Cells from Commensal Cells.* Current fungal infection reports, 2014. **8**(2): p. 179-184.

62. Cleveland, A.A., et al., *Changes in incidence and antifungal drug resistance in candidemia: results from population-based laboratory surveillance in Atlanta and Baltimore, 2008-2011.* Clinical infectious diseases : an official publication of the Infectious Diseases Society of America, 2012. **55**(10): p. 1352-1361.

63. García-Sánchez, S., et al., *Candida albicans biofilms: a developmental state associated with specific and stable gene expression patterns.* Eukaryotic cell, 2004. **3**(2): p. 536-545.

64. Rosenbach, A., et al., *Adaptations of Candida albicans for growth in the mammalian intestinal tract.* Eukaryotic cell, 2010. **9**(7): p. 1075-1086.

65. Bonhomme, J., et al., *Contribution of the glycolytic flux and hypoxia adaptation to efficient biofilm formation by Candida albicans.* Molecular Microbiology, 2011. **80**(4): p. 995-1013.

66. Sohn, K., et al., *EFG1 is a major regulator of cell wall dynamics in Candida albicans as revealed by DNA microarrays.* Molecular Microbiology, 2003. **47**(1): p. 89-102.

67. Andes, D., et al., *Development and characterization of an in vivo central venous catheter Candida albicans biofilm model.* Infection and immunity, 2004. **72**(10): p. 6023-6031.

68. Donlan, R.M., *Biofilms and device-associated infections.* Emerging infectious diseases, 2001. **7**(2): p. 277-281.

69. Nett, J.E., et al., *Host contributions to construction of three device-associated Candida albicans biofilms.* Infection and immunity, 2015. **83**(12): p. 4630-4638.

70. Jabra-Rizk, M.A., W.A. Falkler, and T.F. Meiller, *Fungal biofilms and drug resistance.* Emerging infectious diseases, 2004. **10**(1): p. 14-19.

71. Taff, H.T., et al., *Mechanisms of Candida biofilm drug resistance.* Future microbiology, 2013. **8**(10): p. 1325-1337.

72. Silva, S., et al., *Candida Species Biofilms' Antifungal Resistance.* Journal of fungi (Basel, Switzerland), 2017. **3**(1): p. 8.

73. Kojic, E.M. and R.O. Darouiche, *Candida infections of medical devices.* Clinical microbiology reviews, 2004. **17**(2): p. 255-267.

74. Cirasola, D., et al., *Experimental biofilm-related Candida infections.* Future Microbiology, 2013. **8**(6):799-805..

75. Walraven, C.J. and S.A. Lee, *Antifungal Lock Therapy.* Antimicrobial Agents and Chemotherapy, 2013. **57**(1): p. 1.

76. Giles, C., et al., *The importance of fungal pathogens and antifungal coatings in medical device infections.* Biotechnology Advances, 2018. **36**(1): p. 264-280.

77. Dominic, R.M., S. Shenoy S Fau - Baliga, and S. Baliga, *Candida biofilms in medical devices: evolving trends.* Kathmandu University Medical Journal, 2018. **5**(3):431-6..

78. Cuellar-Cruz, M., et al., *The effect of biomaterials and antifungals on biofilm formation by Candida species: a review.* Eur J Clin Microbiol Infect Dis., 2012. **31**(10):2513-27.

79. Jakobsen, T.H., et al., *Implants induce a new niche for microbiomes.* APMIS, 2018. **126**(8): p. 685-692.

80. Murat, S., et al., *In Vitro Evaluation of Adhesion of Candida albicans on CAD/CAM PMMA-Based Polymers.* Journal of Prosthodontics, 2019. **28**(2): p. e873-e879.

81. Frade, J.P. and B.A. Arthington-Skaggs, *Effect of serum and surface characteristics on Candida albicans biofilm formation.* Mycoses, 2011. **54**(4): p. e154-e162.

82. Holmes, A.R., et al., *Adherence of Candida albicans to silicone is promoted by the human salivary protein SPLUNC2/PSP/BPIFA2.* Mol Oral Microbiol., 2014. **29**(2):90-8.

83. Gorr, S.U., et al., *Dual host-defence functions of SPLUNC2/PSP and synthetic peptides derived from the protein.* Biochem Soc Trans., 2011. **39**(4):1028-32.

84. Holmes, A.R., R.D. Bandara Bm Fau - Cannon, and R.D. Cannon, *Saliva promotes Candida albicans adherence to human epithelial cells.* J Dent Res., 2002. **81**(1):28-32..

85. Holmes, A.R., et al., *Candida albicans binds to saliva proteins selectively adsorbed to silicone.* Oral Surg Oral Med Oral Pathol Oral Radiol Endod., 2006. **102**(4):488-94.

86. O'Sullivan, J.M., R.D. Jenkinson Hf Fau - Cannon, and R.D. Cannon, *Adhesion of Candida albicans to oral streptococci is promoted by selective adsorption of salivary proteins to the streptococcal cell surface.* Microbiology, 2000. **146**: 41–48.

87. Cannon, R.D., H.F. Nand Ak Fau - Jenkinson, and H.F. Jenkinson, *Adherence of Candida albicans to human salivary components adsorbed to hydroxylapatite.* Microbiology, 1995. **141** (Pt 1):213-9.

88. Jones, D.S., et al., *Conditioning film and environmental effects on the adherence of Candida spp. to silicone and poly(vinylchloride) biomaterials.* J Mater Sci Mater Med., 2001. **12**(5):399-405.

89. Cannon, R.D. and W.L. Chaffin, *Oral colonization by Candida albicans.* Critical Reviews in Oral Biology & Medicine, 1999. (1045-4411).

90. Weston, W.M., et al., *Differential display identification of plunc, a novel gene expressed in embryonic palate, nasal epithelium, and adult lung.* J Biol Chem., 1999. **274**(19):13698-703.

91. Bingle, C.D. and L. Bingle, *Characterisation of the human plunc gene, a gene product with an upper airways and nasopharyngeal restricted expression pattern.* Biochim Biophys Acta., 2000. **1493**(3):363-7.

92. Khovidhunkit, W., et al., *Parotid secretory protein is an HDL-associated protein with anticandidal activity.* Am J Physiol Regul Integr Comp Physiol., 2005. **288**(5):R1306-15.

93. Millsap, K.W., et al., *Adhesive interactions between voice prosthetic yeast and bacteria on silicone rubber in the absence and presence of saliva.* Antonie Van Leeuwenhoek, 2001. **79**: 337–343.

94. van der Mei, H.C., et al., *Voice prosthetic biofilm formation and Candida morphogenic conversions in absence and presence of different bacterial strains and species on silicone-rubber.* PLoS One, 2014. **9**(8):e104508.

95. Nagler, R.M. and O. Hershkovich, *Relationships between age, drugs, oral sensorial complaints and salivary profile.* Archive of Oral Biology, 2005. **50** (1): 7-16.

96. Jensen, S.B., et al., *Xerostomia and hypofunction of the salivary glands in cancer therapy.* Support Care Cancer. 2003. **11**(4):207-25.

97. Chandra, J., P.K. Mukherjee, and M.A. Ghannoum, *Candida biofilms associated with CVC and medical devices.* Mycoses, 2012. **55**(s1): p. 46-57.

98. Ramage, G., J.P. Martínez, and J.L. López-Ribot, *Candida biofilms on implanted biomaterials: a clinically significant problem.* FEMS Yeast Research, 2006. **6**(7): p. 979-986.

99. Leonhard, M., et al., *Growth kinetics of candida biofilm on medical polymers: A long-term in vitro study*. The Laryngoscope, 2013. **123**(3): p. 732-737.

100. Chandra, J., et al., *Interaction of Candida albicans with adherent human peripheral blood mononuclear cells increases C. albicans biofilm formation and results in differential expression of pro- and anti-inflammatory cytokines.* Infect Immun, 2007. **75**(5):2612-20.

101. Nett, J.E., *The Host's Reply to Candida Biofilm.* Pathogens (Basel, Switzerland), 2016. **5**(1): p. 33.

102. Alonso, M.F., et al., *Macrophage Migration Is Impaired within Candida albicans Biofilms. J Fungi (Basel), 2017. **3**(3): 31.*

103. Hernández-Chávez, M.J., et al., *Fungal Strategies to Evade the Host Immune Recognition.* Journal of fungi (Basel, Switzerland), 2017. **3**(4): p. 51.

104. Nett, J.E., et al., *Host contributions to construction of three device-associated Candida albicans biofilms.* Infect Immun, 2015. **83**(12):4630-8.

105. Kernien, J.F., et al., *The Interface between Fungal Biofilms and Innate Immunity.* Frontiers in immunology, 2018. **8**: p. 1968-1968.

106. Müller, R., et al., *Fluorescence-Based Bacterial Overlay Method for Simultaneous In Situ Quantification of Surface-Attached Bacteria.* Applied and Environmental Microbiology, 2007. **73**(8): p. 2653.

107. Rickard, A.H., et al., *Bacterial coaggregation: an integral process in the development of multi-species biofilms.* Trends in Microbiology, 2003. **11**(2):94-100.

108. Katsikogianni, M. and Y.F. Missirlis, *Concise review of mechanisms of bacterial adhesion to biomaterials and of techniques used in estimating bacteria-material interactions.* Eur Cell Mater, 2004. **8**:37-57.

109. Chandra, J., et al., *Modification of surface properties of biomaterials influences the ability of Candida albicans to form biofilms.* Appl Environ Microbiol., 2005. **71**(12): 8795–8801.

110. Soll, D.R. and K.J. Daniels, *Plasticity of Candida albicans Biofilms.* Microbiol Mol Biol Rev., 2016. **80**(3):565-95.

111. Chandra, J., et al., *Modification of surface properties of biomaterials influences the ability of Candida albicans to form biofilms.* Applied and environmental microbiology, 2005. **71**(12): p. 8795-8801.

112. Percival, S.L., et al., *Healthcare-associated infections, medical devices and biofilms: risk, tolerance and control.* Journal of Medical Microbiology, 2015. **64**(4): p. 323-334.

113. Nett, J., et al., *β-1,3 Glucan as a Test for Central Venous Catheter Biofilm Infection.* The Journal of Infectious Diseases, 2007. **195**(11): p. 1705-1712.

114. Talpaert, M.J., et al., *Candida biofilm formation on voice prostheses.* Journal of Medical Microbiology, 2015. **64**(3): p. 199-208.

115. Bencharit, S., et al., *Elucidating role of salivary proteins in denture stomatitis using a proteomic approach.* Molecular bioSystems, 2012. **8**(12): p. 3216-3223.

116. Chandra, J., et al., *Antifungal resistance of candidal biofilms formed on denture acrylic in vitro.* Journal of Dental Research, 2001. **80** (3): 903-908.

117. Safavieh, M., et al., *Advances in Candida detection platforms for clinical and point-of-care applications.* Critical reviews in biotechnology, 2017. **37**(4): p. 441-458.

118. Hall, K.K. and J.A. Lyman, *Updated review of blood culture contamination.* Clinical microbiology reviews, 2006. **19**(4): p. 788-802.

119. Morgan, J., et al., *Excess mortality, hospital stay, and cost due to candidemia: a case-control study using data from population-based candidemia surveillance.* Infect Control Hosp Epidemiol., 2005. **26**(6):540-7.

120. Harrington, B.J. and G.J. Hageage, Jr., *Calcofluor White: A Review of its Uses and Applications in Clinical Mycology and Parasitology.* Laboratory Medicine, 2003. **34**(5): p. 361-367.

121. Uzma Mussarat Malik , A.B.K., Muhammad Luqman Satti, *Comparative Evaluation of CHROMagar and API 20C AUX in Isolation and Identification of Candida Species.* JIIMC 2018. **13**(2): p. 85-90.

122. Davey, K.G., et al., *Evaluation of the AUXACOLOR system, a new method of clinical yeast identification.* Journal of clinical pathology, 1995. **48**(9): p. 807-809.

123. *Thermo Scientific™ RapID™ YEAST PLUS System.* . 2019 [cited 2019 June 1]; Available from: https://www.thermofisher.com/order/catalog/product/R8311007.

124. Arvanitis, M., et al., *Molecular and nonmolecular diagnostic methods for invasive fungal infections.* Clinical microbiology reviews, 2014. **27**(3): p. 490-526.

125. Ostrosky-Zeichner, L., et al., *Multicenter Clinical Evaluation of the (1→3) β-D-Glucan Assay as an Aid to Diagnosis of Fungal Infections in Humans.* Clinical Infectious Diseases, 2005. **41**(5): p. 654-659.

126. Lamoth, F., et al., *β-Glucan Antigenemia Assay for the Diagnosis of Invasive Fungal Infections in Patients With Hematological Malignancies: A Systematic Review and Meta-Analysis of Cohort Studies From the Third European Conference on Infections in Leukemia (ECIL-3).* Clinical Infectious Diseases, 2011. **54**(5): p. 633-643.

127. Leinberger, D.M., et al., *Development of a DNA microarray for detection and identification of fungal pathogens involved in invasive mycoses.* Journal of clinical microbiology, 2005. **43**(10): p. 4943-4953.

128. Low, S.Y., J.E. Hill, and J. Peccia, *DNA aptamers bind specifically and selectively to (1-3)-beta-D-glucans.* Biochemical and biophysical research communications, 2009. **378**(4): p. 701-705.

129. Tang, X.L., et al., *Improved detection of deeply invasive candidiasis with DNA aptamers specific binding to (1-->3)-beta-D-glucans from Candida albicans.* Eur J Clin Microbiol Infect Dis., 2016. 35(4):587-95.

130. Gordon, C.K.L., M. Eisenstein, and H.T. Soh, *Direct Selection Strategy for Isolating Aptamers with pH-Sensitive Binding Activity.* ACS Sensors, 2018. **3**(12): p. 2574-2580.

131. Posteraro, B., et al., *Are the Conventional Commercial Yeast Identification Methods Still Helpful in the Era of New Clinical Microbiology Diagnostics? A Meta-Analysis of Their Accuracy.* Journal of clinical microbiology, 2015. **53**(8): p. 2439-2450.

132. Cai, D., et al., *An integrated microfluidic device utilizing dielectrophoresis and multiplex array PCR for point-of-care detection of pathogens.* Lab Chip, 2014. **14**(20):3917-24.

133. LA Neely, M.A., M Blanco, *NMR systems and methods for the rapid detection of analytes.* 2012, T2 Biosystems, Inc: USA.

134. *T2Candida Panel*. 2019 [cited 2019 July 1]; Available from: https://www.t2biosystems.com/products-technology-ous/t2candida-panel-2/.

135. Singhal, N., et al., *MALDI-TOF mass spectrometry: an emerging technology for microbial identification and diagnosis.* Frontiers in microbiology, 2015. **6**: p. 791-791.

136. Yaman, G., I. Akyar, and S. Can, *Evaluation of the MALDI TOF-MS method for identification of Candida strains isolated from blood cultures.* Diagnostic Microbiology and Infectious Disease, 2012. **73**(1): p. 65-67.

137. Pulcrano, G., et al., *Rapid and reliable MALDI-TOF mass spectrometry identification of Candida non-albicans isolates from bloodstream infections.* Journal of Microbiological Methods, 2013. **94**(3): p. 262-266.

138. Alizadeh, M., et al., *Identification of Candida species isolated from vulvovaginitis using matrix assisted laser desorption ionization-time of flight mass spectrometry.* Current medical mycology, 2017. **3**(4): p. 21-25.

139. Daniels, J.S. and N. Pourmand, *Label-Free Impedance Biosensors: Opportunities and Challenges.* Electroanalysis, 2007. **19**(12): p. 1239-1257.

140. Kwasny, D., et al., *Direct Detection of Candida albicans with a Membrane Based Electrochemical Impedance Spectroscopy Sensor.* Sensors, 2018. **18**(7).

141. Biswas, K., S. Sen, and P.K. Dutta, *A constant phase element sensor for monitoring microbial growth.* Sensors and Actuators B: Chemical, 2006. **119**(1): p. 186-191.

142. Park, J.S., et al., *Amyloid Beta Detection by Faradaic Electrochemical Impedance Spectroscopy Using Interdigitated Microelectrodes.* Sensors (Basel, Switzerland), 2018. **18**(2): p. 426.

143. Martin, A.L., et al., *In-situ electrochemical analysis of microbial activity.* AMB Express, 2018. **8**(1): p. 162-162.

144. Lario-García, J. and R. Pallàs-Areny, *Constant-phase element identification in conductivity sensors using a single square wave.* Sensors and Actuators A: Physical, 2006. **132**(1): p. 122-128.

145. Johnson, N., et al., *Evaluation of indirect impedance for measuring microbial growth in complex food matrices.* Food Microbiol, 2014. **42**: p. 8-13.

146. Ribeiro, T., et al., *Development, validation, and applications of a new laboratory-scale indirect impedancemeter for rapid microbial control.* Appl Microbiol Biotechnol, 2003. **63**(1): p. 35-41.

147. Zhong, N., M. Zhao, and Y. Li, *U-shaped, double-tapered, fiber-optic sensor for effective biofilm growth monitoring.* Biomedical Optics Express, 2016. **7**(2): p. 335-351.

148. Zhong, N., et al., *A Fiber-Optic Sensor for Accurately Monitoring Biofilm Growth in a Hydrogen Production Photobioreactor.* Analytical Chemistry, 2014. **86**(8): p. 3994-4001.

149. Cai, Z., et al., *A Photonic Crystal Protein Hydrogel Sensor for Candida albicans.* Angewandte Chemie International Edition, 2015. **54**(44): p. 13036-13040.

150. Kurmoo, Y., et al., *Real time monitoring of biofilm formation on coated medical devices for the reduction and interception of bacterial infections.* Biomaterials Science, 2020. **8**(5): p. 1464-1477.

151. Nguyen, C.T., et al., *Noninvasive in vivo optical detection of biofilm in the human middle ear.* Proceedings of the National Academy of Sciences of the United States of America, 2012. **109**(24): p. 9529-9534.

152. Saitoh, A. and T. Nomura. *Wireless sensor system using surface acoustic wave devices*. in *2009 ICCAS-SICE*. 2009.

153. Muthupillai, R., et al. *Low frequency acoustic shear wave imaging in tissue-like media using magnetic resonance*. in *1995 IEEE Ultrasonics Symposium. Proceedings. An International Symposium*. 1995.

154. Potyrailo, R.A., et al., *Battery-free radio frequency identification (RFID) sensors for food quality and safety.* J Agric Food Chem, 2012. **60**(35): p. 8535-43.

155. Guan, J.-G., Y.-Q. Miao, and Q.-J. Zhang, *Impedimetric biosensors.* Journal of Bioscience and Bioengineering, 2004. **97**(4): p. 219-226.

156. Rao, K.V.S., P.V. Nikitin, and S.F. Lam. *Impedance matching concepts in RFID transponder design*. in *Automatic Identification Advanced Technologies, 2005. Fourth IEEE Workshop on*. 2005.

157. Nikitin, P.V., et al., *Sensitivity and Impedance Measurements of UHF RFID Chips.* Microwave Theory and Techniques, IEEE Transactions on, 2009. **57**(5): p. 1297-1302.

158. Potyrailo, R.A., et al. *Selective quantitation of vapors and their mixtures using individual passive multivariable RFID sensors*. in *2010 IEEE International Conference on RFID (IEEE RFID 2010)*. 2010.

159. Bibi, F., et al., *A review: RFID technology having sensing aptitudes for food industry and their contribution to tracking and monitoring of food products.* Trends in Food Science & Technology, 2017. **62**: p. 91-103.

160. Shellhammer, T.H. and R.P. Singh, *Monitoring Chemical and Microbial Changes of Cottage Cheese using a Full-history Time-temperature Indicator.* Journal of Food Science, 1991. **56**(2): p. 402-405.

161. Taoukis, P.S. and T.P. Labuza, *Applicability of Time-Temperature Indicators as Shelf Life Monitors of Food Products.* Journal of Food Science, 1989. **54**(4): p. 783-788.

162. Amador, C., J.-P. Emond, and M.C.d.N. Nunes, *Application of RFID technologies in the temperature mapping of the pineapple supply chain.* Sensing and Instrumentation for Food Quality and Safety, 2009. **3**(1): p. 26-33.

163. Costa, C., et al., *A Review on Agri-food Supply Chain Traceability by Means of RFID Technology.* Food and Bioprocess Technology, 2013. **6**(2): p. 353-366.

164. Jang, H.-D., et al., *Quantitative determination of Lactobacillus spp. in milk using a series piezoelectric quartz crystal sensor.* European Food Research and Technology, 2009. **229**(2): p. 349-355.

165. Pacquit, A., et al., *Development of a smart packaging for the monitoring of fish spoilage.* Food Chemistry, 2007. **102**(2): p. 466-470.

166. Carstensen, E.L., J. Maniloff, and C.W. Einolf, Jr., *Electrical properties and ultrastructure of Mycoplasma membranes.* Biophysical journal, 1971. **11**(7): p. 572-581.

167. Yuan, M., E.C. Alocilja, and S. Chakrabartty, *A Novel Biosensor Based on Silver-Enhanced Self-Assembled Radio-Frequency Antennas.* IEEE Sensors Journal, 2014. **14**(4): p. 941-942.

168. Karuppuswami, S., et al., *A Wireless RFID Compatible Sensor Tag Using Gold Nanoparticle Markers for Pathogen Detection in the Liquid Food Supply Chain.* IEEE Sensors Letters, 2018. **2**(2): p. 1-4.

169. Mannoor, M.S., et al., *Graphene-based wireless bacteria detection on tooth enamel.* Nat Commun, 2012. **3**: p. 763.

170. Potyrailo, R.A. and W.G. Morris, *Multianalyte Chemical Identification and Quantitation Using a Single Radio Frequency Identification Sensor.* Analytical Chemistry, 2007. **79**(1): p. 45-51.

171. Strand, N., et al., *Chemically Polymerized Polypyrrole for On-Chip Concentration of Volatile Breath Metabolites.* Sensors and actuators. B, Chemical, 2010. **143**(2): p. 516-523.

172. Phillips, M., *Method for the Collection and Assay of Volatile Organic Compounds in Breath.* Analytical Biochemistry, 1997. **247**(2): p. 272-278.

173. Dixon, M.F., *Patterns of inflammation linked to ulcer disease.* Best Practice & Research Clinical Gastroenterology, 2000. **14** (1):27-40.

174. Ong, K.G., et al., *Design and application of a wireless, passive, resonant-circuit environmental monitoring sensor.* Sensors and Actuators A: Physical, 2001. **93**(1): p. 33-43.

175. Chen, P., et al., *Microfabricated Implantable Parylene-Based Wireless Passive Intraocular Pressure Sensors.* Journal of Microelectromechanical Systems, 2008. **17**(6): p. 1342-1351.

176. Chen, L., et al., *An antimicrobial peptide with antimicrobial activity against Helicobacter pylori.* Peptides, 2007. **28**(8): p. 1527-1531.

177. Liao, L., et al., *High-speed graphene transistors with a self-aligned nanowire gate.* Nature, 2010. **467**: p. 305.

178. Potyrailo, R.A., et al. *Label-free biosensing using passive radio-frequency identification (RFID) sensors*. in *TRANSDUCERS 2009 - 2009 International Solid-State Sensors, Actuators and Microsystems Conference*. 2009.

179. Oyeka, D.O., J.C. Batchelor, and A.M. Ziai, *Effect of skin dielectric properties on the read range of epidermal ultra-high frequency radio-frequency identification tags.* Healthcare Technology Letters, 2017. **4**(2): p. 78-81.

180. Dumtoochukwu Oyeka, J.C.B., Mohamed A.Ziai, Joseph S.R. Wheeler, Stephen Yeates, *Tag diversity of inkjet printed body-worn radio frequency identification integrated medical sticking plasters for wireless monitoring.* IET Healthcare Technology Letters, 2016. **3**(4): p. 257-262.

181. Occhiuzzi, C., G. Contri, and G. Marrocco, *Design of Implanted RFID Tags for Passive Sensing of Human Body: The STENTag.* IEEE Transactions on Antennas and Propagation, 2012. **60**(7): p. 3146-3154.

182. Daniel Marques, M.E., and Philippe Pannier, *Broadband UHF RFID Tag Antenna for Bio-Monitoring.* Progress In Electromagnetics Research B, 2016. **67**: p. 31-44.

183. Sunaga, T., et al., *Measurement of the electrical properties of human skin and the variation among subjects with certain skin conditions.* Phys Med Biol, 2002. **47**(1): p. N11-5.

184. *Tissue Properties*. 2019 [cited 2019 July 1]; Available from: https://itis.swiss/virtual-population/tissue-properties/database/dielectric-properties/.

185. Kanesan, M., D.V. Thiel, and S.G.O. Keefe. *The effect of lossy dielectric objects on a UHF RFID meander line antenna*. in *Proceedings of the 2012 IEEE International Symposium on Antennas and Propagation*. 2012.

186. Robson, J.R.K., M. Bazin, and R. Soderstrom, *Ethnic differences in skin-fold thickness.* The American Journal of Clinical Nutrition, 1971. **24**(7): p. 864-868.

187. Freeman, R.G., et al., *Sunlight as a Factor Influencing the Thickness of Epidermis.* Journal of Investigative Dermatology, 1962. **39**(4): p. 295-298.

188. Zuffanelli, S., et al. *An impedance matching method for optical disc-based UHF-RFID tags*. in *2014 IEEE International Conference on RFID (IEEE RFID)*. 2014.

189. Casula, G.A., et al., *Energy-Based Considerations for Ungrounded Wearable UHF Antenna Design.* IEEE Sensors Journal, 2017. **17**(3): p. 687-694.

190. Marrocco, G., *The art of UHF RFID antenna design: impedance-matching and size-reduction techniques.* IEEE Antennas and Propagation Magazine, 2008. **50**(1): p. 66-79.

191. Choo, J., et al. *T-matching networks for the efficient matching of practical RFID tags*. in *2009 European Microwave Conference (EuMC)*. 2009.

192. Makarovaite, V., et al., *Passive Wireless UHF RFID Antenna Label for Sensing Dielectric Properties of Aqueous and Organic Liquids.* IEEE Sensors Journal, 2019. **19**(11): p. 4299-4307.

193. Sharma, V., S. Pattnaik, and T. Garg, *A review of bacterial foraging optimization and its applications.* International Journal of Computer Applications (IJCA), 2012.

194. Yeh, K.-H., et al., *A Novel RFID Tag Identification Protocol: Adaptive n-Resolution and k-Collision Arbitration.* Wireless Personal Communications, 2014. **77**(3): p. 1775-1800.

195. *How Study and Market Your Device*. 2020 [cited 2020 March 1]; Available from: https://www.fda.gov/medical-devices/device-advice-comprehensive-regulatory-assistance/how-study-and-market-your-device

196. *Invention for Innovation*. 2020 [cited 2020 March 1]; Available from: https://www.nihr.ac.uk/explore-nihr/funding-programmes/invention-for-innovation.htm

197. Hillier, A.J.R., et al., *A Passive UHF RFID Dielectric Sensor for Aqueous Electrolytes.* IEEE Sensors Journal, 2019. **19**(14): p. 5389-5395.

198. Lindquist, A.S.A.-A.R.G., *Capacitive Interdigital Sensor with Inhomogeneous Nematic Liquid Crystal Film.* Progress In Electromagnetics Research, 2008. **7**: p. 75-85.

199. Hugo Almeida, M.H.A., Paulo Lobao, *Temperature and pH stimuli-responsive polymers and their applications in controlled and selfregulated drug delivery.* Journal of Applied Pharmaceutical Science, 2012. **2**(6): p. 1-10.

200. Du, K., et al., *Highly Porous Polymer Monolith Immobilized with Aptamer (RNA) Anchored Grafted Tentacles and Its Potential for the Purification of Lysozyme.* Industrial & Engineering Chemistry Research, 2016. **55**(2): p. 499-504.

201. Hayat, A. and J.L. Marty, *Aptamer based electrochemical sensors for emerging environmental pollutants.* Frontiers in chemistry, 2014. **2**: p. 41-41.

202. Leonhard M, Z.B., Moser D, Bertl K, Bigenzahn W, Schneider-Stickler B., *impact of surface roughness on long-term candida biofilm colonization of prosthetic silicone: A pilot study.* Hard Tissue, 2014. **3**(1): p. 1-6.

203. S. E. TEBBS, A.S.A.T.S.J.E., *Influence of surface morphology on in vitro bacterial adherence to central venous catheters.* British Journal of Anaesthesia, 1994. **72**: p. 587-591.

204. Yue Yuan, M.P.H., Philip R. Hardwidge, Jooyoun Kim, *Surface characteristics influencing bacterial adhesion to polymeric substrates.* RSC advances, 2017. **7**: p. 14254-14261.

205. *Portex*. 2020 [cited 2020 March 1]; Available from:https://www.smiths-medical.com/en-gb/brands/portex